Università di Pisa

Dipartimento di Fisica

Laurea Magistrale in Fisica della Materia

Non-local Topological Valley Hall Effect in Bilayer Graphene

Relatore:

Prof: Marco Polini

Candidato:

Francesco Sacco

ANNO ACCADEMICO 2021/2022

Ringraziamenti

Con questa tesi si conclude il mio percorso universitario, in cui per fortuna non sono mai stato solo.

Durante questi anni ho conosciuto un sacco di gente fantastica con cui adesso ho il privilegio di essere amico. E' grazie a voi, con tutti gli indimenticabili ricordi di esperienze passate assieme, che l'università è stata una fantastica esperienza. Credo proprio che senza di voi non sarei riuscito a fare nulla.

Inoltre, al mio fianco, c'è sempre stata la mia famiglia, che nonostante il mio modo di fare sempre tutto a modo mio, mi ha supportato, e cazziato, per il mio bene. Voi lo sapete già anche se non ve lo dico quasi mai, ma vi voglio un mondo di bene.

Ringrazio il personale della mensa, che mi ha dato da mangiare quasi ogni giorno, e senza di loro sarei morto da un pezzo a causa di cattiva, o insufficente alimentazione.

Ringrazio il personale della biblioteca. Non so perchè, ma quando studiavo lì riuscivo a concentrarmi con molta più facilità; ed è quindi grazie a loro che ho potuto studiare in un luogo adeguato alle mie esigenze.

Ringrazio tutto il corpo docenti e collaboratori, che mi ha istruito e fornito dei mezzi necessari per diventare quello che sono, anche se certe volte... va beh qua parlo solo dei ringraziamenti.

In generale ringrazio ogni persona con cui ho interagito questi anni, anche quelli con cui non ho avuto quasi nulla a che fare, ma che a causa dell'effetto farfalla mi hanno cambiato, e cambieranno la vita.

Sono inoltre grato del fatto che non mi sia capitata nessuna disgrazia, anche se in questo caso è un pò difficile capire di chi sia il merito.

Infine ringrazio il mio relatore per avermi seguito e affiancato durante la tesi.

Francesco,
Villabate, 2022

Contents

Introduction

Suppose we start with a infinitely long strip of width W made of a standard conducting material. If we apply a voltage V at two opposite points of the strip a current will flow from one electrode to the other. The current will be the strongest along the segment that unites the electrodes, and will be exponentially weaker the further away it is. This off-axis current is called *Nonlocal Current* and it also generates a voltage along the edges of the strip called *Nonlocal Voltage*.
Experiments in high quality gapped graphene have highlighted the existence of a larger than expected nonlocal dc voltages.

The objective of this thesis is to first explain why this anomalous nonlocal current exists in gapped graphene, and develop a model that can be used to predict and analyze this kind of phenomenon.
The thesis is structured as follows:

The first chapter is devoted to explaining how some of the machinery we'll use work. This includes some of the main concepts of topology in solid state physics, like the Hall effect, Berry phase, Berry curvature. We then use the concept of Berry curvature to generalize the Hall effect and obtain the Kubo formula and the TKNN formula. We also give a quick overview of the electronic properties of graphene and derived like gapped graphene and bilayer graphene where we focus on what happens close to the Dirac points and we introduce the concept of *Valley*.

The second chapter is devoted to see how all this tools come together in fact the nonlocal current arises from the Berry curvature hot spots near the Dirac points in gapped graphene which give rise to a particular kind of anomalous Hall effect called *Valley Hall Effect*. This creates a transverse *Valley Current* that is responsible for the high nonlocal voltage measured in the experiments

In the third and last chapter we create a model that explains in full detail how the voltage and currents behave inside of a graphene strip and develop an approximation that can be used to evaluate the properties of these kind of system and apply it to data from real-world experiments.

Chapter 1

Introduction to relevant topics

In mathematics, topology is concerned with the properties of a geometric object that are preserved under continuous deformations, such as stretching, twisting, crumpling, and bending; that is, without closing holes, opening holes, tearing, gluing, or passing through itself.

Let's start with a simple but important example (figure 1.1): Let's consider the set of all the curves in the plane that do not pass thought the origin and that do not intersect themselves. We can divide this set in two main subsets:

- The set of curves that circle around the origin (in orange)
- The set of curves that do not circle around the origin (in blue)

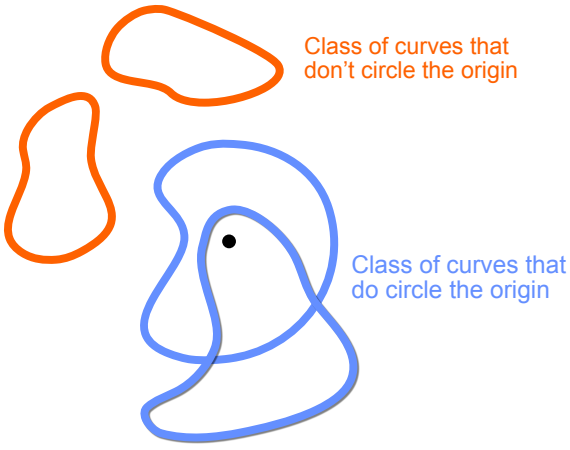

Figure 1.1: The origin in represented with a black dot. On the left the different equivalence classes are shown in different colors

You cannot deform continuously a orange curve in to a blue one without crossing the origin, but you can deform continuously a curve to reach one of the same color, so we say that the two types of curves have different topologies, or alternatively that they form two different classes of equivalence.

As you can see from the image below, if we add noise, most of the time the curves will keep their topology. However, if the noise is strong enough, or the curve close enough to the origin, the curve sometimes changes its topology.

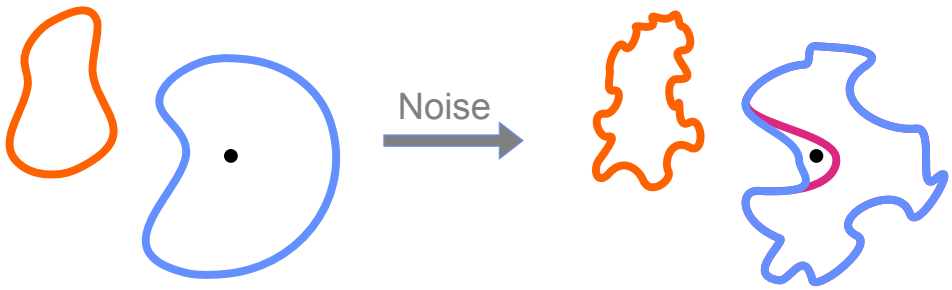

Figure 1.2: In this image the blue curve sometimes under noise keeps its topology, leaving its color unchanged, other times it gets pushed beyond the origin and switches color (here shown in fuchsia)

Why is it important?

For a physicist, things that are inherently topological in nature are important because they are resistant to noise. For example, in quantum computing the main bottleneck comes from environment noise. Because of this researchers are trying to explore the possibility of using topological effects to execute noise-resistant computations.

1.1 Topology and Hamiltonians

In condensed matter physics we can ask whether the Hamiltonian of two quantum systems can be continuously transformed into each other. If that is the case, then we can say that two systems are *topologically equivalent*.

Clearly, every Hamiltonian could be continuously deformed into every other Hamiltonian with the same number of degrees of freedom. This changes drastically if we restrict ourselves to systems with an energy gap. This means that there is a finite energy cost to excite the system above its ground state. If an energy gap is present, then the Hamiltonian of the system has no eigenvalues in a finite interval around zero energy.

We can now create the following topological classes of equivalence: we say that two gapped quantum systems are topologically equivalent if their Hamiltonians can be continuously deformed into each other without ever closing the energy gap.

In order to know whether there is a any path which connects two Hamiltonians H and H' without closing the gap, we can count the number of filled energy levels. This is possible because the eigenvalues of gapped Hamiltonians can move freely as long as they don't cross zero energy. Therefore continuous transformations exist exactly between Hamiltonians with the same number of energy levels below zero.

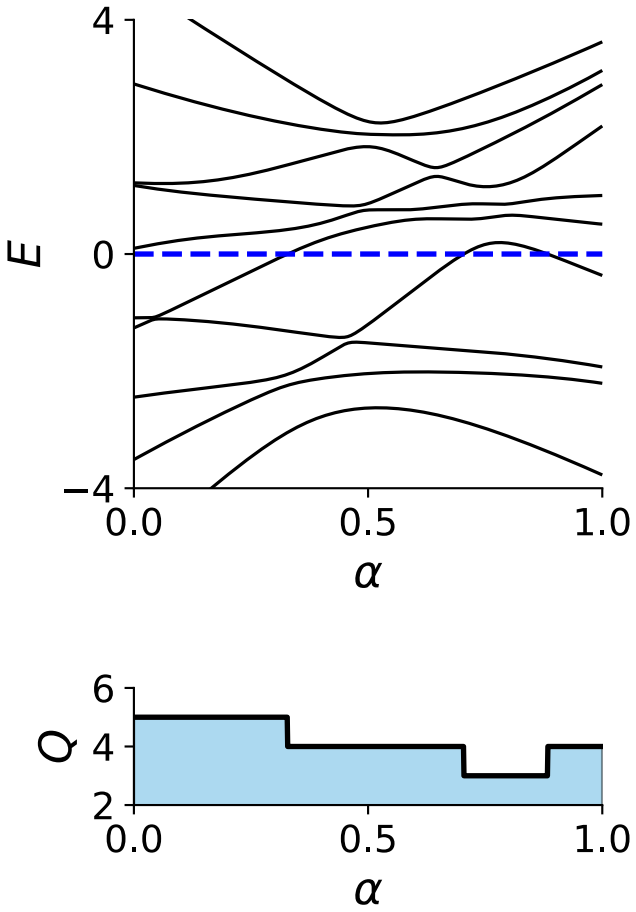

Figure 1.3: In this graph we show how the spectrum of the Hamiltonian changes as we move along a linear path between two randomly generated 10×10 Hamiltonians $H(\alpha) = \alpha H_1 + (1-\alpha)H_0$, so $H(0) = H_0$ and $H(1) = H_1$ In this case the two Hamiltonians are non-equivalent. Image taken from [1]

Since the number of filled levels does not change under continuous transformations inside the set of gapped Hamiltonians we call it the *topological invariant* Q. As you might expect, symmetries play an important role in determining topological equivalence classes, here we are going to explore some of them to

Block diagonal symmetry

If a Hamiltonian is symmetric under the unitary operator $U = \sigma_z \otimes \mathbb{I}$ it means that it can be written in block-diagonal form

$$H = \begin{bmatrix} H_0 & \mathbf{0} \\ \mathbf{0} & H_1 \end{bmatrix} \quad \rightarrow \quad U^\dagger H U = H \,, \tag{1.1}$$

where H_0 and H_1 are matrices with the same size, this means that the system as a whole behaves like two independent systems, each with its topological invariant Q_i. Since the spectrum of the Hamiltonian H is the union of the spectrum of the Hamiltonians H_0 and H_1, it means that the number of filled states of H (which, by definition is Q) is the sum of the number of filled states of H_1 and H_2 (Q_1 and Q_2), so we have that

$$Q = Q_1 + Q_2.$$

However this symmetry, without anything extra does not yield interesting topologies, it only allows us to reduce the dimension of the problem.

Time reversal symmetry

For systems with spin 1/2 the time reversal operator has the form [2]

$$\mathcal{T} = i\sigma_y \mathcal{K}\,, \tag{1.2}$$

With σ_y acting on the spin degree of freedom and where $\mathcal{K}$ is the complex conjugation operator. In that case $\mathcal{T}^2 = -1$. The Hamiltoninas with this kind of time-reversal symmetry obey the equation

$$H = \sigma_y H^* \sigma_y\,. \tag{1.3}$$

Hamiltonian of this kind have every energy eigenvalues doubly degenerate (Kramer's degeneracy), so Q can only have in the end even values. Intuitively this is because particles with spin up behave like particles with spin down, so they have the same energy.

Sublattice symmetry

Let's now take a system where we can split all the degrees of freedom into two groups (say group A and group B) such that the Hamiltonian only has nonzero matrix elements between two groups, and not inside each group.

This naturally arises in crystal systems with sublattice symmetry like graphene (we'll talk about graphene in detail further on). The Hamiltonian has the form

$$H = \begin{bmatrix} \mathbf{0} & H_{AB} \\ H_{AB}^\dagger & \mathbf{0} \end{bmatrix}. \tag{1.4}$$

If we define σ_z such that it acts on the sublattice degree of freedom

$$\sigma_z \begin{bmatrix} \boldsymbol{\psi}_A \\ \boldsymbol{\psi}_B \end{bmatrix} = \begin{bmatrix} \boldsymbol{\psi}_A \\ -\boldsymbol{\psi}_B \end{bmatrix}, \tag{1.5}$$

We have that

$$\sigma_z H \sigma_z = -H\,. \tag{1.6}$$

This means that if $[\psi_A, \psi_B]^T$ is an eigenvector with energy E, then $[\psi_A, -\psi_B]^T$ is an eigenvector with energy $-E$

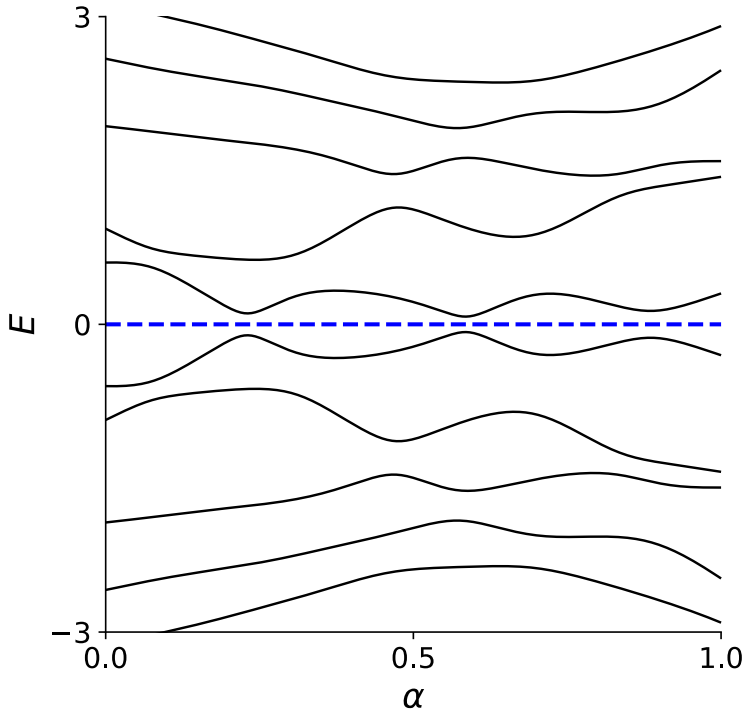

Figure 1.4: In this graph we show how the spectrum of the Hamiltonian changes as we move along a linear path between two randomly generated Hamiltonians in the form of equation 1.4 $H(\alpha) = \alpha H_1 + (1-\alpha)H_0$, so $H(0) = H_0$ and $H(1) = H_1$. As you can see the gap never closes. Image taken from [1]

One way to show why the gap never closes is the following: We can take the Hamiltonian of equation 1.4 and decompose the two sublattice Hamiltonians with the *singular value decomposition*

$$H = U\Sigma V^\dagger \,, \tag{1.7}$$

where U and V are $n \times n$ unitary matrices and Σ is a $n \times n$ diagonal matrix. If we want to find a path that goes from H_0 to H_1 in such a way that it never crosses the zero we just need to deform each one of the three matrices U, Σ and V in such a way that singular values do not appear in the path.

Particle-hole symmetry

Particle-hole symmetry shows up in superconducting systems, its Hamiltonian has the form of

$$\mathcal{H} = \sum_{nm} H_{nm} c_n^\dagger c_m + \frac{1}{2}\left(\Delta_{nm} c_n^\dagger c_m^\dagger + \Delta_{nm}^* c_n c_m, \right) \,, \tag{1.8}$$

where $c_n^\dagger$ and c_n are the creation and annihilation operators of the electrons in the state n. These operators follow the standard anticommutation rule

$$\{c_n, c_m\} = c_n c_m + c_m c_n = 0 \quad \{c_n^\dagger, c_m\} = c_n^\dagger c_m + c_m c_n^\dagger = \delta_{nm}\,. \tag{1.9}$$

We can group all the creation and annihilation operators in a vector

$$C = [c_1, \ldots, c_n, c_1^\dagger, \ldots, c_n^\dagger]\,.$$

We can now write $\mathcal{H}$ in a more compact way

$$\mathcal{H} = \frac{1}{2} C^\dagger H_{BdG} C\,. \tag{1.10}$$

The matrix H_{BdG} is knwon as the Bogoliuvov-de Gennes Hamiltonian

$$H_{BdG} = \begin{bmatrix} H & \Delta \\ -\Delta^* & -H^* \end{bmatrix}, \tag{1.11}$$

Where the matrices H and Δ are defined in equation 1.8. H_{BdG} has the symmetry on exchange of electrons with holes, and there is an antiunitary operator for it $\mathcal{P} = \tau_x \mathcal{K}$ where the Pauli matrix τ_x acts on the particle and hole blocks and $\mathcal{K}$ is the complex conjugation operator. He have that

$$\mathcal{P} H_{BdG} \mathcal{P}^{-1} = -H_{BdG}\,. \tag{1.12}$$

As you can see from figure 1.5 the energy eigenvalues are symmetric around the zero energy. this is because if $[\boldsymbol{\psi}_1, \boldsymbol{\psi}_2]^T$ is an eigenvector with energy E, then $[\boldsymbol{\psi}_2^*, \boldsymbol{\psi}_1^*]^T$ is an eigenvector too, but with energy $-E$

The reason why this crossings come up is because the Bogoljubov-de Gennes Hamiltonian we had to double the degrees of freedom by introducing the holes. Hence a pair of $\pm E$ energy states does not correspond to two distinct quantum states, but to a single quantum state. This state is called a *Bogoljubov quasiparticle* and it is a superposition of electron and hole

$$b^\dagger = uc^\dagger + vc\,. \tag{1.13}$$

The levels sometime cross the zero because some times adding a Bogoljubov quasi particle requires energy, and sometimes it realises energy, when transitioning from one to the other you get a crossing.

Clearly using the topological invariant Q defined above would only give us trivial results, what we want is some kind of number that changes when there is a level crossing. The Eigenvalues of G_{BdG} always come in pairs $\pm E$, so it is equal to

$$\det\left(H_{BdG}\right) = \prod_n -E_n^2\,.$$

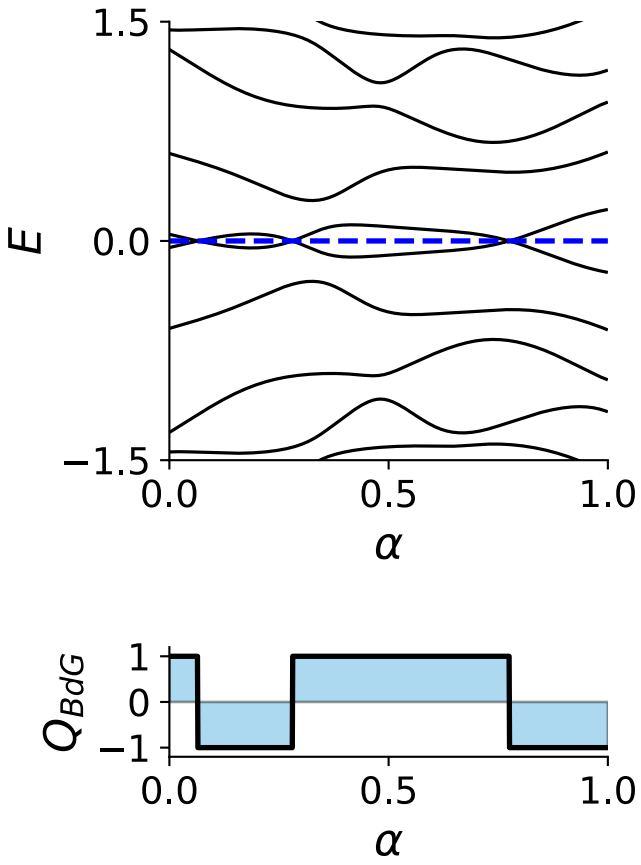

Figure 1.5: In this graph we show how the spectrum of the Hamiltonian changes as we move along a linear path between two randomly generated Bogoljubov-de Gennes Hamiltonians in the form of equation 1.8. This time, however the gap closes from time to time.

If we take the square root of the determinant in such a way that its sign is uniquely determined, also called the *Pfaffian*[1], we can define the following topological invariant

$$Q_{BdG} = [\mathrm{Pf}(iH_{BdG})] \ . \tag{1.14}$$

The results of computing the Pfaffian can be seen in figure 1.5

[1] Actually it is a bit more complicated than taking the square root. The Pfaffian is a property of asymmetric matrices, and H_{BdG} it is not, however though a change of basis it can be cast into one

1.2 Edge states and the bulk-boundary correspondence

A fundamental consequence of the topological classification of gapped states is the emergence of gapless conducting states at interfaces where the topological invariant changes. This edge states are present at the interface between integer Hall state and vacuum [3]. These states can be understood in terms of the skipping motion electrons execute as their cyclotron motion bounce off the edge Arguably the most important property of edge states is their *chirality* in the sense that they only propagate in one direction along the edge. These states are insensitive to disorder because there are no states available for backscattering.

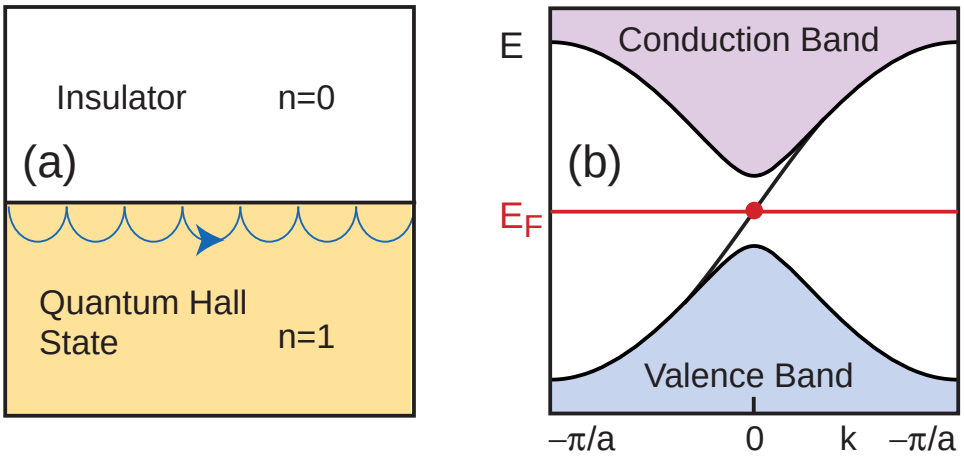

Figure 1.6: In the figure on the left (a) the edge mode is represented as an electron in a skipping motion. On the right (b) is shown the electronic structure of a topological material and the line that unites the conduction band with the valence band represents the edge state. Image taken from [4]

The existence of these one way states are linked to the existence of the topological numbers. If to go from one topological number to the other you need to close the gap, then if we start form inside one material, and we end up to the other material, somewhere along the way the gap has to close and the only reasonable place to do so is the boundary [5]. Keep in mind that one of the two materials can be the vacuum itself

1.3 Spectral Flow

Another example of topology in quantum mechanics is the concept of *spectral flow*. To start off we are going to talk about a very specific case of a quantum particle in a ring around a infinitely long solenoid.
The Hamiltonian of a particle with charge $-e$ moving through a magnetic

field $\mathbf{B} = \nabla \times \mathbf{A}$ is

$$H = \frac{1}{2m}(\mathbf{p} + e\mathbf{A})^2 \,. \tag{1.15}$$

Since

$$\mathbf{p} = p_\theta \hat{\theta} = -\frac{i\hbar\hat{\theta}}{R}\frac{\partial}{\partial\theta}\,,$$

$$\oint \mathbf{A}\cdot d\mathbf{r} = \int \mathbf{B}\cdot d\mathbf{s} = \Phi\,,$$

it means that

$$\mathbf{A} = \frac{\Phi}{2\pi R}\hat{\theta}\,. \tag{1.16}$$

Putting it back into the Hamiltonian

$$H = \frac{1}{2m}\left(-\frac{i\hbar}{R}\frac{\partial}{\partial\theta} + \frac{e\Phi}{2\pi R}\right)^2 . \tag{1.17}$$

The eigenstates of this Hamiltonian are

$$\psi_n(\theta) = \frac{e^{in\theta}}{\sqrt{2\pi R}}; \quad n \in \mathbb{Z}\,.$$

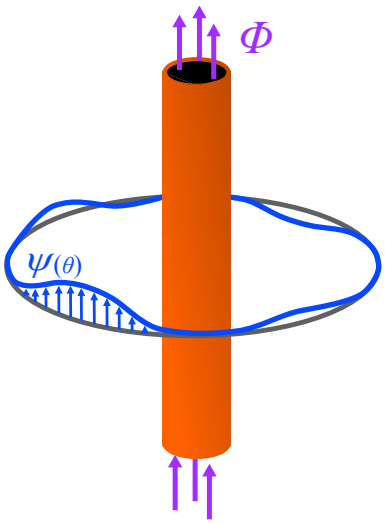

Figure 1.7: Particle in a ring threaded by a solenoid

Interestingly the Energies of the eigenstates are influenced by the vector potential

$$E_n = \frac{1}{2mR^2}\left(\hbar n + \frac{e\Phi}{2\pi}\right)^2 = \tilde{E}\left(n + \frac{\Phi}{\Phi_0}\right)^2 , \tag{1.18}$$

where

$$\tilde{E} = \frac{\hbar^2}{2mR^2} \quad \text{and} \quad \Phi_0 = \frac{2\pi\hbar}{e}\,.$$

Suppose now that we start with the turned solenoid off, and place the particle in the $n = 0$ ground state. If we increase the flux then, by the time we have reached $\Phi = \Phi_0$, the $n = 0$ state has transformed into the state that we previously labelled $n = 1$. Similarly, each state n is shifted to the next state, $n + 1$ [2].

This is an example of a phenomenon is called spectral flow: under a change of parameter the spectrum of the Hamiltonian changes, or "flows". As we change increase the flux by one unit Φ_0 the spectrum returns to itself, but individual states have morphed into each other. [6]

[2] It is tempting to invoke the adiabatic theorem here but, because of level crossing at $\Phi = \Phi_0/2$ it is not valid

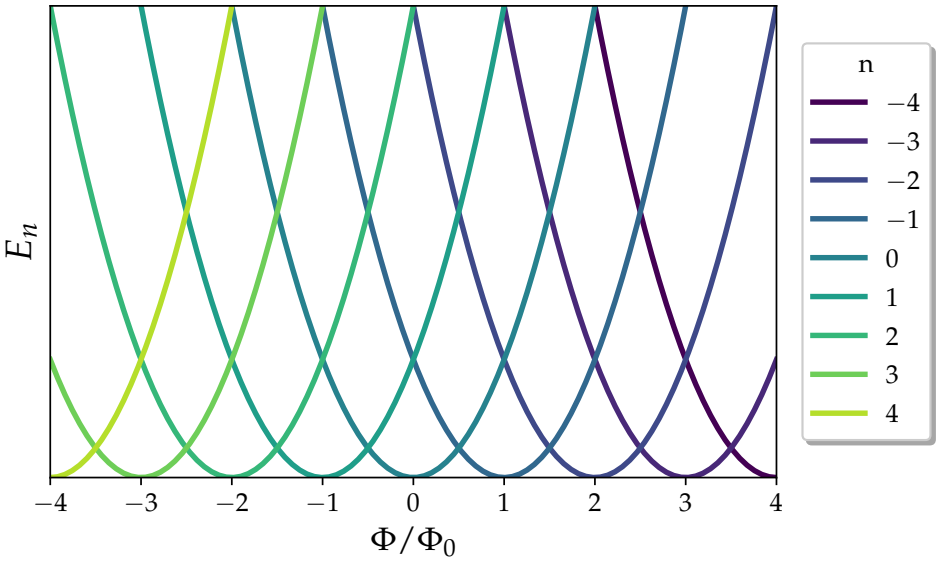

Figure 1.8: Here plotted the energies E_n (eq. 1.18), notice how the states *"flow"* as we change Φ. Image adapted from [6]

Parallelism with Bloch's Theorem

You might have noticed that figure 1.8 is suspiciously similar to a crystal band structure in the limit on which the periodic potential $V \to 0$ with periodicity 2π, let us see if this analogy holds *the test of math.* Let's start by taking the single-particle free propagating Hamiltonian

$$H = \frac{1}{2m} p_\theta^2 \,.$$

The eigenstates this time have to respect the condition that

$$u_{n,q}(\theta) = e^{i2\pi q} u_{n,q}(\theta + 2\pi) \,. \tag{1.19}$$

This also means that if we substitute $q \to q{+}1$ the spectrum doesn't change.[3] We now make the following unitary transformation to obtain a q-depentant Hamiltonian.

$$H(q) = e^{-iq\theta} H e^{iq\theta} = \frac{1}{2m}\left(p_\theta + \frac{\hbar q}{R}\right)^2 .$$

We can easly map this hamiltonian to the one in equation 1.17 just by difining Φ such that $\hbar q = \frac{e\Phi}{2\pi}$.

$$H(\Phi) = \frac{1}{2m}\left(p_\theta + \frac{e\Phi}{2\pi R}\right)^2 . \tag{1.20}$$

[3] This come from the Bloch's theorem that states that the eigenstates of the Hamiltonian of a periodic potential with periodicity a mush obey that $u_{n,q}(x) = e^{iaq} u_{n,q}(x + a)$. In our case the periodicity $a = 2\pi$ and the variable of the function is θ instead of x

Since before we said that the system doesn't change if we substitute $q \to q+1$, it means that now the system remains unchanged if we send $\Phi \to \Phi + \Phi_0$. This is exactly the result obtained in the previous page.

And the tranformed eigenstates $\psi_{n,q} = e^{-iq\theta} u_{n,q}$ is just the cell-periodic part of the Bloch function. It satified the stricter periodic boundary condition

$$\psi_{n,q}(\theta) = \psi_{n,q}(\theta + 2\pi)\,. \tag{1.21}$$

As you can see equations 1.20 and 1.21 create a system that is mathematically equivalent to the particle moving in a ring around a flux tube [7].

Conditions to have spectral flow

Up until now we looked spectral flow the case where the particle is freely propagating, let's see what happens when we add a periodic potential $V(\theta) = V(\theta + 2\pi)$

$$H = \frac{1}{2m} p_\theta^2 + V(\theta)\,.$$

Now the spectrum is still periodic, however the energy bands do not necessarily cross, this means that when abiabatically changing q, (or equivalently Φ) the states won't flow, instead they will return to their original state.

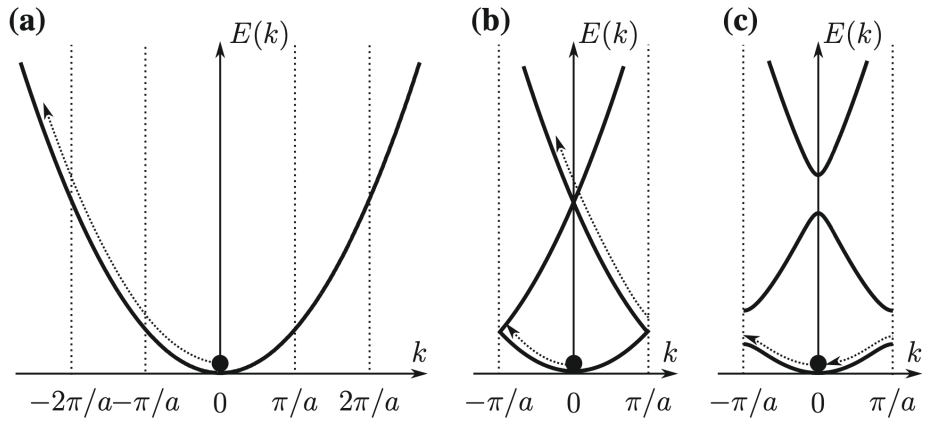

Figure 1.9: Pictorial representation of what happens when changing q. Image taken from [8]

Conversely if there are n degeneracies, on every cycle more the i-th state will flow to the $i + n$-th state.

Spectral flow in a more general context

The spectral flow is applicable in much more complex geometries than the one we have seen so far.
Suppose that now the particle can moove in a 3D potential $V(\mathbf{r})$, the Hamiltonian is

$$H(\mathbf{A}) = \frac{1}{2m}(\mathbf{p} + e\mathbf{A})^2 + V(\mathbf{r})\,,$$

since the solenoid is still the same, the formula for $\mathbf{A}$ remains unchanged (eq. 1.16)

$$H(\Phi) = \frac{1}{2m}\left(\mathbf{p} + \frac{e\Phi}{2\pi R}\hat{\theta}\right)^2 + V(\mathbf{r})\,,$$

and since it's expressed in cylindrical coordinates it's better to express also $\mathbf{p}$ in cylindrical coordinates.

$$\mathbf{p} = -i\hbar\nabla = -i\hbar\left(\hat{\mathbf{r}}\frac{\partial}{\partial r} + \frac{\hat{\theta}}{r}\frac{\partial}{\partial\theta} + \hat{\mathbf{z}}\frac{\partial}{\partial z}\right) \equiv \hat{\mathbf{r}}p_r + \hat{\theta}p_\theta + \hat{\mathbf{z}}p_z\,.$$

Of course if we send $\theta \to \theta + 2\pi$ the system should be unchanged.

$$\psi(r,\theta,z) = \psi(r,\theta+2\pi,z)\,.$$

Following the inverse reasoning done in the previous subsection we make the following unitary transformation

$$H = e^{i\theta\Phi/\Phi_0}H(\Phi)e^{-i\theta\Phi/\Phi_0} = \frac{\mathbf{p}^2}{2m} + V(\mathbf{r})\,.$$

This means that the eigenvalue problem is now written like so

$$He^{i\theta\Phi/\Phi_0}\psi(r,\theta,z) = E(\Phi)e^{i\theta\Phi/\Phi_0}\psi(r,\theta,z)\,.$$

If we send $\Phi \to \Phi + \Phi_0$ we get an equivalent equation

$$He^{i\theta\Phi/\Phi_0}\psi(r,\theta,z) = E(\Phi+\Phi_0)e^{i\theta\Phi/\Phi_0}\psi(r,\theta,z)\,.$$

This means that the energy spectrum is unchanged if we send $\Phi \to \Phi + \Phi_0$. This is true regardless of the shape or geometry of $V(\mathbf{r})$.

The quantum Hall effect

We'll now see the effects of the spectral flow on physical properties of materials. Suppose we have a system like the one of the figure on the side. Now we slowly increase Φ from 0 to Φ_0 in a total time T. This introduces a electromagnetic force around the ring $\mathcal{E} = -\partial_t\Phi = -\Phi_0/T$.

Due to spectral flow n electrons are transferred form the inner circle to the outer circle in this time T. This would result in a radial current $I_r = -ne/T$. This means that the resistance is

$$R_{xy} = \frac{\mathcal{E}}{I_r} = \frac{2\pi\hbar}{e^2}\frac{1}{n}\,. \tag{1.22}$$

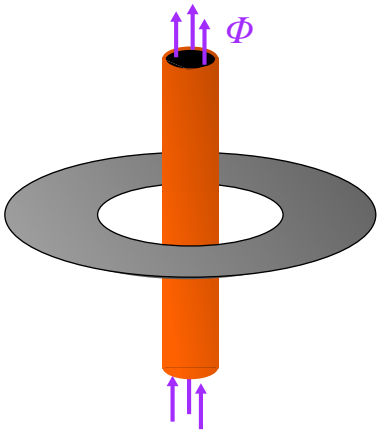

In the case there is no spectral flow, it is equivalent as saying $n = 0$, so this treatment works is still valid.
To be able to calculate n we need to calculate how is the spectrum of the system as we change Φ. This means that n depends on the system, but equation 1.22 is independent of the system.
This effect to be observed the system has to be in a definite quantum state, so in real life scenario the material has to be cooled to low enough temperatures.

1.4 Berry phase

Berry phase is the simplest demonstration of how geometry and topology can emerge from quantum mechanics and it is at heart of the quantum Hall effect.
Let us consider a physical system described by a Hamiltonian that depends on a set of parameters $\boldsymbol{\lambda} = (\lambda_1, \lambda_2, \dots)$. These parameters do not represent the degrees of freedom of the system like position and momentum, rather they describe things such as the mass of a particle, the strength of a potential and so on.
For each $H(\boldsymbol{\lambda})$ there exists a set of eigenstates such that

$$H(\boldsymbol{\lambda})\,|n, \boldsymbol{\lambda}\rangle = E_n(\boldsymbol{\lambda})\,|n, \boldsymbol{\lambda}\rangle\ , \tag{1.23}$$

however the equation above does not completely determine the basis function $|n, \boldsymbol{\lambda}\rangle$; We can change arbitrarily the phase $\gamma_n(\boldsymbol{\lambda})$ of any eigenstate which is called **Berry phase**

$$|n, \boldsymbol{\lambda}\rangle \to \underbrace{e^{i\gamma_n(\boldsymbol{\lambda})}}_{\text{Berry phase}}\ |n, \boldsymbol{\lambda}\rangle\ . \tag{1.24}$$

Suppose we start off with a Hamiltonian and then we slowly change the parameters for a time T until it reaches a different Hamiltonian, this means that $\boldsymbol{\lambda} = \boldsymbol{\lambda}(t)$. For the adiabatic theorem we can say that if we start on an energy eigenstate, and the system changes slowly enough,and has no degeneracies, then the system will cling on that energy eigenstate.How slow

you have to be in changing the parameters depends on the energy gap from the state you're in to the nearest other state. The smaller the gap, the slower you have to change the parameters. A way of showing this without doing long calculations is the following:
We know from the Heisenberg uncertainty principle that $T\Delta E \geq \hbar/2$. We want the uncertainty in the Energy to be way smaller than the energy gap $E_g \gg \Delta E$, so $E_g \gg \frac{\hbar}{2T}$, therefore if we make T big enough it can be achieved.

The equation of motion of a particle that for time $t = 0$ is equal to $|\psi_n(t=0)\rangle = |n, \boldsymbol{\lambda}(0)\rangle$ is

$$|\psi_n(t)\rangle = \underbrace{e^{i\gamma_n(\boldsymbol{\lambda}(t))}}_{\text{Berry phase}} \cdot \underbrace{e^{-\frac{i}{\hbar}\int_0^t E_n(\boldsymbol{\lambda}(t'))dt'}}_{\text{dynamical phase}} |n, \boldsymbol{\lambda}(t)\rangle \,, \tag{1.25}$$

where the first exponent comes from eq. 1.24. We now insert the equation above into the time-dependent Schrodinger equation

$$i\hbar\partial_t|\psi_n(t)\rangle = H(\boldsymbol{\lambda}(t))|\psi_n(t)\rangle \,. \tag{1.26}$$

By plugging equation 1.25 into the *right* term term of equation 1.26 we get we get that

$$H(\boldsymbol{\lambda}(t))|\psi_n(t)\rangle = E_n(t)\,|\psi_n(t)\rangle \ , \tag{1.27}$$

and by plugging equation 1.25 into the *left* term term of equation 1.26 we get we get that

$$i\hbar\partial_t|\psi_n(t)\rangle = -\hbar\dot{\gamma}_n(t)|\psi_n(t)\rangle + E_n(t)|\psi_n(t)\rangle + e^{i\phi_n(t)}\partial_t|n,t\rangle \,, \tag{1.28}$$

where we have defined $e^{i\phi_n(t)} \equiv e^{i\gamma_n(\boldsymbol{\lambda}(t))}e^{-\frac{i}{\hbar}\int_0^t E_n(\boldsymbol{\lambda}(t'))dt'}$.

By equating the right terms in equations 1.27 and 1.28 we get that

$$i\hbar e^{i\phi_n t(t)}\partial_t|n,t\rangle = \hbar\dot{\gamma}_n(t)\,|\psi_n(t)\rangle = \hbar\dot{\gamma}_n(t)e^{i\phi_n(t)}\,|n,t\rangle \tag{1.29}$$

now we multiply the term on the left and on the right of equation 1.29 by $\hbar^{-1}e^{-i\phi_n(t)}\,\langle n,t|$

$$\dot{\gamma}_n(t) = i\,\langle n,t|\,\partial_t\,|n,t\rangle \tag{1.30}$$

We can re-express it in terms of $\boldsymbol{\lambda}$

$$\dot{\gamma}_n(t) = \dot{\boldsymbol{\lambda}}\cdot\underbrace{i\,\langle n,t|\,\partial_{\boldsymbol{\lambda}}\,|n,t\rangle}_{\equiv\mathbf{A}_n(\boldsymbol{\lambda})} , \tag{1.31}$$

where

$$\boldsymbol{A}_n(\boldsymbol{\lambda}) = i\,\langle n,t|\,\partial_{\boldsymbol{\lambda}}\,|n,t\rangle \ . \tag{1.32}$$

$\mathbf{A}_n(\boldsymbol{\lambda})$ called the **Berry connection** This means that we can calculate the total change in $\gamma_n(t)$ can be obtained by doing a line integral in the space

of parameters $\boldsymbol{\lambda}$ over the path $\mathcal{P}$ of values that $\boldsymbol{\lambda}$ assumes during the time evolution

$$\gamma_n = \int_{\mathcal{P}} \mathbf{A}_n(\boldsymbol{\lambda}) \cdot d\boldsymbol{\lambda}\,, \tag{1.33}$$

$$|n, \boldsymbol{\lambda}\rangle \to e^{if_n(\boldsymbol{\lambda})} |n, \boldsymbol{\lambda}\rangle\ . \tag{1.34}$$

Keep in mind however that the eigenstates are defined up to a phase, meaning that we can re-define the base vectors like so (equation 1.34). If we apply this substitution into the formula of $\mathbf{A}_n$ we have that

$$\mathbf{A}_n(\boldsymbol{\lambda}) = i \langle n, t| \partial_{\boldsymbol{\lambda}} |n, t\rangle \to i \langle n, t| \partial_{\boldsymbol{\lambda}} |n, t\rangle - \partial_{\boldsymbol{\lambda}} f_n(\boldsymbol{\lambda})\,,$$

$$\mathbf{A}_n \to \mathbf{A}_n - \partial_{\boldsymbol{\lambda}} f_n\,. \tag{1.35}$$

So the system is invariant under the gauge transformation in equation 1.35. If we do this transformation to equation 1.33 we have that

$$\gamma_n = \int_{\mathcal{P}} \mathbf{A}_n(\boldsymbol{\lambda}) \cdot d\boldsymbol{\lambda} - \int_{\mathcal{P}} \partial_{\boldsymbol{\lambda}} f_n(\boldsymbol{\lambda}) \cdot d\boldsymbol{\lambda} = \int_{\mathcal{P}} \mathbf{A}_n(\boldsymbol{\lambda}) \cdot d\boldsymbol{\lambda} + f(\boldsymbol{\lambda}(0)) - f(\boldsymbol{\lambda}(T))\,.$$

This means that if the path $\mathcal{P}$ is open we can always choose a function f_n such that $f(\boldsymbol{\lambda}(0)) - f(\boldsymbol{\lambda}(T)) = \int_{\mathcal{P}} \mathbf{A}_n(\boldsymbol{\lambda}) \cdot d\boldsymbol{\lambda}$, thus we can conclude that one can always choose a suitable $f(\boldsymbol{\lambda})$ such that γ_n accumulated along the path $\mathcal{P}$ is calceled out leaving equation 1.25 with only the dynamical phase. However if the path is closed $\boldsymbol{\lambda}(0) = \boldsymbol{\lambda}(T)$, in order to make the phase change in equation 1.34 single valued we must have that

$$e^{f(\boldsymbol{\lambda}(0)) - f(\boldsymbol{\lambda}(T))} = 1\,,$$

so

$$f(\boldsymbol{\lambda}(0)) - f(\boldsymbol{\lambda}(T)) = 2n\pi \quad n \in \mathbb{Z}\,.$$

This leads us to the important result that

$$\gamma_n = \oint_{\mathcal{P}} \mathbf{A}_n(\boldsymbol{\lambda}) \cdot d\boldsymbol{\lambda} + 2n\pi\,. \tag{1.36}$$

This time, if the line integral is not a multiple of 2π (and there is no reason why it should) there is no way of choosing a suitable f_n to cancel it out and the Berry phase in equation 1.25 is there to stay

1.5 Berry curvature

You might have noticed that equation 1.35 is analogous to what happens in Electromagnetism with the vector potential. This means that we can try using the same mathematics and see where it leads us. However, in classic and relativistic electromagnetism $\dim(\boldsymbol{A}_\mu)$ is equal to respectively 3 and 4, in the case of the Berry curvature it can have any integer value.

In EM from the gauge-dependent $\boldsymbol{A}$ are defined the gauge-indipendent field as follows:

1. in 3D the magnetic field is defined as follows $B_i = \epsilon_{ijk}\partial_j A_k$
2. in $(3+1)$D the Field tensor is defined as $F_{\mu\nu} = \partial_\mu A_\nu - \partial_\nu A_\mu$

In both cases the resulting field is asymmetric under the exchange of the indices of the derivative and the indices of the vector potential. This requirement is what makes the resulting field gauge independent.

With the same logic we can define a gauge field tensor derived from the Berry connection:

$$\boxed{\Omega^n_{\mu\nu} = \partial_\mu A^n_\nu(\boldsymbol{\lambda}) - \partial_\nu A^n_\mu(\boldsymbol{\lambda})\,.} \tag{1.37}$$

This new field tensor is defined as **Berry curvature**, and it is gauge independent just like $\boldsymbol{B}$ and $F_{\mu\nu}$![4]

From now on it can be useful to introduce the external product operator $\wedge$ that act as follows: Given two vectors $\boldsymbol{v}$ and $\boldsymbol{w}$ we have that

$$\boldsymbol{v} \wedge \boldsymbol{w} \equiv v_\mu w_\nu - v_\nu w_\mu\,. \tag{1.38}$$

With this definition we can write

$$\boldsymbol{\Omega}^n(\boldsymbol{\lambda}) = \nabla \wedge \boldsymbol{A}^n(\boldsymbol{\lambda})\,. \tag{1.39}$$

Other formulas for $\Omega_{\mu\nu}$

With a few mathematical steps it is possible to re cast the Berry curvature into a different form that might be useful later

$$\partial_\mu A^n_\mu = i\partial_\mu \langle n, \boldsymbol{\lambda}|\, \partial_\nu n, \boldsymbol{\lambda}\rangle = i\,\langle \partial_\mu n, \boldsymbol{\lambda}|\, \partial_\nu n, \boldsymbol{\lambda}\rangle + i\,\langle n, \boldsymbol{\lambda}|\, \partial_\mu\partial_\nu n, \boldsymbol{\lambda}\rangle\,,$$

$$\boxed{\Omega^n_{\mu\nu} = i\,\langle \partial_\mu n|\, \partial_\nu n\rangle - i\,\langle \partial_\nu n|\, \partial_\mu n\rangle} \tag{1.40}$$

or, equivalently

$$\boldsymbol{\Omega}^n = i\,\langle \nabla n| \wedge |\nabla n\rangle\ . \tag{1.41}$$

[4]The notation has changed a bit, now $A^n_\mu \equiv (\mathbf{A}_n)_\mu$

It is also possible to express Ω in terms of the eigenstates of the Hamiltonian with some mathematical manipulation

$$\begin{gathered}
\langle n'| H |n\rangle = \delta_{n'n} \to \partial_\mu \langle n'| H |n\rangle = 0\,, \\
\partial_\mu \langle n'| H |n\rangle = \langle \partial_\mu n'| H |n\rangle + \langle n'| H |\partial_\mu n\rangle + \langle n'| \partial_\mu H |n\rangle\ , \\
E_n \langle \partial_\mu n'| n\rangle + E_{n'} \langle n'| \partial_\mu n\rangle = \langle n'| \partial_\mu H |n\rangle\ , \\
(E_{n'} - E_n) \langle n'| \partial_\mu n\rangle = \langle n'| \partial_\mu H |n\rangle\ , \\
\langle n'| \partial_\mu n\rangle = \frac{\langle n'| \partial_\mu H |n\rangle}{E_{n'} - E_n}\,. \qquad (1.42)
\end{gathered}$$

Now we write equation 1.40 like so

$$\Omega^n_{\mu\nu} = i \langle \partial_\mu n| \partial_\nu n\rangle - (\mu \leftrightarrow \nu) = i \sum_{n' \neq n} \langle \partial_\mu n| n'\rangle \langle n'| \partial_\nu n\rangle - (\mu \leftrightarrow \nu)\,.$$

By plugging in above equation 1.42 we get

$$\boxed{\Omega^n_{\mu\nu} = i \sum_{n' \neq n} \frac{\langle n| \partial_\mu H |n'\rangle \langle n'| \partial_\nu H |n\rangle}{(E_{n'} - E_n)^2} - (\mu \leftrightarrow \nu)} \qquad (1.43)$$

This last form of the Berry curvature has the advantage that no differentiation of the wavefunction is needed. This equation also tells us that

$$\sum_n \Omega^n_{\mu\nu}(\boldsymbol{\lambda}) = 0\,.$$

Equation 1.43 can also be written as

$$\boldsymbol{\Omega}^n = \sum_{n' \neq n} \frac{\langle n| \nabla H |n'\rangle \wedge \langle n'| \nabla H |n\rangle}{(E_{n'} - E_n)^2}\,. \qquad (1.44)$$

1.6 Stokes' Theorem

From the Stokes theorem we have that

$$\gamma_n = \oint_{\mathcal{P}} A^n_\mu \, d\lambda^\mu = \frac{1}{2} \int_\Sigma \Omega^n_{\mu\nu} \, d\lambda^\mu \wedge d\lambda^\nu\,, \qquad (1.45)$$

where we have used the Einstein convention of summation.
There is a subtelty in this last equation, as we know the Berry curvature tensor in Gauge-invariant, so the integral over the surface is too, but the integral over the closed path of the Berry connection is defined up to a factor $2n\pi$ that is gauge dependant. So is there a modulo 2π ambiguity or not?
The answer is that if γ_n is to be determined using the knowledge of $|n, \boldsymbol{\lambda}\rangle$

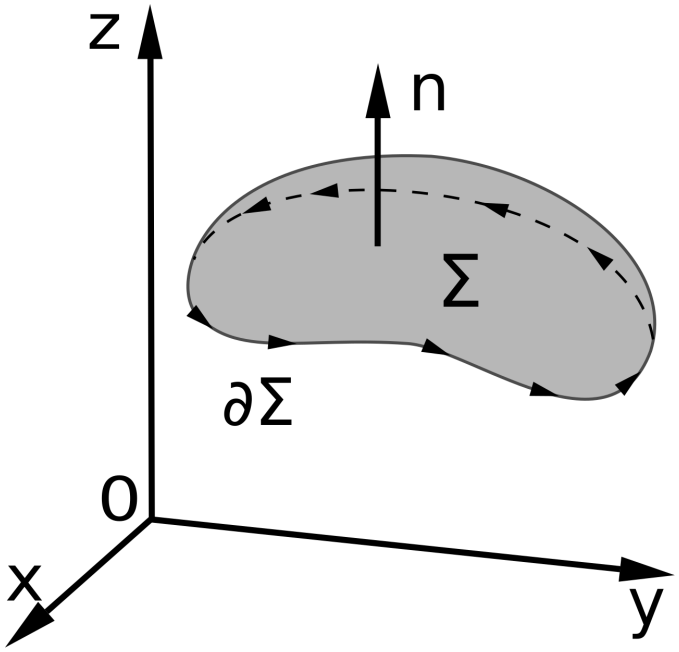

Figure 1.10: Here we divide the surface of the sphere in two different surfaces $\mathcal{A}$ and $\mathcal{B}$ that share the edge $\mathcal{P}$

only on the curve $\mathcal{P}$ then it is really well defined modulo 2π. In this case we can re-write equation 1.45 as

$$\frac{1}{2}\int_{\Sigma}\Omega^{n}_{\mu\nu}\,d\lambda^{\mu}\wedge d\lambda^{\nu} := \oint_{\mathcal{P}} A^{n}_{\mu}\,d\lambda^{\mu}\,. \tag{1.46}$$

Meaning that the integral over the surface Σ is equal to *one of the values of* the integrals along the closed path $\mathcal{P}$.

But what kind of Gauge gives the "correct" answer? If we choose a gauge that is continuous and smooth everywhere along the surface Σ including on its boundary $\mathcal{P}$ then equation 1.45 becomes unambiguous.
While it is possible to make a radical gauge transformation that shifts γ_n by 2π when regarding $|n,\boldsymbol{\lambda}\rangle$ as a function defined only in the neighborhood of $\mathcal{P}$, such a gauge change cannot be smoothly continued into the interior $\mathcal{S}$ without creating a vortex-like singularity of $\gamma_n(\boldsymbol{\lambda})$.

1.7 Chern Theorem

Let's take as an example Gauss's theorem. It tells us that the flux of the field through a closed surface is equal to the charges inside.
Now let's calculate the flux of the Berry curvature through a closed surface. We can divide the closed surface as two different open surfaces that share the same edge $\mathcal{P}$.

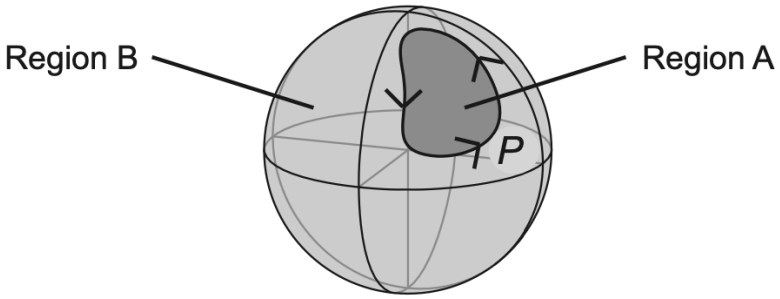

Figure 1.11: Here we divide the surface of the sphere in two different surfaces $\mathcal{A}$ and $\mathcal{B}$ that share the edge $\mathcal{P}$

Thanks to stokes theorem the flux through the surface $\mathcal{A}$ is $\oint_{\mathcal{P}} \mathbf{A} \cdot d\boldsymbol{\lambda}$, but the flux through the surface $\mathcal{B}$ is $-\oint_{\mathcal{P}} \mathbf{A} \cdot d\boldsymbol{\lambda}$.
Theese two integrals must be equal modulo 2π, so

$$\oint_{\mathcal{S}} \Omega^n_{\mu\nu} d\lambda^\mu \wedge d\lambda^\nu = 2\pi C_n \qquad C_n \in \mathbb{Z}\,. \tag{1.47}$$

This means that the flux thought a closed surface of the Berry curvature is quantized

The constant C in known as the Chern number. Note that when the Chern index is nonzero, it is impossible to construct a smooth and continuous gauge over the entire surface $\mathcal{S}$. If such a gauge did exist, then we could apply Stokes' theorem directly to the entire surface and conclude that the Chern number vanishes, in contradiction with the assumption.
But what are these "pseudo-charges" inside the closed surface that generate the flux?
In E.M. a simple way to spot charges (or monopoles) is to look at the fields and see if as some point it diverges as $1/(\mathbf{r}-\mathbf{r_0})^2$. Let's take a look at $\Omega_{\mu\nu}$ (eq. 1.43) and see if we can spot anything similar [5]

$$\Omega^n_{\mu\nu} = i \sum_{n' \neq n} \frac{\langle n|\, \partial_\mu H\, |n'\rangle \wedge \langle n'|\, \partial_\nu H\, |n\rangle}{\underbrace{[E_{n'}(\boldsymbol{\lambda}) - E_n(\boldsymbol{\lambda})]^2}_{\substack{\text{what happens if for some } \boldsymbol{\lambda}=\boldsymbol{\lambda}_d \\ \text{the two energies are the same?}}}}\,. \tag{1.48}$$

So, suppose that for some $\boldsymbol{\lambda} = \boldsymbol{\lambda}_d$ we have that $E_n(\boldsymbol{\lambda}_d) = E_m(\boldsymbol{\lambda}_d)$, now we expand the energies near $\boldsymbol{\lambda}_d$ at first order

$$\begin{cases} E_n(\boldsymbol{\lambda}) \approx E_n(\boldsymbol{\lambda}_d) + \partial_{\boldsymbol{\lambda}} E_n|_{\boldsymbol{\lambda}=\boldsymbol{\lambda}_d} \cdot (\boldsymbol{\lambda} - \boldsymbol{\lambda}_d) \\ E_m(\boldsymbol{\lambda}) \approx E_n(\boldsymbol{\lambda}_d) + \partial_{\boldsymbol{\lambda}} E_m|_{\boldsymbol{\lambda}=\boldsymbol{\lambda}_d} \cdot (\boldsymbol{\lambda} - \boldsymbol{\lambda}_d) \end{cases}\,.$$

[5] In the equation below I expressed explicitly the $\boldsymbol{\lambda}$ dependence in the denominator and condensed the formula using the wedge product $\wedge$

This means that

$$E_n(\boldsymbol{\lambda}) - E_m(\boldsymbol{\lambda}) \approx \partial_{\boldsymbol{\lambda}}(E_n - E_m)|_{\boldsymbol{\lambda}=\boldsymbol{\lambda}_d} \cdot (\boldsymbol{\lambda} - \boldsymbol{\lambda}_d)\,,$$

so the denominator of the berry curvature near $\boldsymbol{\lambda}_d$ goes like $1/(\boldsymbol{\lambda} - \boldsymbol{\lambda}_d)^2$. This means that there are "charges" or "monopoles" that induce the flux through the closed surface, and they are localized where 2 (or more) energy levels cross

1.8 Kubo Formula

We'll derive the Kubo formula for a general, multi-particle (or, if you prefer, single particle) Hamiltonian H_0 where the subscript 0 means that this is the unperturbed Hamiltonian before we apply an electric field. We denote the eigentstates of the Hamiltonian as $|m\rangle$ with $H_0 |m\rangle = E_m |m\rangle$.

$$H_0 = \sum_i \left[\frac{1}{2m} (\boldsymbol{p}_i - e\boldsymbol{A}_0)^2 + V_0(\boldsymbol{r}_i) \right] + \sum_{i \neq j} V_{ee}(\boldsymbol{r}_i - \boldsymbol{r}_j)\,, \tag{1.49}$$

where $\boldsymbol{A}_0$ and V_0 are due to an existing EM field. Now we add a background electric field.

$$H = \sum_i \left[\frac{1}{2m} (\boldsymbol{p}_i - e\boldsymbol{A}_0 - e\boldsymbol{A})^2 + V_0(\boldsymbol{r}_i) - e\boldsymbol{r}_i\phi(\boldsymbol{r}_i) \right] + \sum_{i \neq j} V_{ee}(\boldsymbol{r}_i - \boldsymbol{r}_j)\,. \tag{1.50}$$

Which can be written as

$$H = H_0 + \sum_i -\frac{e}{m}\boldsymbol{\pi}_i \cdot \boldsymbol{A} - e\boldsymbol{r}_i\phi(\boldsymbol{r}_i)\,, \tag{1.51}$$

where $\boldsymbol{\pi}_i = \boldsymbol{p} - e\boldsymbol{A}_0 = m\dot{\boldsymbol{r}}$ is the mechanical momentum, furthermore we can use the fact that the electric charge operator $\rho(\boldsymbol{r}) = -e\sum_i \delta(\boldsymbol{r} - \boldsymbol{r}_i)$ current operator $\boldsymbol{I}$ is equal to

$$\boldsymbol{I} = -e\sum_i \dot{\boldsymbol{r}}_i = -\sum_i \frac{e}{m}\boldsymbol{\pi}_i\,. \tag{1.52}$$

We can now re-write equation 1.51 like so

$$H = H_0 + \boldsymbol{I} \cdot \boldsymbol{A} + \int \rho(\boldsymbol{r})\phi(\boldsymbol{r})d\boldsymbol{r}\,. \tag{1.53}$$

however, we can assume that the density of charge ρ is always zero. It is usually considered when investigating dielectric properties of a material, but here we are interested in conduction, so we are ignoring it. This means that equation 1.53 becomes

$$H(\boldsymbol{A}) = H_0 + \boldsymbol{I} \cdot \boldsymbol{A}\,. \tag{1.54}$$

At this point we need to write the perturbation in terms of the electric field, we can choose a gauge where $\boldsymbol{E} = -\partial_t \boldsymbol{A}$ and assume that the wave is monochromatic $\boldsymbol{E}(t) = \boldsymbol{E}e^{-i\omega t}$, so

$$A = \frac{\boldsymbol{E}}{i\omega} e^{i\omega t} \,. \tag{1.55}$$

Our goal is to compute the current $\langle \boldsymbol{I} \rangle$ that flows due to the perturbation ΔH. To do so we'll work in the *interaction picture*, this means that the operators evolve as $\mathcal{O}(t) = V^{-1}\mathcal{O}V$ with $V = e^{-iH_0 t/\hbar}$. This means that the states evolve by

$$|\psi(t)\rangle = U(t,t_0)\,|\psi(t_0)\rangle\,; \quad U(t,t_0) = T\exp\left(-\frac{i}{\hbar}\int_{t_0}^{t} \Delta H(t')dt'\right) \,, \tag{1.56}$$

where T is the time ordering. Keep in mind that since we are in the interaction picture $\Delta H(t) = V^{-1}\Delta H V$.
We now prepare the system at time $t = -\infty$ in a specific many body state $\rho_0 = \sum_i p_i \,|i\rangle\,\langle i|$ (it usually is either the ground state or a thermodynamic distribution). Keep in mind that the density operator, in the interaction picture evolves with the states

$$\begin{aligned} \rho(t) =& \sum_i p_i \,|\psi_i(t)\rangle\,\langle\psi_i(t)| = \\ =& \sum_i p_i U(t,t_0)\,|\psi_i(t_0)\rangle\,\langle\psi_i(t_0)|\,U^{-1}(t,t_0) = \\ =& U(t,t_0)\rho(t_0)U^{-1}(t,t_0)\,. \end{aligned} \tag{1.57}$$

Then, writing $U(t) = T(t, t_0 \to -\infty)$, the expectation value of the current is

$$\begin{aligned} \langle \boldsymbol{I}(t)\rangle &= \mathrm{tr}\left[\rho(t)\boldsymbol{I}(t)\right] = \\ &= \mathrm{tr}\left[U(t)\rho_0 U^{-1}(t)\boldsymbol{I}(t)\right] = \\ &= \mathrm{tr}\left[\rho_0 U^{-1}(t)\boldsymbol{I}(t)U(t)\right] = \\ &= \langle U^{-1}(t)\boldsymbol{I}(t)U(t)\rangle_0 \approx \\ &\approx \langle \boldsymbol{I}(t)\rangle_0 + \left\langle \frac{i}{\hbar}\int_{-\infty}^{t} [\Delta H(t'), \boldsymbol{I}(t)]dt' \right\rangle_0 \,, \end{aligned} \tag{1.58}$$

where in the last passage we've expanded the exponential in the U operator (equation 1.56), and $\langle \ldots \rangle_0$ means the average with respect to ρ_0. The first term is the current in the absence of an electric field, therefore it is zero. Using equation 1.54 and 1.55 and plugging it in the last equation we have that the current due to the electric field is then

$$\langle I_i(t)\rangle = \frac{1}{\hbar\omega}\int_{\infty}^{t} \langle [I_j(t'), I_i(t)]\rangle_0 E_j e^{-i\omega t'} dt' \,. \tag{1.59}$$

Because the system is invariant under time translations, the correlation function above can bony depend on $t'' = t - t'$, we can rewrite the expression above as

$$\frac{E_j e^{-i\omega t}}{\hbar\omega} \int_0^\infty e^{i\omega t''} \langle [I_j(0), I_i(t'')] \rangle_0 dt'' \,. \tag{1.60}$$

The only t dependence in the formula above sits outside as $e^{-i\omega t}$. This means that the proportionality constant is the conductance. To get the conductivity σ (conductance per unit area, we just have to divide the surface S), and the off diagonal part is the *Hall conductivity*

$$\sigma_{xy} = \frac{1}{S\hbar\omega} \int_0^\infty e^{i\omega t} \langle [I_x(0), I_y(t)] \rangle_0 dt \tag{1.61}$$

This is the **Kubo formula** for the Hall conductivity.

1.9 Quantization of Hall conductivity

Our job here is not done, we got Kubo formula the Hall conductivity 1.61, but to capture the most important property we need to do some mathematical manipulation. Using the fact hat $\boldsymbol{I}(t) = V^{-1}\boldsymbol{I}(0)V$ with $V = e^{-iH_0 t/\hbar}$ we can write

$$\sigma_{xy}(\omega) = \frac{1}{S\hbar\omega} \int_0^\infty e^{i\omega t} \sum_{nm} p_n \left[\langle n|I_y|m\rangle \langle m|I_x|n\rangle e^{-iE_{nm}t/\hbar} - (n \leftrightarrow m) \right] dt \,.$$

Now we can perform the integral in dt, since the states with $n = m$ cancel out we have that

$$\sigma_{xy}(\omega) = -\frac{i}{\omega S} \sum_{nm} p_n \left[\frac{\langle n|I_y|m\rangle \langle m|I_x|n\rangle}{\hbar\omega - E_{nm}} - (n \leftrightarrow m) \right] . \tag{1.62}$$

To get the Hall conductivity for DC current we have to evaluate $\sigma_{xy}(\omega \to 0)$, in this limit

$$\lim_{\omega\to 0} \frac{1}{\hbar\omega - E_{nm}} = -\frac{1}{E_{nm}} + \frac{\hbar\omega}{(E_{nm})^2} \,.$$

Plugging the zeroth-order we get

$$\begin{aligned} \sigma_{xy} =& \frac{i}{\omega S} \sum_{nm} p_n \left[\frac{\langle n|I_y|m\rangle \langle m|I_x|n\rangle}{E_{nm}} - (n \leftrightarrow m) \right] = \\ =& \frac{i}{\omega S} \sum_{nm} \frac{p_n}{E_{nm}} \left[\langle n|I_y|m\rangle \langle m|I_x|n\rangle + (n \leftrightarrow m) \right] = \\ =& 0 \,. \end{aligned} \tag{1.63}$$

That is equal to zero because the terms inside the summation are asymmetric under the exchange of $(n \leftrightarrow m)$, and we are summing over all the possible n

and m. For the first order term we have

$$\boxed{\sigma_{xy} = \frac{i\hbar}{S} \sum_{nm} \frac{p_n}{(E_{nm})^2} \left[\langle n|I_y|m\rangle \langle m|I_x|n\rangle - (n \leftrightarrow m) \right]} \tag{1.64}$$

This is also called the **Kubo formula** but is only valid for DC currents usually it is possible to say to which formula people are referring from the context. Since the Hall effect is generally studied in the DC case this formula will be useful. From equation 1.54 we can see that $I_i = \partial H / \partial A_i$, this means that the equation above becomes

$$\begin{aligned}
\sigma_{xy} =& \frac{i\hbar}{S} \sum_{nm} \frac{p_n}{(E_{nm})^2} \left[\langle n|I_y|m\rangle \langle m|I_x|n\rangle - (n \leftrightarrow m) \right] = \\
=& \frac{\hbar}{S} \sum_n p_n \sum_{m \neq n} \frac{i}{(E_{nm})^2} \left[\left\langle n \middle| \frac{\partial H}{\partial A_y} \middle| m \right\rangle \left\langle m \middle| \frac{\partial H}{\partial A_x} \middle| n \right\rangle - (n \leftrightarrow m) \right] = \\
=& \frac{\hbar}{S} \sum_n p_n \Omega^n_{A_x A_y} \,.
\end{aligned} \tag{1.65}$$

This is a nice formula, however it doesn't explain why σ_{xy} is quantized, however if we average over all possible values of $\boldsymbol{A}$, which comes from all the possible value of the fluxes

$$\begin{aligned}
\langle \sigma_{xy} \rangle =& \frac{\int \sigma_{xy} d^2\boldsymbol{A}}{\int d^2\boldsymbol{A}} = \\
=& \left(\frac{S}{\Phi_0^2} \right) \frac{\hbar}{S} \sum_n p_n \int \Omega^n_{A_x A_y} d^2\boldsymbol{A} = \\
=& \left(\frac{e^2}{4\pi^2\hbar^2} \right) 2\pi\hbar \sum_n p_n C_n = \\
=& \frac{e^2}{2\pi\hbar} \sum_n p_n C_n \qquad \text{with } C_n \in \mathbb{Z} \,.
\end{aligned} \tag{1.66}$$

Where we have defined the Chern numbers $2\pi C_n = \int \Omega^n_{A_x A_y} d^2\boldsymbol{A}$ and for the Stokes theorem it is a multiple of 1. The most emblematic passage here is why $\int d^2\boldsymbol{A} = \Phi_0^2 / S$.

$\boldsymbol{\sigma_{xy}}$ at low temperatures

In equation 1.66 we had a contribution that is the average of C_n over all the states, if we are at low temperature there are two possibilities depending on the treatment we had on the wavefunction

- **Many body interacting wavefunction** For $T \to 0$ we have that it will be at the fundamental state $p_0 \to 1$ and $p_i \to 0$ for $i \neq 0$, this means that $\sum_n p_n C_n \to C_0$, therefore a quantized conductivity will be observed.

- **Non-interacting single particle wavefunctions** For $T \to 0$ the electrons will settle in a Fermi-Dirac distribution, so

$$\sum_n p_n C_n = N^{-1} \sum_n C_n \theta(E_F - E_n)\,.$$

  where N is the total number of electrons and E_F is the Fermi energy. Although it's not as easy to prove that is generally quantized due to the N^{-1} factor,[6] we'll see that it's much easier to calculate the precise value for real world scenarios, and it's going to be the subject of the next section.

1.10 Berry phase in Bloch bands

The band structure of crystals provides a natural platform to investigate the occurrence of the Berry phase effect. Within the independent electron approximation, the band structure of a crystal is determined by the Bloch Hamiltonian:

$$H = \frac{\boldsymbol{p}^2}{2m} + V(\boldsymbol{r})\,, \tag{1.67}$$

where $V(\boldsymbol{r} + \boldsymbol{a}) = V(\boldsymbol{r})$ is the periodic potential with a being the Bravais lattice vector. According to Bloch's theorem the eigenstates satisfy

$$\psi_{n\boldsymbol{k}}(\boldsymbol{r} + \boldsymbol{a}) = e^{i\boldsymbol{k}\cdot\boldsymbol{a}} \psi_{n\boldsymbol{k}}(\boldsymbol{r})\,, \tag{1.68}$$

where n is the band index and $\hbar\boldsymbol{k}$ is the crystal momentum. To comply with the general formalism of the Berry phase, we make the following unitary transformation to obtain a $\boldsymbol{k}$-dependent Hamiltonian

$$e^{-i\boldsymbol{k}\cdot\boldsymbol{r}} H e^{i\boldsymbol{k}\cdot\boldsymbol{r}} \equiv H(\boldsymbol{k}) = \frac{(\boldsymbol{p} + \hbar\boldsymbol{k})^2}{2m} + V(\boldsymbol{r})\,. \tag{1.69}$$

The transformed eigenstate $u_{n\boldsymbol{k}}(\boldsymbol{r}) = e^{-i\boldsymbol{k}\cdot\boldsymbol{r}} \psi_{n\boldsymbol{k}}(\boldsymbol{r})$ is just the cell-periodic part of the Bloch function. It satisfies the strict periodic boundary condition

$$u_{n\boldsymbol{k}}(\boldsymbol{r} + \boldsymbol{a}) = u_{n\boldsymbol{k}}(\boldsymbol{r})\,. \tag{1.70}$$

[6] Even thought we know for sure it must be quantized, because we can always re-parametrize Non-interacting single particle wavefunctions into many body interacting wavefunction

We can now identify the Brillouin zone $\mathcal{B}$ as the parameter space of the transformed Hamiltonian $H(\boldsymbol{k})$, and $u_{n\boldsymbol{k}} = |n, \boldsymbol{k}\rangle$ as the basis function.
In this regime the Kubo formula 1.64 becomes

$$\sigma_{xy} = i\hbar \sum_{m, E_n < E_F} \int_{\mathcal{B}} \frac{\langle n, \boldsymbol{k}|J_y|m, \boldsymbol{k}\rangle \langle m, \boldsymbol{k}|J_x|n, \boldsymbol{k}\rangle - (n \leftrightarrow m)}{E_m(\boldsymbol{k}) - E_n(\boldsymbol{k})} \frac{d^2\boldsymbol{k}}{(2\pi)^2} \,. \quad (1.71)$$

And it is called the **TKNN formula** [9]. We can define the current in terms of the group velocity of the wavepackets.

$$\boldsymbol{J} = \frac{e}{\hbar} \frac{\partial H}{\partial \boldsymbol{k}} \,, \quad (1.72)$$

this means that equation 1.71 is equal to

$$i\frac{e^2}{\hbar} \sum_{m, E_n < E_F} \int_{\mathcal{B}} \frac{\langle n, \boldsymbol{k}|\partial_y H|m, \boldsymbol{k}\rangle \langle m, \boldsymbol{k}|\partial_x H|n, \boldsymbol{k}\rangle - (n \leftrightarrow m)}{E_m(\boldsymbol{k}) - E_n(\boldsymbol{k})} \frac{d^2\boldsymbol{k}}{(2\pi)^2} \,. \quad (1.73)$$

Using equation 1.43 we have that the equation above becomes

$$\sigma_{xy} = \frac{e^2}{\hbar} \sum_{E_n < E_F} \int_{\mathcal{B}} \Omega^n_{k_x k_y} \frac{d^2\boldsymbol{k}}{(2\pi)^2} \,. \quad (1.74)$$

Finally, using the Chern theorem 1.47 we have that the equation above is equal to

$$\sigma_{xy} = \frac{e^2}{2\pi\hbar} \sum_{n}^{N} C_n \,, \quad (1.75)$$

where C_n is the Chern number of the n-th band and the bands up to the N-th band are occupied, therefore we sum over the occupied bands.
This is an important result, because it tells us that the transversal component of the conductivity arising from Berry curvature effects is quantized if the system has a finite number of fully occupied bands.
But what happens at non zero temperature, or when the Fermi level intersects one or more bands? To do so we have to make some modification the the TKNN formula (equation 1.71).

Generalized TKNN formula

In the TKNN formula (equation 1.71) we assume to have a Fermi-Dirac step function that lies in between two bands when summing over $E_n < E_F$. This means that

$$\sum_{E_n < E_\mathrm{F}} \to \sum_n f\left[E_n(\boldsymbol{k}), \mu, T\right] \,, \quad (1.76)$$

where $f\left[E_n(\boldsymbol{k}), \mu, T\right]$ is the Fermi-Dirac distribution with chemical potential μ and temperature T

$$f\left[E_n(\boldsymbol{k}), \mu, T\right] = \frac{1}{e^{\beta[E(\boldsymbol{k}) - \mu]} + 1} \,, \quad (1.77)$$

Where $\beta = 1/K_b T$. This means that the TKNN formula becomes

$$\sigma_{xy} = i\hbar \sum_{mn} \int_{\mathcal{B}} f\left[E_n(\boldsymbol{k}), \mu, T\right] \frac{\langle n, \boldsymbol{k}|J_y|m, \boldsymbol{k}\rangle \langle m, \boldsymbol{k}|J_x|n, \boldsymbol{k}\rangle - (n \leftrightarrow m)}{E_m(\boldsymbol{k}) - E_n(\boldsymbol{k})} \frac{d^2\boldsymbol{k}}{(2\pi)^2} \,. \tag{1.78}$$

Doing the same steps we did going form equation 1.71 to equation 1.74 we get that

$$\sigma_{xy}(\mu, T) = \frac{e^2}{\hbar} \sum_n \int_{\mathcal{B}} f\left[E_n(\boldsymbol{k}), \mu, T\right] \Omega^n_{k_x k_y} \frac{d^2\boldsymbol{k}}{(2\pi)^2} \,. \tag{1.79}$$

The Fermi-Dirac distribution prohibits us from using the Chern theorem (equation 1.47), so it is not granted for general μ and T that the conductivity in quantized, however this last equation can be used to calculate the conductivity in a more general setting.

1.11 Anomalous velocity

Finally, as a last phenomenon of the Berry curvature we talk about how it changes the velocity of electrons inside crystals. The velocity operator of a particle in a periodic potential with crystal impulse $\boldsymbol{k}$ is given by [8]

$$\boldsymbol{v}(\boldsymbol{k}) = \frac{\partial H(\boldsymbol{k})}{\hbar \partial \boldsymbol{k}} \,, \tag{1.80}$$

where $H(\boldsymbol{k})$ is the Hamiltonian from equation 1.69. so the velocity of the n-th state with impulse $\boldsymbol{k}$ is simply

$$\boldsymbol{v}_n(\boldsymbol{k}) = \langle \psi_n | \, \boldsymbol{v}(\boldsymbol{k}) \, |\psi_n\rangle = \frac{\partial E_n(\boldsymbol{k})}{\hbar \partial \boldsymbol{k}} \,. \tag{1.81}$$

Now lets see what happens if we apply a weak uniform external electric field through a uniform vector potential $\boldsymbol{A}(t)$. Using the Peierls substitution, the Hamiltonian is written as

$$H(\boldsymbol{k}, t) = \frac{[\boldsymbol{p} + \hbar\boldsymbol{k} + e\boldsymbol{A}(t)]^2}{2m} + V(\boldsymbol{r}) \,. \tag{1.82}$$

We can now introduce a gauge invariant crystal momentum $\boldsymbol{\pi}(\boldsymbol{k}, t) = \boldsymbol{k} + e\boldsymbol{A}(t)$ and we can notice that

$$H(\boldsymbol{k}, t) = H(\boldsymbol{\pi}) \,. \tag{1.83}$$

Since $\boldsymbol{A}(t)$ preserves the translational symmetry, $\boldsymbol{k}$ is still a good quantum number and it is a constant of motion $\dot{\boldsymbol{k}} = 0$ it follows from derivating with respect to time this equation $\boldsymbol{\pi}(\boldsymbol{k}, t) = \hbar\boldsymbol{k} + e\boldsymbol{A}(t)$ that

$$\dot{\boldsymbol{\pi}} = -e\boldsymbol{E} \,. \tag{1.84}$$

To evaluate the velocity we have to use first order perturbation theory [10]

$$\left|\psi_n'\right\rangle = \left|\psi_n\right\rangle + \sum_{n'\neq n} \frac{\langle\psi_{n'}|\Delta H|\psi_n\rangle}{E_{n'} - E_n} \left|\psi_{n'}\right\rangle \,. \tag{1.85}$$

Since in the interaction picture $\Delta H \left|\psi_n\right\rangle = -i\hbar \left|\partial_t \psi_n\right\rangle$ we have that the equation above becomes

$$\left|\psi_n'\right\rangle = \left|\psi_n\right\rangle - i\hbar \sum_{n'\neq n} \frac{\langle\psi_{n'}|\partial_t\psi_n\rangle}{E_{n'} - E_n} \left|\psi_{n'}\right\rangle \,. \tag{1.86}$$

From equation 1.80 we have that the velocity with the new states becomes

$$\begin{aligned} \boldsymbol{v}_n(\boldsymbol{k}) &= \left\langle\psi_n'\right| \boldsymbol{v}(\boldsymbol{k}) \left|\psi_n'\right\rangle = \\ &= \left\langle\psi_n\right| \boldsymbol{v}(\boldsymbol{k}) \left|\psi_n\right\rangle - i \sum_{n\neq 0} \left\langle \psi_n \middle| \frac{\partial H}{\partial \boldsymbol{k}} \middle| \psi_{n'} \right\rangle \frac{\langle\psi_{n'}|\partial_t\psi_n\rangle}{E_{n'} - E_n} - \text{c.c.} \,. \end{aligned} \tag{1.87}$$

From equation 1.42 we can say that

$$\left\langle \psi_n \middle| \frac{\partial H}{\partial \boldsymbol{k}} \middle| \psi_{n'} \right\rangle \frac{1}{E_{n'} - E_n} = \langle \partial_{\boldsymbol{k}} \psi_n | \psi_{n'} \rangle \,, \tag{1.88}$$

And using equation 1.80, equation 1.87 becomes

$$\boldsymbol{v}_n(\boldsymbol{k}) = \frac{\partial E_n(k)}{\hbar \partial \boldsymbol{k}} - i \sum_{n'\neq n} \langle \partial_{\boldsymbol{k}} \psi_n | \psi_{n'} \rangle \langle \psi_{n'} | \partial_t \psi_n \rangle - \text{c.c.} \,. \tag{1.89}$$

The second term in the equation above is the Berry curvature (equation 1.40), so in the end we get that.

$$\boldsymbol{v}_n(\boldsymbol{k}) = \frac{\partial E_n(k)}{\hbar \partial \boldsymbol{k}} - \Omega^n_{\boldsymbol{k}t} \,. \tag{1.90}$$

Also, since $\frac{\partial}{\partial \boldsymbol{\pi}} = \frac{\partial}{\hbar \partial \boldsymbol{k}}$ and $\hbar \frac{\partial \boldsymbol{k}}{\partial t} = -e\boldsymbol{E}$ (equation 1.84) we have that

$$\frac{\partial}{\partial t} = -\frac{e}{\hbar} \nabla_{\boldsymbol{k}} \cdot \boldsymbol{E} \,.$$

Thought some mathematical manipulation it can be shown that parsing the equation above into equation 1.90 we get that [11]

$$\boldsymbol{v}_n(\boldsymbol{k}) = \frac{\partial E_n(k)}{\hbar \partial \boldsymbol{k}} - \frac{e}{\hbar} \boldsymbol{E} \times \boldsymbol{\Omega}^n(\boldsymbol{k}) \,, \tag{1.91}$$

where $\boldsymbol{\Omega}^n(\boldsymbol{k})$ is the Berry curvature of the n-th band

$$\boldsymbol{\Omega}^n(\boldsymbol{k}) = i \left\langle \nabla_{\boldsymbol{k}} \psi_n \right| \times \left| \nabla_{\boldsymbol{k}} \psi_n \right\rangle \,. \tag{1.92}$$

From equation 1.91 we can see that, in addition to the usual band dispersion contribution of equation 1.80, an extra term previously known as an anomalous velocity contributes to $\boldsymbol{v}_n(\boldsymbol{k})$. This velocity is transverse to the electric field, and it gives us yet another way of interpreting the Hall effect.

1.12 Symmetry considerations for the Berry curvature

The velocity formula of equation 1.91 shows us that, in addition to the band energy, the Berry curvature is required for a complete description of electron dynamics. However, the conventional formula of equation 1.80 has had great success describing electronic properties in the past. This suggests us that the Berry curvature term in most cases does not contribute.

The general form of the Berry curvature $\Omega^n(\boldsymbol{k})$ can be obtained via symmetry analysis. The velocity formula 1.91 should be invariant under time reversal and spatial inversion symmetry if the unperturbed system possesses these symmetries to begin with. Under time reversal, $\boldsymbol{v}_n$ and $\boldsymbol{k}$ changes sign while $\boldsymbol{E}$ does not, in that case from 1.91 we have that

$$\Omega^n(-\boldsymbol{k}) = -\Omega(\boldsymbol{k})\,. \tag{1.93}$$

Under spatial inversion, $\boldsymbol{v}_n$, $\boldsymbol{k}$ and $\boldsymbol{E}$ changes sign, so from equation 1.91

$$\Omega^n(-\boldsymbol{k}) = \Omega(\boldsymbol{k})\,. \tag{1.94}$$

Therefore, fore crystals with simultaneous time-reversal and spatial inversion symmetry the Berry curvature vanish identically throughout the Brillouin zone, this reduces equation 1.91 to equation 1.80.

There are many important systems where both symmetries are not simultaneously present, for example in materials where the ferromagnetic ordering breaks the time reversal symmetry (figure 1.12). Another example is provided by single-layered graphene stacked on top of a substrate of Boron nitrite which breaks the inversion symmetry, it will be one of the main focuses of the thesis, but before delving into that we need to talk in more detail about the structure and electronic properties of graphene.

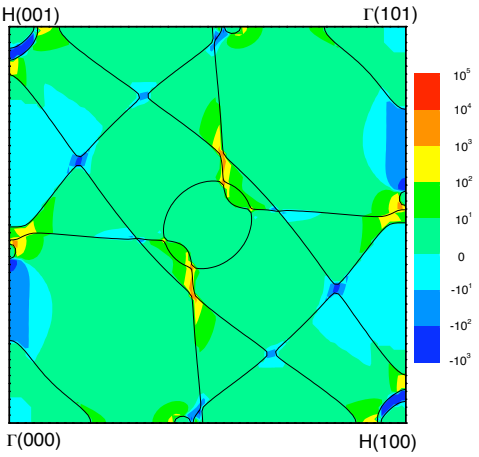

Figure 1.12: This plot represents the intersection of the be Brillouin zone with the 010 plane. The solid line i where the fermi surface intersects the 010 plane and in color in shown the magnitude of the Berry curvature $\Omega_z(\boldsymbol{k})$ in atomic units. Image taken from [12].

1.13 Graphene

Graphene is a two-dimensional lattice of carbon atoms, arranged in a honeycomb structure as shown in the figure 1.13 Although it is straightforward to build many layers of these lattices (a substance known as graphite), it was long thought that a purely two-dimensional lattice would be unstable to thermal fluctuations and impossible to create. This changed in 2004 when Andre Geim and Konstantin Novoselov succeeded in isolating two-dimensional graphene [13]. For this, they won the 2010 Nobel prize. As we now show, the band structure of graphene is particularly interesting.

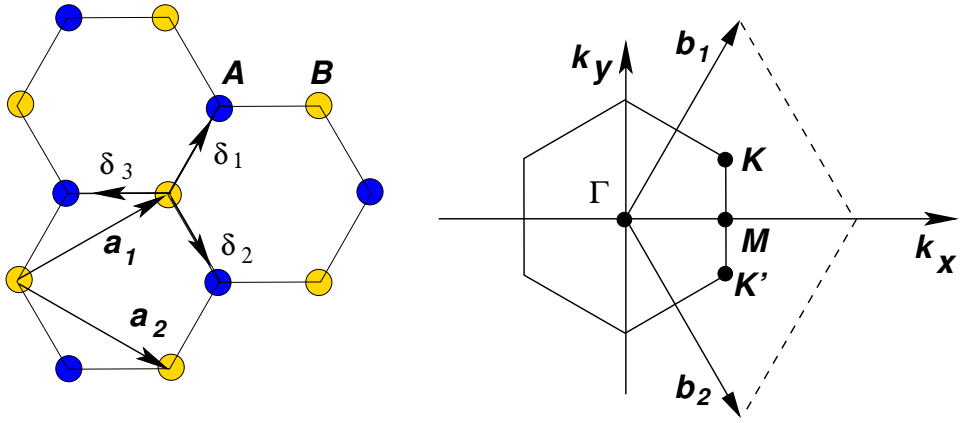

Figure 1.13: On the left there is the lattice structure of graphene made out of two interpenetrating triangular lattices (a_1 and a_2 are the lattice unit vectors, and δ_i with $i \in 1, 2, 3$ are the nearest neighbors. On the right the corresponding Brillouin zone, the Dirac cones are located at the K_0 and K_1 points). Image taken from [14].

We define the primitive lattice vectors $\boldsymbol{a}_1$ and $\boldsymbol{a}_2$ as follows:

$$\boldsymbol{a}_1 = \frac{a}{2}\begin{bmatrix} 3 \\ \sqrt{3} \end{bmatrix}, \qquad \boldsymbol{a}_2 = \frac{a}{2}\begin{bmatrix} 3 \\ -\sqrt{3} \end{bmatrix}. \tag{1.95}$$

Where a is the distance between two neighboring atoms, which in graphene is $\approx 1.4 \times 10^{-10}$m. The sublattice A is defined as all the points $\boldsymbol{r} = n_1\boldsymbol{a}_1 + n_2\boldsymbol{a}_2$ with $n_i \in \mathbb{Z}$ (yellow points in figure 1.13), sublattice B is defined as all points $\boldsymbol{r} = n_1\boldsymbol{a}_1 + n_2\boldsymbol{a}_2 + \boldsymbol{\delta}$ with $\boldsymbol{\delta} = (a, 0)$ (blue points in figure 1.13).

The reciprocal lattice vectors $\boldsymbol{b}_i$ are the vectors that satisfy $\boldsymbol{a}_i \cdot \boldsymbol{b}_j = \delta_{ij}$ and are equal to

$$\boldsymbol{b}_1 = \frac{2\pi}{3a}\begin{bmatrix} 1 \\ \sqrt{3} \end{bmatrix}, \qquad \boldsymbol{b}_2 = \frac{2\pi}{3a}\begin{bmatrix} 1 \\ -\sqrt{3} \end{bmatrix}. \tag{1.96}$$

This reciprocal lattice is also triangular. The Brillouin zone is constructed in the usual manner by drawing perpendicular boundaries between the origin

and each other point in the reciprocal lattice giving rise to a hexagonal Brillouin zone with $\boldsymbol{K}_0$ and $\boldsymbol{K}_1$ as the vertices of the hexagon, where

$$\boldsymbol{K}_0 = \frac{1}{3}(2\boldsymbol{b}_1 + \boldsymbol{b}_2)\,, \qquad \boldsymbol{K}_1 = \frac{1}{3}(\boldsymbol{b}_1 + 2\boldsymbol{b}_2)$$

,

$$\boldsymbol{K}_0 = \frac{2\pi}{3a}\left(1, \frac{1}{\sqrt{3}}\right)\,, \qquad \boldsymbol{K}_1 = \frac{2\pi}{3a}\left(1, -\frac{1}{\sqrt{3}}\right)\,. \tag{1.97}$$

The tight binding approach

To investigate the band structure of graphene, we are going to use the tight binding approach [15, 16]. First we write the Hamiltonian.

$$H = \frac{\boldsymbol{p}^2}{2m} + \sum_{\boldsymbol{R}\in C} V_a(x - \boldsymbol{R})\,, \tag{1.98}$$

where V_a is the potential of the single carbon atom, the set
$C = \{n_1\boldsymbol{a}_1 + n_2\boldsymbol{a}_2 + \nu\boldsymbol{\delta}\,|\,n_1, n_2 \in \mathbb{Z},\, \nu \in \{0,1\}\}$ is the set of all the positions of the atoms.
We can re-write the potential of the Hamiltonian in this more convenient manner.

$$\sum_{\boldsymbol{R}\in C} V_a(x - \boldsymbol{R}) = V_a(x) + V'(x)\,, \tag{1.99}$$

where $V'(x)$ the potential of the other atoms, this way the can be divided in two parts:

$$H = \underbrace{\frac{\boldsymbol{p}^2}{2m} + V_a(x)}_{\substack{\text{single-atom}\\ \text{Hamiltonian}}} + \underbrace{V'(x)}_{\text{perturbation}}\,. \tag{1.100}$$

Let $|n, \boldsymbol{R}\rangle$ be the n-th eingenstate of the Hamiltonian of single carbon atom placed in $\boldsymbol{R}$. Due to translational symmetry, the wave function must satisfy the Bloch theorem, this tells us that the eingenstates of the Hamiltonian can be written as

$$|n, \nu, \boldsymbol{k}\rangle = \sum_{\boldsymbol{R}_\nu \in C_\nu} e^{i\boldsymbol{k}\cdot\boldsymbol{R}_\nu}\,|n, \boldsymbol{R}_\nu\rangle\,, \tag{1.101}$$

with $\nu \in \{0,1\}$ and C_ν si defined as

$$C_\nu = \{n_1\boldsymbol{a}_1 + n_2\boldsymbol{a}_2 + \nu\boldsymbol{\delta}\,|\,n_1, n_2 \in \mathbb{Z}\}\,.$$

With this we can now calculate the matrix elements of the Hamiltonian

$$\big\langle n, \nu, \boldsymbol{k}\big|H\big|n', \nu', \boldsymbol{k}'\big\rangle = \sum_{\boldsymbol{k}\boldsymbol{k}', \boldsymbol{R}\boldsymbol{R}'} e^{i\boldsymbol{k}\cdot(\boldsymbol{R}+\nu\boldsymbol{\delta}) - i\boldsymbol{k}'\cdot(\boldsymbol{R}+\nu'\boldsymbol{\delta})}\big\langle n, \nu, \boldsymbol{R}\big|H\,\big|n', \nu', \boldsymbol{R}'\big\rangle\,. \tag{1.102}$$

Since the matrix elements inside the summation do not depend on k we have that the terms with $k \neq k'$ are equal to zero. So the equation above becomes

$$\langle n, \nu, \boldsymbol{k} | H | n', \nu', \boldsymbol{k}' \rangle = \langle n, \nu, \boldsymbol{k} | H | n', \nu', \boldsymbol{k} \rangle \delta_{\boldsymbol{k},\boldsymbol{k}'} \, .$$

This means that

$$\langle n, \nu, \boldsymbol{k} | H | n', \nu', \boldsymbol{k} \rangle = \sum_{\boldsymbol{k},\boldsymbol{R}\boldsymbol{R}'} e^{i\boldsymbol{k}\cdot(\boldsymbol{R}-\boldsymbol{R}'+\nu\boldsymbol{\delta}-\nu'\boldsymbol{\delta})} \langle n, \nu, \boldsymbol{R} | H | n', \nu', \boldsymbol{R}' \rangle \, ,$$

and, since it only depends on $\boldsymbol{R} - \boldsymbol{R}'$ we have that

$$\langle n, \nu, \boldsymbol{k} | H | n', \nu', \boldsymbol{k} \rangle = \sum_{\boldsymbol{k},\boldsymbol{R}} e^{i\boldsymbol{k}\cdot\boldsymbol{R}+i(\nu-\nu')\boldsymbol{k}\cdot\boldsymbol{\delta}} \langle n, \nu, \boldsymbol{R} | H | n', \nu', \boldsymbol{0} \rangle \, . \quad (1.103)$$

Now we need to calculate the matrix elements $\langle n, \nu, \boldsymbol{R} | H | n', \nu', \boldsymbol{0} \rangle$. Using equation 1.100 we get that if $\boldsymbol{R} = \boldsymbol{0}$

$$\langle n, \nu, \boldsymbol{0} | H | n', \nu', \boldsymbol{0} \rangle = E_n \langle n, \nu, \boldsymbol{0} | n', \nu', \boldsymbol{0} \rangle + \langle n, \nu, \boldsymbol{0} | V'(\boldsymbol{r}) | n', \nu', \boldsymbol{0} \rangle \, . \quad (1.104)$$

For $\nu = \nu'$ the first term ($E_n \langle n, \nu, \boldsymbol{0} | n', \nu, \boldsymbol{0} \rangle = \delta_{nn'}$) and the second term, which is called crystal field integral is usually neglected because in most cases they simply produce a rigid shift of the energy bands $E_n(\boldsymbol{k})$ without affecting their dispersion. [8]
For $\nu \neq \nu'$ the second term is much bigger than the first one, so

$$\langle n, \nu, \boldsymbol{0} | H | n', \nu', \boldsymbol{0} \rangle \approx E_n \delta_{nn'} \delta_{\nu\nu'} + \langle n, \nu, \boldsymbol{0} | V'(\boldsymbol{r}) | n', \nu', \boldsymbol{0} \rangle (1 - \delta_{\nu\nu'}) \, . \quad (1.105)$$

Since we consider the wavefunctions as strongly localized, the second term is much smaller than the first one, so we can ignore it.
Usually the matrix elements $\langle n, \nu, \boldsymbol{0} | V'(\boldsymbol{r}) | n', \nu', \boldsymbol{0} \rangle$ are conveniently expressed in terms of a a small number of independent parameters, and are evaluated either analytically, or numerically, or semi-empirically.

In the case of carbon atoms we only need to work with atomic orbitals of type s and p, this means that the independent matrix elements to evaluate are shown in table 1.1

These parameters can be pictorially shown in figure 1.14
The Hamiltonian matrix should be a 8×8 matrix. Nevertheless, from group theory we know that at a general point k the Bloch functions derived from s, p_x and p_y atomic functions never mix with the Bloch function p_z because of the symmetry operation of reflection through the xy plane. We can thus classify the energy states as even or odd with respect to this transformation; the former give rise to the so-called σ-bands and the latter to the so-called π-bands. Moreover, the problem is decomposed into two decoupled sub-problems and, instead of diagonalizing a single 8×8 matrix, we have to cope separately with a 2×2 matrix (π-bands) and a 6×6 matrix (σ-bands).

$\langle\ s\ ,\nu,\mathbf{0}\big\vert V'(\boldsymbol{r})\ \vert\ s\ ,\nu',\mathbf{0}\rangle = V(ss\sigma)$
$\langle\ s\ ,\nu,\mathbf{0}\big\vert V'(\boldsymbol{r})\ \vert p_x,\nu',\mathbf{0}\rangle = l_x V(sp\sigma)$
$\langle p_x,\nu,\mathbf{0}\big\vert V'(\boldsymbol{r})\ \vert p_x,\nu',\mathbf{0}\rangle = l_x^2 V(pp\sigma) + (1-l_x^2)V(pp\pi)$
$\langle p_x,\nu,\mathbf{0}\big\vert V'(\boldsymbol{r})\ \vert p_y,\nu',\mathbf{0}\rangle = l_x l_y\left[V(pp\sigma) - V(pp\pi)\right]$
$\langle p_x,\nu,\mathbf{0}\big\vert V'(\boldsymbol{r})\ \vert p_z,\nu',\mathbf{0}\rangle = l_x l_z\left[V(pp\sigma) - V(pp\pi)\right]$

Table 1.1: Here we have defined $\boldsymbol{\delta} = (l_x, l_y, l_z)|\delta|$

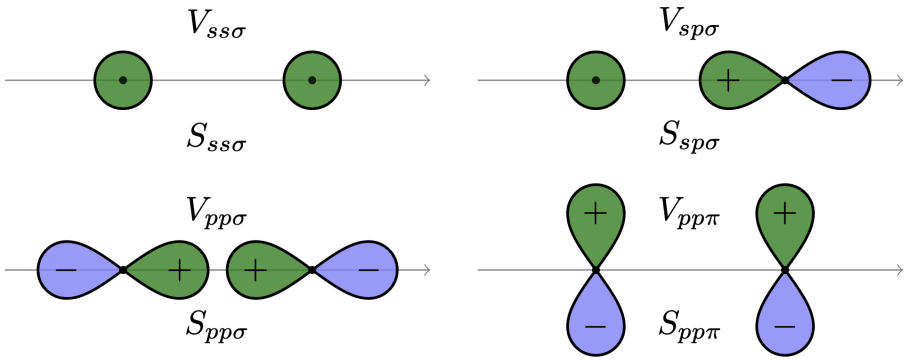

Figure 1.14: Each one of the potentials $V(ss\sigma), V(sp\sigma), V(pp\sigma), V(pp\pi)$ represent a different kind of bonding between the two orbitals. The first two indices represent the orbitals (s and p), the last one represent the bonding type (σ and π). Image taken from [17].

Fortunately the σ-bands are fully below the Fermi-level, so they do not have any contribution to the electron-transport phenomenon, so we only have to deal with the 2×2 matrix of the π-bands

$$\langle p_z,\nu,\mathbf{0}\big\vert H\ \vert p_z,\nu',\mathbf{0}\rangle = \begin{bmatrix} E_p & V(pp\pi) \\ V(pp\pi) & E_p \end{bmatrix}. \tag{1.106}$$

Now we can evaluate equation 1.103 considering just the nearest-neighbors

$$\langle p_z,0,\boldsymbol{k}\big\vert H\ \vert p_z,0,\boldsymbol{k}\rangle = \sum_{\boldsymbol{k},\boldsymbol{R}} e^{i\boldsymbol{k}\cdot\boldsymbol{R}}\langle p_z,0,\boldsymbol{R}\big\vert H\ \vert p_z,0,\mathbf{0}\rangle \approx E_p\,; \tag{1.107}$$

$$\begin{aligned}\langle p_z,0,\boldsymbol{k}\big\vert H\ \vert p_z,1,\boldsymbol{k}\rangle =& \sum_{\boldsymbol{k},\boldsymbol{R}} e^{i\boldsymbol{k}\cdot\boldsymbol{R}+i\boldsymbol{k}\cdot\boldsymbol{\delta}}\langle p_z,0,\boldsymbol{R}\big\vert H\ \vert p_z,1,\mathbf{0}\rangle \approx \\ \approx& \sum_i e^{i\boldsymbol{k}\cdot\boldsymbol{\delta}_i} V(pp\pi) \equiv \\ \equiv& V(pp\pi)F(\boldsymbol{k})\,.\end{aligned} \tag{1.108}$$

Where $F(\boldsymbol{k})$ is defined as the geometrical form factor, and it is equal to

$$F(\boldsymbol{k}) = \sum_{\boldsymbol{\delta}_i} e^{i\boldsymbol{k}\cdot\boldsymbol{\delta}_i} = 1 + 2\cos\frac{k_x\delta}{2}e^{-i\frac{\sqrt{3}}{2}k_y\delta}\,. \tag{1.109}$$

Therefore, the k-dependent Hamiltonian for the π-bands is

$$\langle p_z, \nu, \boldsymbol{k}|H\,|p_z, \nu', \boldsymbol{k}'\rangle = \delta_{kk'}\begin{bmatrix} E_p & V(pp\pi)F(\boldsymbol{k}) \\ V(pp\pi)F(\boldsymbol{k}) & E_p \end{bmatrix}. \tag{1.110}$$

However before diagonalizing the Hamiltonian we have to keep in mind that we do not start off with an orthonormal base of states

$$\langle p_z, \nu, \boldsymbol{k}|p_z, \nu', \boldsymbol{k}\rangle \equiv S_{\nu\nu'}(\boldsymbol{k}) = \begin{bmatrix} 1 & sF(\boldsymbol{k}) \\ sF(\boldsymbol{k}) & 1 \end{bmatrix}. \tag{1.111}$$

This means that the eigenvalue equation is

$$\det|H_{\nu\nu'}(\boldsymbol{k}) - E(\boldsymbol{k})S_{\nu\nu'}(\boldsymbol{k})| = 0\,. \tag{1.112}$$

The eigenvalues of the Hamiltonian gives us the dispersion relation 1.15

$$E(\boldsymbol{k}) = \frac{E_p \pm V(pp\pi)|F(\boldsymbol{k})|}{1 \mp s|F(\boldsymbol{k})|}\,. \tag{1.113}$$

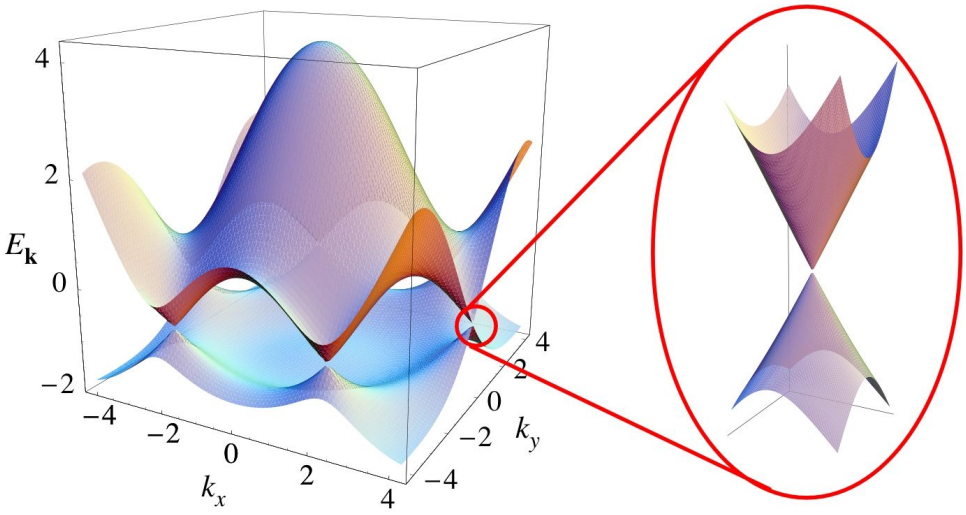

Figure 1.15: This is the dispersion relation for the single layer graphene, notice how near the vertices of the reciprocal lattice we get a cone-like dispersion relation typical of relativistic massless particles. Image taken from [14].

The Dirac cones

Near the degenerate points $\boldsymbol{K}_0$ and $\boldsymbol{K}_1$ (eq. 1.97), the geometrical form factor can be expanded in Taylor series to first order in the wavevector measured from the $\boldsymbol{K}_0$ and $\boldsymbol{K}_1$ points. The resulting expression of the form factors are

$$F_{\boldsymbol{K}_0}(\boldsymbol{k}) = -F^*_{\boldsymbol{K}_1}(\boldsymbol{k}) = -\frac{\sqrt{3}}{2}\delta(k_x - ik_y)\,. \tag{1.114}$$

This means that the matrix Hamiltonians near the degeneracies can be recast in the form

$$H_{\boldsymbol{K}_0}(\boldsymbol{k}) = -H^*_{\boldsymbol{K}_1}(\boldsymbol{k}) = \begin{bmatrix} 0 & v_F\hbar(k_x - ik_y) \\ v_F\hbar(k_x + ik_y) & 0 \end{bmatrix}; \quad v_f = \frac{\sqrt{3}}{2}\frac{\delta}{\hbar}V(pp\pi)\,. \tag{1.115}$$

The eigenvalues of both Hamiltonians are

$$E(k) = \pm v_F\hbar k \quad \text{with} \quad k = \sqrt{k_x^2 + k_y^2}\,. \tag{1.116}$$

This means that electrons near the Dirac cones behave pretty much like photons, except that they move at the Fermi speed v_F instead of the speed of light.
The eigenstates of this Hamiltonian are called **Dirac-fermions** and are equal To

$$|\pm, \boldsymbol{k}\rangle = \frac{1}{\sqrt{2}}\begin{bmatrix} e^{-i\lambda\theta} \\ \pm e^{i\lambda\theta} \end{bmatrix}; \quad \boldsymbol{k} = k\begin{bmatrix} \cos\theta \\ \sin\theta \end{bmatrix}\,, \tag{1.117}$$

where $\lambda = 1$ in K_0 and $\lambda = -1$ in K_1. Hence, the low-energy quasiparticles in graphene can be interpreted as massless Dirac fermion, and described by a spinor wave function in which the spin degree-of-freedom is substituted with a sublattice degree-of-freedom, that is defined as **pseudospin**. We can also go further on this, since an electron can be in a superposition between the two cones we can add an additional spin-like degree of freedom. The Hamiltonian 1.115 becomes

$$H(\boldsymbol{k}) = \hbar v_{\mathrm{F}}(\sigma_x\tau_z k_x + \sigma_y k_y)\,. \tag{1.118}$$

Here $\boldsymbol{\sigma}$ and $\boldsymbol{\tau}$ are Pauli matrices with $\sigma_z = \pm 1$ describing states on the $A(B)$ sublattice and $\tau_z = \pm 1$ describing states at the $\boldsymbol{K}_0(\boldsymbol{K}_1)$ points.

Why Dirac cones appear in the first place

Many of the properties of crystalline band structure can be infered by the symmetries of their spatial structure [18], in this subsection we are going to talk about some of the properties of that give rise the Dirac cones.

The Hamiltonian of graphene can be written as 2×2 Hamiltonian that depends from a parameter $\boldsymbol{k}$ though the Peierls substitution that we introduced in section 1.10

$$H(\boldsymbol{k}) = \boldsymbol{h}(\boldsymbol{k}) \cdot \boldsymbol{\sigma}\,, \tag{1.119}$$

where $\boldsymbol{h}(\boldsymbol{k}) = (h_x(\boldsymbol{k}), h_z(\boldsymbol{k}), h_z(\boldsymbol{k}))$ the parity operator $\mathcal{P}$ sends $\boldsymbol{k} \to -\boldsymbol{k}$ and exchanges the two sites so it acts as a σ_x operator, so we have that

$$H(\boldsymbol{k}) = \mathcal{P}^{-1} H(\boldsymbol{k}) \mathcal{P} = \sigma_x H(-\boldsymbol{k}) \sigma_x\,, \tag{1.120}$$

and since

$$\mathcal{P}^{-1} \boldsymbol{\sigma} \mathcal{P} = \sigma_x \boldsymbol{\sigma} \sigma_x = (\sigma_x, -\sigma_y, -\sigma_z)\,, \tag{1.121}$$

we have that

$$\begin{vmatrix} h_x(\boldsymbol{k}) \\ h_y(\boldsymbol{k}) \\ h_z(\boldsymbol{k}) \end{vmatrix} = \begin{vmatrix} h_x(-\boldsymbol{k}) \\ -h_y(-\boldsymbol{k}) \\ -h_z(-\boldsymbol{k}) \end{vmatrix}\,. \tag{1.122}$$

The time reversal operator $\mathcal{T}$ sends $\boldsymbol{k} \to -\boldsymbol{k}$ and it is antinunitary, so the system to have time reversal symmetry must obey

$$H(\boldsymbol{k}) = \mathcal{T}^{-1} H(\boldsymbol{k}) \mathcal{T} = H^*(-k)\,, \tag{1.123}$$

however doesn't exchange the particle sites, it only does the complex conjucation

$$\mathcal{T}^{-1} \boldsymbol{\sigma} \mathcal{T} = (\sigma_x, -\sigma_y, \sigma_z)\,, \tag{1.124}$$

so we have that

$$\begin{vmatrix} h_x(\boldsymbol{k}) \\ h_y(\boldsymbol{k}) \\ h_z(\boldsymbol{k}) \end{vmatrix} = \begin{vmatrix} h_x(-\boldsymbol{k}) \\ -h_y(-\boldsymbol{k}) \\ h_z(-\boldsymbol{k}) \end{vmatrix}\,. \tag{1.125}$$

Uniting the conditions from equation 1.122 and equation 1.125 we have that

$$h_z(\boldsymbol{k}) = 0\,. \tag{1.126}$$

The Dirac points occur because the two component $\boldsymbol{h}(\boldsymbol{k})$ can have point zeros in two dimensions. In graphene they occur at two points $\boldsymbol{K}_0$ and $\boldsymbol{K}_1 = -\boldsymbol{K}_0$ [4, 19].

1.14 Gapped graphene

If either the sublattice symmetry $\mathcal{P}$ or the time reversal symmetry $\mathcal{T}$ are broken the Hamiltonian near the $\boldsymbol{K}$ points becomes a massive Dirac Hamiltonian. This means that for materials that do not have the parity symmetry

$\mathcal{P}$ such as Boron Nitrite exhibit an open gap in the $\boldsymbol{K}$ points, alternatively one could layer graphene on top of another honeycomb lattice that doesn't have sublattice symmetry, therefore subjecting it with a periodic potential that breaks the symmetry and opens the gap by adding a mass term Δ in both the Dirac cones.
Finding a crystalline structure that breaks time reversal symmetry can be a little more cumbersome, these kind of structures had been theorized by Haldane in 1987 [20], then Kane and Mele [21] proved that this happens in graphene itself if we take into account spin-orbit coupling,

Mathematically speaking, the tight binding Hamiltonian has two different energies for the two different atoms in the sub-lattice. With respect to equation 1.115 it becomes

$$H(\boldsymbol{k}) = \begin{bmatrix} \Delta & v_F\hbar(\tau_z k_x - ik_y) \\ v_F\hbar(\tau_z k_x + ik_y) & -\Delta \end{bmatrix}, \tag{1.127}$$

where Δ is half the difference of the diagonal energy on the two sublattices, and the energy zero has been shifted at the center of the energy gap. The dispersion relation now becomes

$$E(\boldsymbol{k}) = \pm\sqrt{\Delta^2 + (v_F\hbar k)^2}\,. \tag{1.128}$$

It is seen that the above dispersion curves are formally the same produced by the Dirac equations, with the light velocity c replaced by the Fermi velocity v_F and the rest mass $m_0 = \Delta/v_F^2$.

1.15 Bilayer graphene

In the tight-binding description of bilayer graphene, we take into account $2p_z$ orbitals on the four atomic sites in the unit cell, labelled as $j = A_1, B_1, A_2, B_2$. Then, the transfer integral matrix of bilayer graphene is a 4×4 matrix given by [22]

$$H(\boldsymbol{k}) = \begin{bmatrix} E_{A_1} & -\gamma_0 F(\boldsymbol{k}) & \gamma_4 F(\boldsymbol{k}) & -\gamma_3 F(\boldsymbol{k}) \\ -\gamma_0 F(\boldsymbol{k}) & E_{B_1} & -\gamma_1 & \gamma_4 F(\boldsymbol{k}) \\ \gamma_4 F(\boldsymbol{k}) & \gamma_1 & E_{A_2} & -\gamma_0 F(\boldsymbol{k}) \\ -\gamma_3 F(\boldsymbol{k}) & \gamma_4 F(\boldsymbol{k}) & -\gamma_0 F(\boldsymbol{k}) & E_{B_2} \end{bmatrix}, \tag{1.129}$$

where the tight-binding parameters are defined as

$$\begin{aligned} \gamma_0 &= -\langle A_1|H|B_1\rangle = -\langle A_2|H|B_2\rangle\ ; \\ \gamma_1 &= \langle A_2|H|B_1\rangle\ ; \\ \gamma_3 &= -\langle A_1|H|B_2\rangle\ ; \\ \gamma_4 &= \langle A_1|H|A_2\rangle = \langle B_1|H|B_2\rangle\ . \end{aligned} \tag{1.130}$$

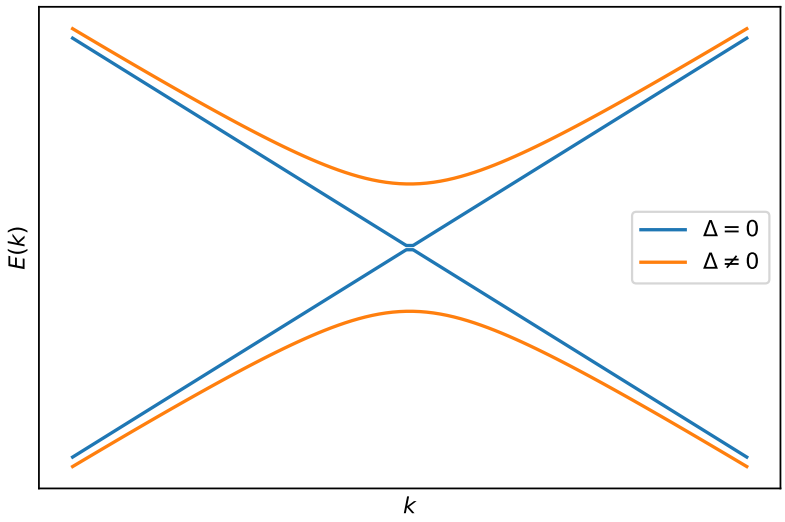

Figure 1.16: Difference between the gapless and the gapped Dirac dispersion relation. In blue is showed the gapless Dirac Hamiltonian, while in orange the gapped Dirac Hamiltonian.

The upper-right and lower-left square 2×2 blocks of H describe inter-layer coupling. Parameter γ_1 describes coupling between pairs of orbitals on sites that are directly above each other B_1 and A_2 (also called dimer sites): since this is a vertical coupling, the corresponding terms in H do not contain $F(\boldsymbol{k})$ which describes in-plane hopping. The other γ factors do have an in plane component, which causes the $F(\boldsymbol{k})$ term to show up.
The overlap matrix S form equation 1.111 becomes in the bilayer case

$$S = \begin{bmatrix} 1 & s_0 F(\boldsymbol{k}) & 0 & 0 \\ s_0 F(\boldsymbol{k}) & 1 & s_1 & 0 \\ 0 & s_1 & 1 & s_0 F(\boldsymbol{k}) \\ 0 & 0 & s_0 F(\boldsymbol{k}) & 1 \end{bmatrix}. \tag{1.131}$$

Here we only include two parameters: $s_0 = \langle A_1 | B_1 \rangle = \langle A_2 | B_2 \rangle$ describing non-orthogonality of intra-layer nearest-neighbours and $s_1 = \langle A_2 | B_1 \rangle$ describing non-orthogonality of orbitals on dimer sites A1 and B2. In principle, it is possible to introduce additional parameters analogous to γ_3, γ_4, etc., but generally they will be small and irrelevant, infact in the bilayer case it is common practice to neglect completely the overlap matrix if we are dealing with. The resulting energy bands are plotted in figure 1.18

Parameter	Value [eV]
γ_0	3.16 ± 0.03
γ_1	0.381 ± 0.003
γ_3	0.38 ± 0.06
γ_4	0.14 ± 0.03

Table 1.2: Values in eV of γ_i [23]

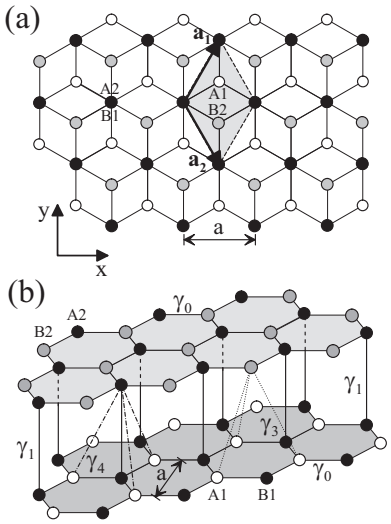

Figure 1.17: Schematic representation of the bilayer graphene structure. Image taken from [22]

To describe the properties of the electrons near the K we just have to approximate $F(\boldsymbol{k})$ just like we did in equation 1.114. This results in a Hamiltonian that is the generalization of the one we had in equation 1.127

$$H_{\boldsymbol{K}_0} = \begin{bmatrix} E_{A_1} & v_F\pi^\dagger & -v_4\pi^\dagger & v_3\pi \\ v_F\pi & E_{B_1} & \gamma_1 & -v_4\pi^\dagger \\ -v_4\pi & \gamma_1 & E_{A_2} & v_F\pi^\dagger \\ v_3\pi^\dagger & -v_4\pi & v_F\pi & E_{B_2} \end{bmatrix}. \tag{1.132}$$

Where $\pi = \hbar(\tau_z k_x + ik_y)$, $\pi^\dagger = \hbar(\tau_z k_x - ik_y)$, and the velocities $v_{3,4} = a\gamma_{3,4}/\hbar$ are effective fermi velocities that come from the coupling γ_3 and γ_4

Effective two-band Hamiltonian at low energy

Most of the properties we are interested in graphene are about the electronic properties near the Dirac points.
First we consider the energy eigenvalue equation considering separate blocks in the Hamiltonina corresponding to low-energy $\boldsymbol{\theta} = (\psi_{A1}, \psi_{B2})$ and dimer $\boldsymbol{\chi} = (\psi_{A_2}, \psi_{B_1})$

$$\begin{bmatrix} h_\theta & u \\ u^\dagger & h_\chi \end{bmatrix} \begin{bmatrix} \boldsymbol{\theta} \\ \boldsymbol{\chi} \end{bmatrix} = E \begin{bmatrix} \boldsymbol{\theta} \\ \boldsymbol{\chi} \end{bmatrix}. \tag{1.133}$$

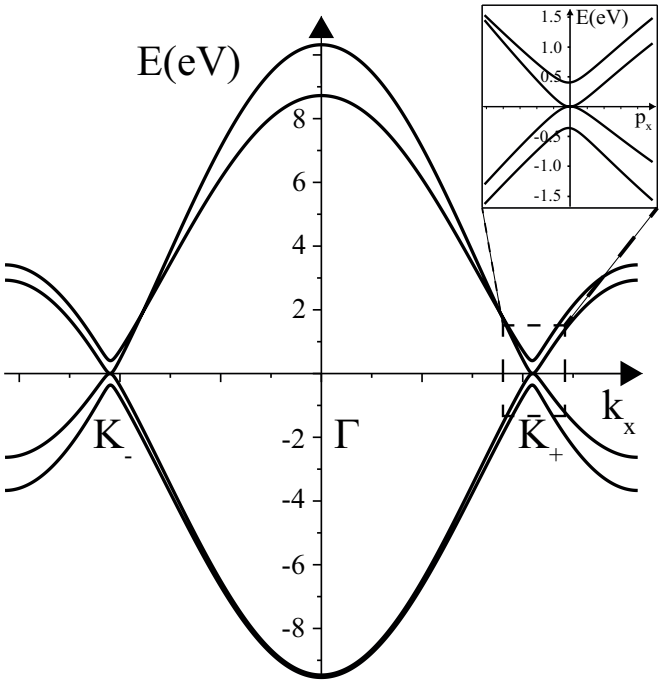

Figure 1.18: Here are plotted the p_z orbitals along the k_x axis in the reciprocal space intersecting the corners K_0 and K_1 and the center Γ of the Brillouin zone. Notice how now we have four bands, this because we have four atoms in the fundamental cell, two for each layer. Image taken from [22]

The second row of 1.133 allows the dimer components to be expressed in terms of the low energy ones.

$$\boldsymbol{\chi} = (E - h_\chi)^{-1} u^\dagger \boldsymbol{\theta}\,, \tag{1.134}$$

substituting this into equation 1.133 gives us an effective eigenvalue equation depending on low the low energy components

$$[h_\theta + u(E - h_\chi)^{-1} u^\dagger]\boldsymbol{\theta} = E\boldsymbol{\theta}\,. \tag{1.135}$$

Note that this is not anymore a simple eigenvector problem because the eigenvalue E is a parameter of the matrix we wish to diagonalize, making an approximation it is possible to write the equation above, up to linear terms of the energy like so:

$$[h_\theta + u h_\chi^{-1} u^\dagger]\boldsymbol{\theta} \approx ES\boldsymbol{\theta}\,, \tag{1.136}$$

where $S = 1 + u h_\chi^{-2} u^\dagger$ and the second equation is accurate up to a linear term in E. We now define $\boldsymbol{\Phi} = S^{1/2}\boldsymbol{\theta}$ and substitute it in the equation above

$$S^{-1/2}[h_\theta + u h_\chi^{-1} u^\dagger] S^{-1/2}\boldsymbol{\Phi} = E\boldsymbol{\Phi}\,. \tag{1.137}$$

With this we can define the effective 2×2 Hamiltonian, find its eigenvectors $\boldsymbol{\phi}$, and then mutliply it by $S^{-1/2}$ to get $\boldsymbol{\theta} = S^{-1/2}\boldsymbol{\Phi}$, and then use equation 1.134 to get the $\boldsymbol{\chi}$ component. Remember however that since we have a 2×2 matrix we are going to get two eigenvalues instead of 4 of the original Hamiltonian if equation 1.133. These two energies are going to be the ones that touch the Fermi level (figure 1.18), and $k_bT \ll \Delta E$ higher energy states can be ignored (here ΔE is the gap of the high energy states)
The effective Hamiltonian is [24, 25]

$$\begin{aligned} H =& H_2 + h_w + h_4 + h_\Delta + h_U + h_{AB}\,, \\ H_2 =& -\frac{1}{2m}\begin{bmatrix} 0 & (\pi^\dagger)^2 \\ \pi^2 & 0 \end{bmatrix}\,, \end{aligned} \tag{1.138}$$

where H_2 can is the dominant term and describes massive electrons, and it may be written like so $H_2 = -(1/2m)[\sigma_x(p_x^2 - p_y^2) + 2\tau_z\sigma_y p_x p_y]$. And it dominates at low energies, the other terms may be considered as perturbations of it. the term h_w represents a triangular distortion of the Fermi circle around the $\boldsymbol{K}$. the terms h_U and h_{AB} produce a band gap while h_4 and h_Δ introduce electron-hole asymmetry. The solutions of H_0 are massive chiral electrons with parabolic dispersion $E = \pm p^2/2m$, $m = \gamma_1/2v^2$ and the corresponding wavefunctions are

$$|\pm, \boldsymbol{k}\rangle = \frac{1}{\sqrt{2}}\begin{bmatrix} 1 \\ \mp e^{2i\tau_z\phi} \end{bmatrix} e^{i\boldsymbol{k}\cdot\boldsymbol{r}}\,, \tag{1.139}$$

where the wavefunction components describe the electronic amplitudes pf the $A1$ and $B2$ sites.

1.16 Graphene synthesis

Recently, there are several methods used to synthesize graphene. After the first exfoliation of graphene [13] several other techniques were developed to produce graphene sheets each with its own advantages and disadvantages [26]:

Mechanical exfoliation

Mechanical exfoliation is also known as Scotch tape or peel-off method. It was the first method to be used by Novoselov and Geim for the production of graphene with the help of an adhesive tape to force the graphene layers apart, with this method flakes of on the order of μm$\sim$cm can be obtained [13, 27, 28]. One the peeling process in completed, usually acetone is used to detach the flakes from the tape. The main drawback of this process is that

is slow and imprecise, hence the process is used to study the properties of graphene rather than using it commercially.

Electrochemical exfoliation

This method involves the use of various forms of graphite such as graphite foils, plates, rods and graphite powders as electrodes in an aqueous or non-aqueous electrolyte and electric current to bring about the expansion of electrodes [29–31].
The cathode is made of graphite, and a persistent voltage of 5V are applied, after a few minutes the anode is covered by a thin layers of a black material, by cleaning the anode a graphene powder made of flakes of around 500 $\sim$ 700nm can be obtained.

Pyrolysis

The meaning of the word is *separating with fire*.One of the common techniques of graphene synthesis is the thermal decomposition of silicon carbide (SiC). At high temperature, Si is desorbed leaving behind C atom which forms few graphene layers. The advantages of this method is the production of high purity graphene mono-layer up to cm size over the entire SiC coated surface, however it has proven challenging doing so at large scales [32–35].

Chemical vapor deposition

Chemical vapor deposition (CVD) is a bottom-up synthesis technique used for production of high-quality graphene [36], this method involves combining a gas molecule with a surface substrate inside a reaction chamber. Different substrates are used in CVD for graphene film growth, they include Nickel (Ni) [37] Copper (Cu) [38], Iron (Fe) [39], and Stainless steel [40]. Methane (CH4) and acetylene (C2H2) are normally used as a carbon source. At high temperatures the hydrogen and carbon detach forming hydrogen gas and pure carbon, the carbon when it comes in contact with the substrate it attaches itself creating graphene. With this technique it is possible to create graphene flakes of the size of several cm, however scaling it up has proven challenging.

Chapter 2

Anomalous Hall effect

The anomalous Hall effect refers to the appearance of a large spontaneous Hall current in ferromagnet in response to an electric field alone [41], and it was first discovered by Hall in 1881 [42]. Despite its century long history and importance, the microscopic characterization of the anomalous Hall effect has been a controversial subject. In the past three main mechanisms have been identified:

- Berry curvature induced Hall effect [43]
- Skew scattering [44]
- Side-jump scattering [45]

The Berry curvature induced Hall effect can be regarded as an **intrinsic contribution** to the conductivity, the other two are regarded as **extrinsic contributions**, this is because they are related to some kind of asymmetry to the scattering with impurities. More precisely the skew scattering deals with the asymmetry that arises with spin-orbit coupling between the electrons and the impurity, while the side jump is a sudden shift in of the electron coordinates during scattering [45]. The effects are illustrated in figure 2.1. The total Hall conductivity is the sum of all three contributions

$$\sigma_H = \sigma_H^{\text{in}} + \sigma_H^{\text{sk}} + \sigma_H^{\text{sj}}\,, \tag{2.1}$$

where σ_H^{in} is the intrinsic contribution given from equation 1.74, σ_H^{sk} is the skew scattering term, which is proportional to the relaxation time τ, and σ_H^{sj} is the side-jump term that is independent of τ.

An important question is to identify the dominant contribution to the anomalous Hall effect (AHE). The way to compare theoretically the magnitude of the contribution rely mainly on semiclassical conduction theory [47], and they express the dominance of the Berry induced Hall effect. In addition, a number of experimental results also gave favorable evidence for the dominance of the intrinsic contribution [48]. Because of this we are going to

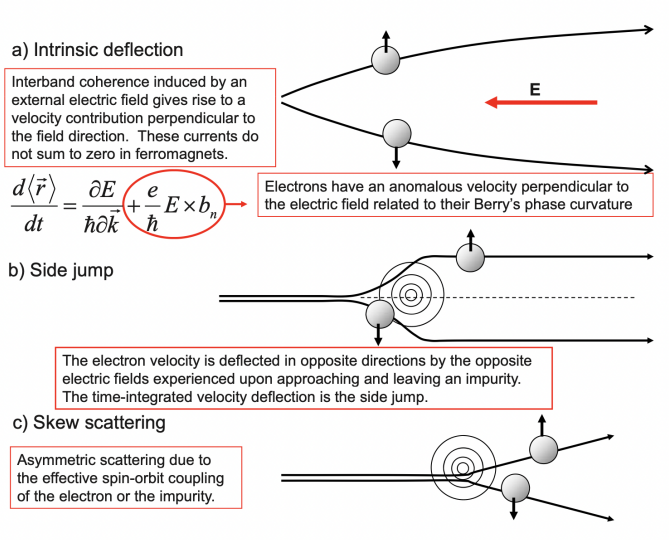

Figure 2.1: All three contributions to the anomalous Hell effect, as you can see the intrinsic contribution does not need an impurity to scatter from. Image taken from [46]

ignore σ_H^{sk} and σ_H^{sj}.
To get used to the math used thought the whole thesis we'll calculate all the anomalous Hall effects exclusively in gapped graphene, however it can be done in several other materials with different hamiltonians.

2.1 Berry curvature in gapped graphene

The Hamiltonian for the gapped graphene near the point K_1 and K_2 is (eq 1.127)

$$\begin{aligned} H_{\boldsymbol{K}_1} &= \begin{bmatrix} \Delta & \hbar v_F(k_x + ik_y) \\ \hbar v_f(k_x - ik_y) & -\Delta \end{bmatrix}; \\ H_{\boldsymbol{K}_2} &= \begin{bmatrix} \Delta & \hbar v_F(-k_x + ik_y) \\ \hbar v_f(-k_x - ik_y) & -\Delta \end{bmatrix}. \end{aligned} \tag{2.2}$$

The last equation can be written in a more concise way following the notation used in 1.118

$$H(\boldsymbol{k}) = \hbar v_{\text{F}}(\sigma_x \tau_z k_x + \sigma_y k_y) + \Delta\sigma_z\,, \tag{2.3}$$

where Δ is the energy gap and v_F is the Fermi velocity and $\tau_z = \pm 1$ represents the valleys $\boldsymbol{K}_1, \boldsymbol{K}_2$. For ease of computation we define $\boldsymbol{q} = \hbar v_F \boldsymbol{k}$

$$H(\boldsymbol{k}) = \sigma_x \tau_z q_x + \sigma_y q_y + \Delta\sigma_z\,. \tag{2.4}$$

Here the energy vector $\boldsymbol{E}$ is defined as $\boldsymbol{E} = (\tau_z q_x, q_y, \Delta)$. The nice things about it is that $E = |\boldsymbol{E}| = \sqrt{q_x^2 + q_y^2 + \Delta^2}$ is the positive eigenvalue of the Hamiltonian (the negative eigenvalue is just $-E$).
To calculate the Berry curvature we are first going to calculate the Berry connection 1.31, and to calultate the Berry connection we need the eigenvectors which are well known for the Hamiltonian of the form $\boldsymbol{\sigma} \cdot \boldsymbol{E}$.

$$|+;\theta,\phi\rangle = \begin{bmatrix} \cos\frac{\theta}{2} \\ e^{i\tau_z\phi}\sin\frac{\theta}{2} \end{bmatrix}, \quad |-;\theta,\phi\rangle = \begin{bmatrix} -e^{-i\tau_z\phi}\sin\frac{\theta}{2} \\ \cos\frac{\theta}{2} \end{bmatrix}, \tag{2.5}$$

where θ and ϕ are the coordinates of $\boldsymbol{E}$ in the polar representation

$$\begin{bmatrix} \tau_z q_x \\ q_y \\ \Delta \end{bmatrix} = E \begin{bmatrix} \tau_z \sin\theta\cos\phi \\ \sin\theta\sin\phi \\ \cos\theta \end{bmatrix}. \tag{2.6}$$

Now we can calculate the Berry connection (equation 1.32)

$$\begin{aligned} A_\theta^\pm =& i\,\langle \pm;\theta,\phi|\partial_\theta|\pm;\theta,\phi\rangle \;; = 0 \\ A_\phi^+ =& i\,\langle +;\theta,\phi|\partial_\phi|+;\theta,\phi\rangle = -A_\phi^- = \tau_z \sin^2\frac{\theta}{2}\,. \end{aligned} \tag{2.7}$$

This means that the Berry curvature is

$$\Omega_{\theta\phi}^+ = -\Omega_{\theta\phi}^- = \partial_\theta A_\phi^+ = \tau_z \frac{\sin\theta}{2}\,. \tag{2.8}$$

From now on we are going to work with Ω^+ and we are going to drop the $+$ sign to make the notation lighter.
We want to express Ω in terms of $\boldsymbol{q}$, however it's more convenient to write it in terms fo $\cos\theta$ and ϕ, so we do a small coordinate transformation

$$\Omega_{\theta\phi} = \frac{\partial\cos\theta}{\partial\theta}\Omega_{\cos(\theta)\phi} \to \Omega_{\cos(\theta)\phi} = \frac{\tau_z}{2}\,. \tag{2.9}$$

Now we can easily make the transformation to express Ω in terms of $\boldsymbol{q}$. The Berry curvature transforms like any other tensor under coordinate transformation, so

$$\Omega_{q_x q_y} = \frac{\partial\cos\theta}{\partial q_x}\frac{\partial\phi}{\partial q_y}\Omega_{\cos(\theta)\phi} + \frac{\partial\phi}{\partial q_x}\frac{\partial\cos\theta}{\partial q_y}\Omega_{\phi\cos(\theta)}\,. \tag{2.10}$$

That can be rewritten as

$$\Omega_{q_x q_y} = \frac{\tau_z}{2}\det\left[\frac{\partial(cos\theta,\phi)}{\partial(q_x,q_y)}\right] = \frac{\tau_z}{2}\frac{\Delta}{E^3}\,. \tag{2.11}$$

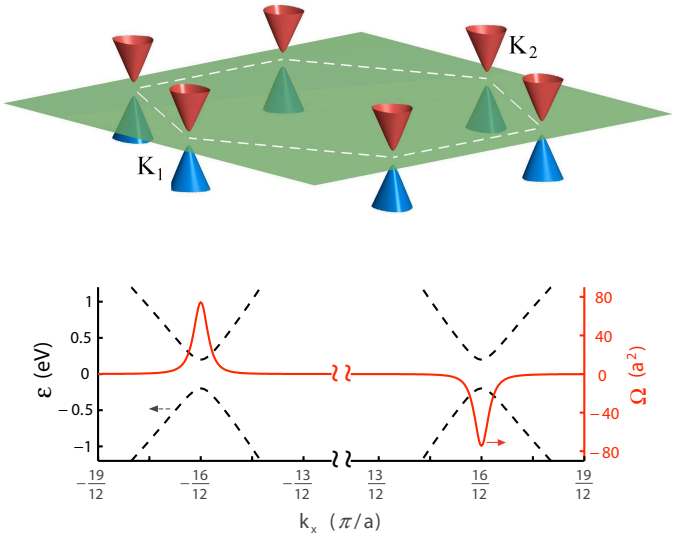

Figure 2.2: In the top panel are displayed the Energy bands in 2D. In the bottom panel with the dotted line are displayed a section of the energy bands, and with the continuous red line the Berry curvature. Image taken from [49]

And finally we can express it in terms of $\boldsymbol{k}$

$$\Omega_{k_x k_y} = (\hbar v_{\mathrm{F}})^2 \Omega_{q_x q_y} = \frac{\tau_z}{2} \frac{(\hbar v_{\mathrm{F}})^2 \Delta}{E^3} \,. \tag{2.12}$$

Notice how from figure 2.2 most of the berry curvature lies near the cones. The nice thing about it is that to calculate the total curvature in any given band, we can calculate the Berry in the two cones, and then sum the results. This is because we know that the total Berry curvature over the band has to be quantized.

Now let's calculate the Chern number in any given cone from equation 2.11.

$$\begin{aligned} C = & \int \Omega_{q_x q_y} dq_x dq_y = \\ = & \frac{\tau_z \Delta}{2} \int \frac{dq_x dq_y}{(q^2 + \Delta^2)^{3/2}} = \\ = & \frac{\tau_z \Delta}{2} \int \frac{2\pi q dq}{(q^2 + \Delta^2)^{3/2}} = \\ = & \pi \tau_z \Delta \frac{1}{|\Delta|} \\ = & \pi \tau_z \mathrm{sign}(\Delta) \,. \end{aligned} \tag{2.13}$$

This means that the two cones have opposite total Berry curvature, so the entire Brillouin zone has zero total Berry curvature. In the next section we

are going to see how it is possible to give rise to a honeycomb system with a non zero total Berry curvature.

2.2 The Haldane model

The Haldane model is a toy model of a spinless particle in a honeycomb lattice purposely made to exhibits a nonzero quantization of the Hall conductance a in the absence of an external magnetic field.
The idea is to start with the classic nearest neighbor hopping with hopping parameter t_1, and then to break time reversal symmetry, Haldane introduced the next-nearest neighbour hopping parameter that is a imaginary number $t_2 e^{i\phi}$ (figure 2.3). The full Hamiltonian becomes

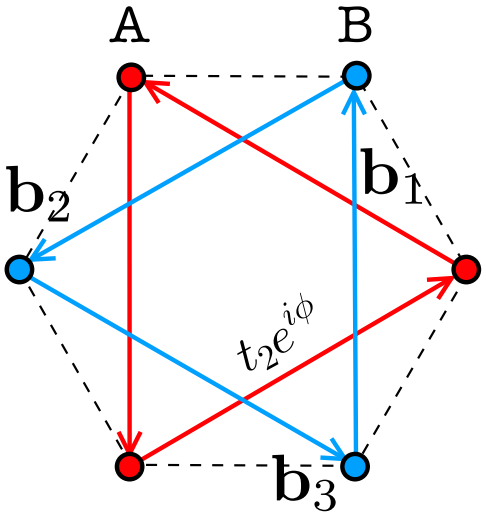

Figure 2.3: Honeycomb lattice showing nearest neighbor hopping with dashed line and next-nearest neighbor with the colored arrows, the red ones link only the atoms in the A sites, while the blue one link the atoms in the B sites. The transition amplitudes for the next-nearest are complex. Image adapted from [1].

$$H(\boldsymbol{k}) = H_0(\boldsymbol{k}) + \Delta\sigma_z - 2t_2\sigma_z\tau_z \sin\phi \sum_i \sin(\boldsymbol{k}\cdot\boldsymbol{b}_i)\,. \tag{2.14}$$

Where Δ is a mass term and $\boldsymbol{b}_i$ are the vectors that unite the atoms in the same sublattice site (figure 2.3). Near the Dirac cones it assumes this form:

$$H(\boldsymbol{k}) = \hbar v_{\mathrm{F}}(\sigma_x\tau_z k_x + \sigma_y k_y) + (\Delta - \tau_z\Delta_T \sin\phi)\sigma_z\,, \tag{2.15}$$

Where

$$\Delta_T = 2t_2 \sum_i \sin(\boldsymbol{K}\cdot\boldsymbol{b}_i)\,. \tag{2.16}$$

Notice ho the σ_z term now has a τ_z term in it. Effectively this is the same as taking a massive Dirac Hamiltonian and then sending $\Delta \to \Delta + \tau_z \Delta_t \sin\phi$. This means that we can use equation 2.13 to calculate the Chern number.

$$C = \pi \tau_z \text{sign}(\Delta - \tau_z \Delta_T \sin\phi)\,. \tag{2.17}$$

Notice how in this case, if $\Delta < |\Delta_T \sin\phi|$ the Chern number is $C = \pi$ and since it doesn't depend on the valley index both valleys have the same Chern number, and the total Berry curvature of the band is 2π, making the material topological.
If $\Delta = |\Delta_T \sin\phi|$ then we have that one of the two cones is closed, while if $\Delta > |\Delta_T \sin\phi|$ then both cones are open and the Chern number of the full band is 0, so the material is non-topological.
To go to the topological state to the non-topological one the gap has to close in one of the two valleys (figure 2.5).

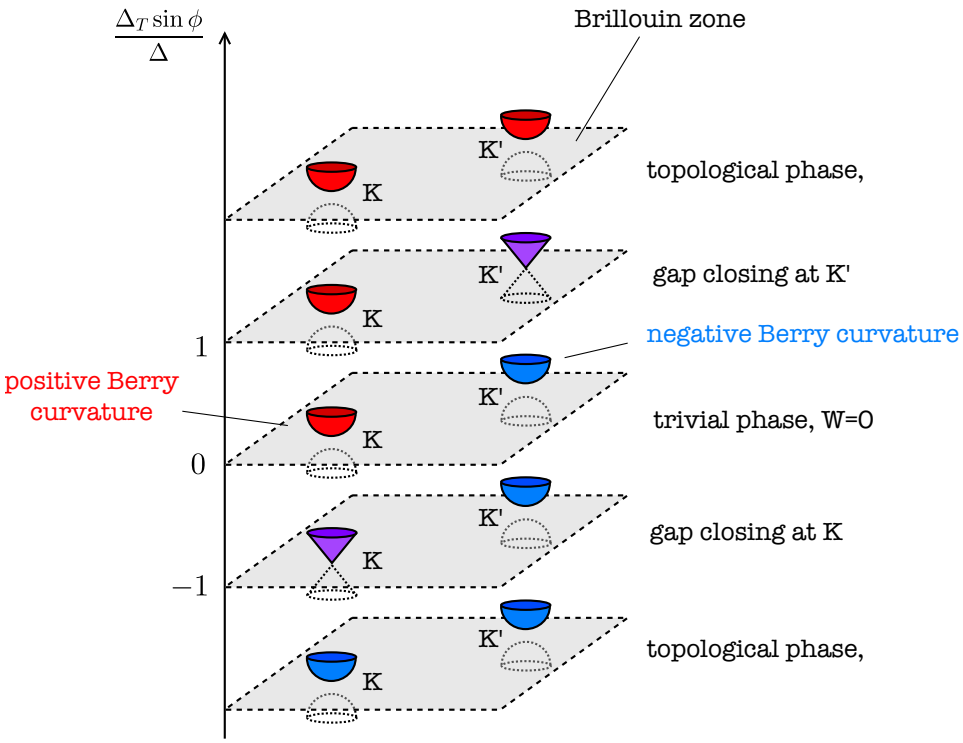

Figure 2.4: Phase diagram showing the topological phases ($\Delta < |\Delta_T \sin\phi|$), the trivial ones ($\Delta > |\Delta_T \sin\phi|$) and the phase change happens in the points where $\Delta = |\Delta_T \sin\phi|$. Image adapted from [1].

Although this model seems unphisical it will be of crucial importance when explaining the Spin Hall effect.

2.3 Spin Hall effect

The most famous example of anomalous Hall effect is the spin Hall effect (SHE). It is a phenomenon arising due to spin-orbit coupling in which change current passing thought a sample leads to spin transport in the transverse direction [50]. This phenomenon has been attracting continuous interest, and it is one of the protagonists of the field of spintronics [51].

Due to relativistic corrections, an electron moving with velocity $\boldsymbol{v}$ in an electric field $\boldsymbol{E}$ will experience a magnetic field equal to [52]

$$\boldsymbol{B} = -\frac{1}{c}(\boldsymbol{v} \times \boldsymbol{E})\,. \tag{2.18}$$

This means that the spin-orbit coupling term of the Hamiltonian is

$$H_{\mathrm{SO}} = -\frac{g\mu_B}{2}\boldsymbol{B}\cdot\boldsymbol{s} = \alpha_R(\boldsymbol{k}\times\boldsymbol{E})\cdot\boldsymbol{s}\,, \tag{2.19}$$

where $-g\mu_B/2$ is the electron magnetic moment, and $\alpha_R = g\mu_B/2\hbar mc$. We can assume that the electric field is equal to $\boldsymbol{E} = E_z\hat{\boldsymbol{z}}$, this is achieved either by a perpendicular electric field or by interaction with a substrate. With this we get the Rashba spin-orbit interaction also called as the external spin-orbit interaction[53]

$$H_{\mathrm{SO}}^{\mathrm{ext}} = \alpha_R E_z(\boldsymbol{s}\times\boldsymbol{k})\cdot\hat{\boldsymbol{z}}\,. \tag{2.20}$$

It can be show that this is equal to [21]

$$H_{\mathrm{SO}}^{\mathrm{ext}} = \lambda_R(\sigma_x\tau_z s_y - \sigma_y s_x)\,, \tag{2.21}$$

where in the last equation the same notation from equation 1.118. Another contribution due to the spin-orbit interaction comes from the interaction with the honeycomb periodic potential. If we plug $\boldsymbol{E} = \nabla V$ into equation 2.19 we get

$$H_{\mathrm{SO}}^{\mathrm{int}} = \alpha_R(\boldsymbol{k}\times\nabla V)\cdot\boldsymbol{s}\,. \tag{2.22}$$

Kane and Mele [21] showed that this is equivalent to

$$H_{\mathrm{SO}}^{\mathrm{int}} = \Delta_{\mathrm{SO}}\,\sigma_z\tau_z s_z\,. \tag{2.23}$$

Combining equations 1.118, 2.21 and 2.23 we get that

$$\begin{aligned} H(\boldsymbol{k}) =& H_0 + H_{\mathrm{SO}}^{\mathrm{int}} + H_{\mathrm{SO}}^{\mathrm{ext}} = \\ =& \hbar v_{\mathrm{F}}(\sigma_x\tau_z k_x + \sigma_y k_y) + \Delta_{\mathrm{SO}}\,\sigma_z\tau_z s_z + \lambda_R(\sigma_x\tau_z s_y - \sigma_y s_x)\,. \end{aligned} \tag{2.24}$$

For now we are going to ignore the external spin-orbit contribution, so we work with the Hamiltonian

$$H(\boldsymbol{k}) = \hbar v_{\mathrm{F}}(\sigma_x\tau_z k_x + \sigma_y k_y) + \Delta_{\mathrm{SO}}\,\sigma_z\tau_z s_z\,. \tag{2.25}$$

The gap generated by $\sigma_z\tau_z s_z$ is different from the gap that would be generated by a staggered sublattice potential σ_z or $\sigma_z s_z$.The gap generated by $\sigma_z\tau_z s_z$ produces an opposite sign mass on each of the $\boldsymbol{K}$ points.
Taken separately the Hamiltonians for the $s_z = \pm 1$ spins violate time reversal and are equivalent to Haldane's model for spinless electrons.
The Chern number for each spin has opposite sign and it leads to quantized Hall conductance of $\sigma_{xy} = \pm e^2/\hbar$ computed by the Kubo formula (equation 1.64).
Since the Hall conductivity has different sign for different spin, an electric field will induce opposite transversal currents for opposite spin. This effect has been observed in several experiments [54–57] using optical techniques

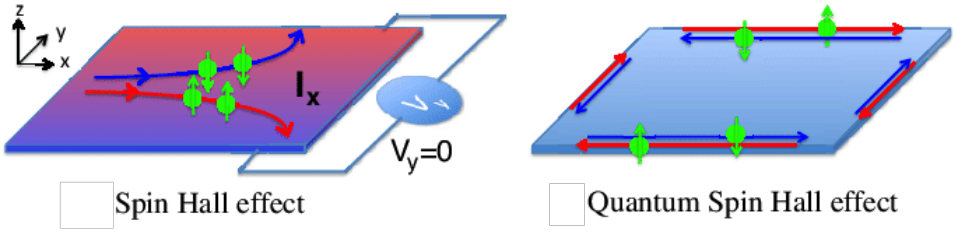

Figure 2.5: In nonmagnetic conductor, equivalent currents in both spin channels with opposite "anomalous velocity" leads to balanced electron concentration at both sides while net spin current in transversal direction. This leads to opposite moving spin edge states. Image taken from [58].

2.4 Valley-Hall effect

Up until now all of the various Hall effects we studied relied on a non-zero Chern number over the entire band. To do so, time symmetry breaking was needed.
The valley Hall effect is a particular kind of Hall effect that doesn't rely of time reversal breaking, however as explained in section 1.12 this means that to have a non zero Berry curvature, space inversion symmetry has to be broken. As explained in section 1.14 the inversion symmetry breaking can be achieved by resting the graphene sheet on top of a another honeycomb lattice that does not have sublattice symmetry like Molybdenum disulfide (MoS_2).
The problem with this approach is that no matter how strong the sublattice potential is, the Chern number of the valence and conduction band will always be zero.
However, if we treat the two valleys a two distinct quantum degrees of freedom, we have from equation 2.13 that for each of the valley equal and opposite non-zero Chern number.

$$C = \pi\tau_z \,. \tag{2.26}$$

This will lead to equal and opposite integer Hall conductivities in different Valleys. Now let's do more accurate calculations.

Calculation of the Hall conductivity as a function of the Fermi level

In this section we are going to calculate the anomalous Hall conductivity for each valley as we change the chemical potential μ (or equivalently the Fermi level E_{F}). We can start by using the generalized TKNN formula 1.79, so the Hall conductivity σ_{xy} is

$$\sigma_{xy}(\mu) = \tau_z \frac{e^2}{\hbar} \int_{\mathbb{R}^2} f[E^+(k)]\Omega^+_{k_x k_y} + f[E^-(k)]\Omega^-_{k_x k_y} \frac{d^2\boldsymbol{k}}{2\pi} \,, \tag{2.27}$$

where $f(E) = \left[e^{\beta(E-\mu)} + 1\right]^{-1}$ is the Fermi-Dirac distribution, it is applied once for the states with positive energy and once for the states with negative energy, and the $\pm$ sign represent the conduction band and the valence band quantum numbers (± 1).
We are going to analyze the system at low temperatures ($k_\beta T \ll 1$), so our Fermi-Dirac distribution can be considered like a step-function, for simplicity we are going to assume $\Delta > 0$, if that is not true the resulting Hall conductivity will be reversed.
First let's integrate the conductivity for the conduction band.

$$\sigma^+_{xy}(\mu) = \frac{1}{(2\pi)^2}\frac{e^2}{\hbar}\int_{\mathbb{R}^2} f[E^+(k)]\Omega^+_{k_x k_y} dk_x dk_y = \frac{1}{(2\pi)^2}\frac{e^2}{\hbar}\int_{\mathbb{R}^2} f[E^+(q)]\Omega^+_{q_x q_y} dq_x dq_y \approx$$

$$= \frac{1}{(2\pi)^2}\frac{e^2}{\hbar}\int_{\mathbb{R}^2} f[E^+(q)]\frac{\tau_z}{2}\frac{\Delta}{E^3} dq_x dq_y \approx \frac{\Delta\tau_z}{2(2\pi)^2}\frac{e^2}{\hbar}\int_0^{2\pi}\int_0^{q_{\mathrm{F}}} \frac{q dq d\theta}{E^3} =$$

$$= \frac{\tau_z\Delta}{4\pi}\frac{e^2}{\hbar}\int_0^{q_f} \frac{q dq}{E^3} = \frac{\tau_z\Delta}{4\pi}\frac{e^2}{\hbar}\int_0^{q_f} \frac{q dq}{(\Delta^2+q^2)^{3/2}} =$$

$$= \frac{\tau_z\Delta}{4\pi}\frac{e^2}{\hbar}\left(\frac{1}{\Delta} - \frac{1}{\sqrt{\Delta^2+q_F^2}}\right) = \frac{\tau_z}{2}\frac{e^2}{2\pi\hbar}\left(1 - \frac{\Delta}{\mu}\right)\theta(\mu-\Delta)\,.$$

In the third passage we used equation 2.11 to express $\Omega_{q_x q_y}$, in the fourth passage we approximated the Fermi-Dirac to a step function.
The $\theta(\mu-\Delta)$ is there to make sure that if no states are inside the Fermi-Dirac the integral is zero.
So in the end we have that for the conduction band

$$\sigma^+_{xy}(\mu) = \frac{\tau_z}{2}\frac{e^2}{2\pi\hbar}\left(1 - \frac{\Delta}{\mu}\right)\theta(\mu-\Delta)\,. \tag{2.28}$$

One thing to notice is that if you have $\mu \gg \Delta$ (aka. all states in the band are occupied) then the integral is equal to -2π. The integral of the lower band is very similar, the main difference is that the Berry curvature has opposite sign, and when integrating the Fermi-Dirac as a step function behaves like this:

$$\begin{aligned} \int_{\mathbb{R}^2} f[E^+(q)] dq_x dq_y &= 2\pi \int_0^{q_F} dq\,, \\ \int_{\mathbb{R}^2} f[E^-(q)] dq_x dq_y &= 2\pi \int_{q_F}^{\infty} dq\,. \end{aligned} \tag{2.29}$$

In the end the conductivity contribution fro the valence band is

$$\sigma_{xy}^{-}(\mu) = -\frac{\tau_z}{2}\frac{e^2}{2\pi\hbar}\frac{\Delta}{\mu}\theta(\Delta - \mu)\,. \tag{2.30}$$

By the end equation of the conductivity for every μ is 2.27 becomes

$$\sigma_{xy}(\mu) = -\frac{\tau_z}{2}\frac{e^2}{2\pi\hbar}\left[\frac{\Delta}{|\mu|}\theta\left(\mu^2 - \Delta^2\right) + \theta\left(\Delta^2 - \mu^2\right)\right]. \tag{2.31}$$

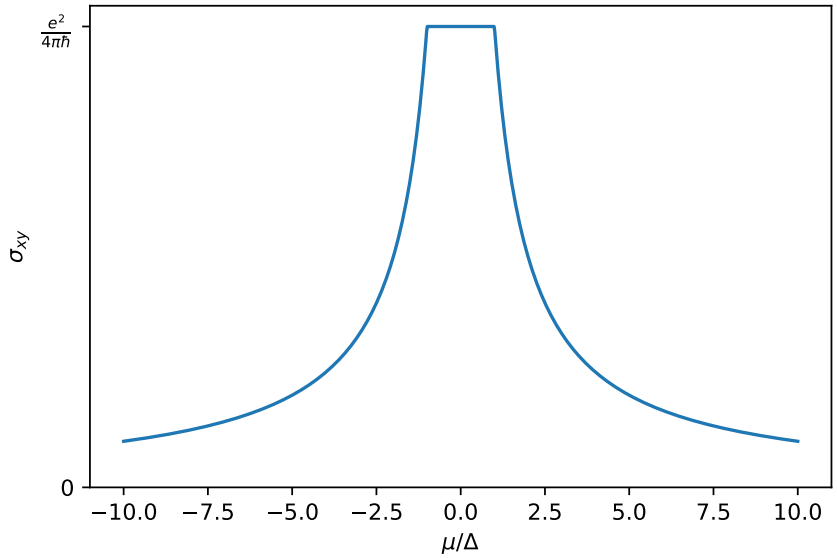

Figure 2.6: Here is shown $\sigma_{xy}(\mu)$ (eq. 2.31). Notice how, when $\mu \in [-\Delta, \Delta]$ then $\sigma_{xy} = \frac{e^2}{4\pi\hbar}$

However in most cases it's safe to assume that the chemical potential is inside the energy gap, so equation 2.31 becomes

$$\sigma_{xy} = \frac{\tau_z}{2}\frac{e^2}{2\pi\hbar}\,. \tag{2.32}$$

2.5 Topological properties of bilayer graphene

As explained in section 1.15 the Hamiltonian for the low energy states bilayer graphene is (equation 1.138)

$$\begin{aligned} H =& H_2 + h_w + h_4 + h_\Delta + h_U + h_{AB}\,, \\ H_2 =& -\frac{1}{2m}\begin{bmatrix} 0 & (\pi^\dagger)^2 \\ \pi^2 & 0 \end{bmatrix}, \end{aligned} \tag{2.33}$$

where H_2 is the dominant term and the others are perturbations. For a given momentum $\boldsymbol{p} = [p\cos\phi, p\sin\phi]$ a Hamiltonian H_J can be written in the form

$$H_J = E(p)\boldsymbol{n}(\phi)\cdot\boldsymbol{\sigma}\,, \tag{2.34}$$

where $\boldsymbol{n}(\phi) = -[\cos(J\phi), \sin(J\phi)]$ and $\boldsymbol{\sigma}$ is the vector made of Pauli matrices. For bilayer graphene $J = 2$ while for monolayer $J = 1$, this convention of using J thus helps us compare what happens between the two cases. The eigenstates in both cases are (equations 1.117 and 1.139)

$$|\pm, \boldsymbol{k}\rangle = \frac{1}{\sqrt{2}}\begin{bmatrix} 1 \\ \mp e^{i2\phi} \end{bmatrix} e^{i\boldsymbol{k}\cdot\boldsymbol{r}}\,, \quad \boldsymbol{k} = kn(\phi)\,. \tag{2.35}$$

The eigenstates of H_J correspond to pseudospins polarized parallel (electrons) or antiparallel (holes) to the 'quantization' axis $\boldsymbol{n}$. An adiabatic evolution of such pseudospin states, which accompanies the rotation of momentum $\boldsymbol{k}$ by angle ϕ, also corresponds to the rotation of axis $\boldsymbol{n}$ by angle $J\phi$.
As a result, if a electron encircles a closed contour in the momentum space (that is $\phi = 2\pi$), a phase shift $\Phi = J\pi$ known as Berry's phase is gained by the quasiparticle's wavefunction.
As a result the Chern number on each Dirac cone in bilayer graphene is double the one of single layer graphene, this means that the Hall effect is doubled in bilayer graphene.

2.6 Non-local Charge transport

If we apply a voltage V in two opposite points of a strip of a ohmic material of width W and infinite lenght, and we see a current that flows from one point to another figure 2.7.
Clearly the current isn't completely localized along the axis that unites the two injection points, and so does the voltage difference.
If we probe the voltage from two different points with an offset of x from the injection points and we divide it by the total current between the contacts we see that

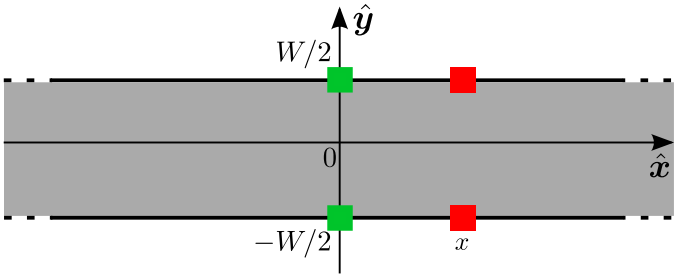

Figure 2.7: Representation of the strip. The current goes from one of the green squares in the middle to the other, while the voltage is measured from the two red squares on the right. Image taken from [59]

$$\frac{V(x)}{I} = \frac{2\rho}{\pi} \ln \left| \coth\left(\frac{\pi x}{2W}\right) \right|, \tag{2.36}$$

where ρ is the resistivity. We will later give a proof for this formula.

Two-dimensional material like gapped graphene [60–62] and transition metal dichalcogenides [63–65], do not obey this equation. This is because these materials display the Valley Hall effect we talked about previously.

Non-local transport can be a useful tool to probe the existence of anomalous Hall effect [66–71]

2.7 Theory of non local charge transport

The charges inside the material get pushed around from the electrochemical potential ψ_K

$$\psi_K(\boldsymbol{r}) = V(\boldsymbol{r}) - \frac{1}{e}\mu_K[n_{K_1}(\boldsymbol{r}), n_{K_2}(\boldsymbol{r}), T]\,, \tag{2.37}$$

where ϕ is the electrical potential, and $\mu_K = \frac{\partial}{\partial n_K} F[n_{K_1}(\boldsymbol{r}), n_{K_2}(\boldsymbol{r}), T]$ is the chemical potential of the material and F is the free energy.

The current generated from this potential in the valley K_α in the $i-$th direction is

$$-eJ_{K_\alpha,i}(\boldsymbol{r}) = \sum_{j,b} \underbrace{-\sigma_{K_\alpha K_\beta,ij}}_{\text{conductivity}} \partial_j \psi_{K_\beta}(\boldsymbol{r})\,. \tag{2.38}$$

From now we are going to set $T \approx 0$[1] and ignore intervalley scattering, so if $K_\alpha \neq K_\beta$ $\sigma_{K_\alpha K_\beta,ij} = 0$, also because of this the free energy can be written

[1] A more precise statement is that the thermal De Broglie wavelenght λ_T must be much larger than the average distance between the electrons. We are not going into the math here, but if you want to calculate it, keep in mind that the dispersion relation is relativistic, so the formula of λ_T is going to be a bit different

as the sum of the two Free energies

$$F(n_{K_1}, n_{K_2}) = F_1(n_{K_1}(\mathbf{r})) + F_2(n_{K_2}(\mathbf{r}))\,, \tag{2.39}$$

and so the chemical potential of a given valley depend only on the number of electron in the same valley

$$\mu_\alpha(n_{K_\alpha}(\mathbf{r})) = \frac{\partial}{\partial n_{K_\alpha}} F(n_{K_0}, n_{K_1}) = \frac{\partial}{\partial n_{K_\alpha}} F_\alpha(n_{K_\alpha}(\mathbf{r}))\,. \tag{2.40}$$

This simplifies the trasport equation in

$$-e\mathbf{J}_{K_\alpha}(\mathbf{r}) = \sigma_{K_\alpha}(\mathbf{r})\nabla\psi_{K_\alpha}(\mathbf{r})\,. \tag{2.41}$$

Where σ_{K_α} is the following matrix

$$\sigma_{K_\alpha} = \begin{bmatrix} \sigma_{K_\alpha K_\alpha, xx} & \sigma_{K_\alpha K_\alpha, xy} \\ -\sigma^*_{K_\alpha K_\alpha, xy} & \sigma_{K_\alpha K_\alpha, xx} \end{bmatrix}.$$

Now we need to write the gradient electrochemical potential $\nabla\psi(\boldsymbol{r})$

$$\nabla\psi_{K_\alpha}(\mathbf{r}) = \nabla V(\mathbf{r}) - \frac{1}{e}\frac{\partial}{\partial n_{K_\alpha}}\mu_\alpha(n_{K_\alpha}(\mathbf{r}))\nabla n_{K_\alpha}\,. \tag{2.42}$$

For gapped Dirac Hamiltonians

$$\frac{\partial \mu_{K_\alpha}}{\partial n_{K_\alpha}} = \frac{\pi}{\sqrt{2\pi|n| + \Delta^2}} + \Delta\delta(n) \approx \frac{\pi}{\Delta} + \Delta\delta(n) \quad \forall\alpha\,.$$

In this equation we assumed that there are very few charge carries, so $\frac{n}{\Delta^2} \approx 0$. We can shorten the equation 2.42 by defining

$$e^2 D_{K_\alpha, ij} = \sigma_{K_\alpha, ij}\frac{\partial \mu_\alpha}{\partial n_{K_\alpha}}[n_{K_\alpha}(\mathbf{r})]\,, \tag{2.43}$$

so equation 2.41 becomes

$$-eJ_{K_\alpha, i}(\mathbf{r}) = \sigma_{K_\alpha, ij}E_j(\mathbf{r}) - eD_{K_\alpha, ij}\partial_j n_{K_\alpha}(\mathbf{r})\,, \tag{2.44}$$

or, written in matrix form

$$-e\mathbf{J}_{K_\alpha}(\mathbf{r}) = \sigma_{K_\alpha}\mathbf{E}(\mathbf{r}) - eD_{K_\alpha}\nabla n_{K_\alpha}(\mathbf{r})\,, \tag{2.45}$$

where σ_{K_α} and $-eD_{K_\alpha}$ are matrices.

2.7.1 Re-writing the equations in terms of charge current and valley current

Measuring the currents in different valley can be cumbersome, however measuring the charge current $\mathbf{J}_c = \mathbf{J}_{K_1} + \mathbf{J}_{K_2}$ is straightforward, and for mathematical convenience we also define the valley current $\mathbf{J}_v = \mathbf{J}_{K_1} - \mathbf{J}_{K_2}$.

Since we no longer describe the currents in terms of their valley index, but on the sum and the difference of what happens at the different valleys, we are going to reparametrize also the other quantities in the same fashion.

$$\begin{cases} \sigma_c = \sigma_{K_1} + \sigma_{K_2} = 2\sigma_{xx}\delta_{ij} \\ \sigma_v = \sigma_{K_1} - \sigma_{K_2} = \sigma_v = 2\sigma_{xy}\epsilon_{ij} \end{cases} . \tag{2.46}$$

The term $-eD_{K_\alpha}\nabla n_{K_\alpha}(\mathbf{r})$ is a little harder to translate. First off we are going to impose the local charge conservation

$$n(\mathbf{r}) = n_{K_0} + n_{K_1} \approx 0\,,$$

and so

$$n_v(\mathbf{r}) = n_{K_1} - n_{K_2} = 2n_{K_1} = -2n_{K_2}\,. \tag{2.47}$$

Now let's do the sum of the $D_{K_\alpha}\nabla n_{K_\alpha}(\mathbf{r})$ terms to write them in terms of charge and valleys degrees of freedom

$$D_{K_1}\nabla n_{K_1} + D_{K_2}\nabla n_{K_2} = (D_{K_1} - D_{K_2})\nabla n_v(\mathbf{r})/2\,,$$

$$D_{K_1} - D_{K_2} = \sigma\frac{\partial\mu_1}{\partial n_{K_1}} - \sigma^T\frac{\partial\mu_2}{\partial n_{K_2}}\,.$$

Since $\mu_v = 2\mu_1 = -2\mu_2$ and $n_v = 2n_{K_1} = -2n_{K_2}$

$$D_{K_1} - D_{K_2} = \frac{1}{e^2}(\sigma - \sigma^T)\frac{\partial\mu_v}{\partial n_v} = \frac{2}{e^2}\sigma_v\frac{\partial\mu_v}{\partial n_v}\,.$$

So I define

$$D_{cv} = \frac{2}{e^2}\sigma_v\frac{\partial\mu_v}{\partial n_v} \approx \frac{2}{e^2}\frac{\pi}{\Delta}\sigma_v\,,$$

and we get that

$$D_{K_1}\nabla n_{K_1} + D_{K_2}\nabla n_{K_2} = D_{cv}n_v\,.$$

Putting it all together we have that

$$\mathbf{J}_c(\mathbf{r}) = \sigma_c\mathbf{E}(\mathbf{r}) + eD_{cv}\nabla n_v(\mathbf{r})\,.$$

Writing all the indices

$$J_{c,i}(\boldsymbol{r}) = \sum_j \sigma_{c,xx}\delta_{ij}E_i(\boldsymbol{r}) + eD_{cv,xy}\epsilon_{ij}\partial_j n_v(\boldsymbol{r})\,, \tag{2.48}$$

so we can rewrite them as

$$\mathbf{J}_c = \sigma_{c,xx}\mathbf{E}_i + D_{cv,xy}\nabla \times n_v\,, \tag{2.49}$$

where $\sigma_{c,xx}$ and $D_{cv,xy}$ are scalars.

And now the difference of the $D_{K_\alpha}\nabla n_{K_\alpha}(\mathbf{r})$ terms to write them in terms of charge and valleys degrees of freedom

$$D_{K_0}\nabla n_{K_0} - D_{K_1}\nabla n_{K_1} = (D_{K_0} + D_{K_1})\nabla n_v(\mathbf{r})/2\,,$$

and with some calculations done in a similar fashion to the one we use to calculate $\mathbf{J}_c$ we have that

$$D_v = \frac{1}{2}(D_{K_0} + D_{K_1}) = \frac{1}{e^2}\sigma_c\frac{\partial\mu_c}{\partial n_c}\,,$$

so, in matrix form

$$\mathbf{J}_v(\mathbf{r}) = \sigma_v\mathbf{E}(\mathbf{r}) + eD_v\nabla n_v(\mathbf{r})\,, \tag{2.50}$$

which can be re-written as

$$J_{v,i}(\mathbf{r}) = \sum_j \sigma_{c,xy}\epsilon_{ij}E_j(\mathbf{r}) + eD_{v,xx}\delta_{ij}\partial_j n_v(\mathbf{r})\,, \tag{2.51}$$

where $\sigma_{c,xy}$ and $D_{v,xx}$ are scalars.

2.7.2 Laplace equation

Now that we have the charge and valley currents differential equations we calculate the laplacians to solve them. Let's start from the equation for the charge currents 2.49

$$\nabla\cdot\boldsymbol{J}_c = \nabla\cdot(\sigma_c\mathbf{E}) + eD_{cv,xx}\nabla\cdot(\nabla\times n_v)\,. \tag{2.52}$$

Inside the material the are no sources of charge current, so $\nabla\cdot\boldsymbol{J}_c =$, and the divergence of a rotor is zero, so $\nabla\cdot(\nabla\times n_v) = 0$. This means that inside the material

$$\boxed{\nabla^2 V(x,y) = 0} \tag{2.53}$$

So, to be able to solve the laplace equation we just need to impose the boundary conditions that the current is injected in a single point at $x = 0$ along the $\hat{\boldsymbol{y}}$ direction.

$$-e\boldsymbol{J}_c(x, \pm W/2) = I\delta(x)\hat{\boldsymbol{y}}\,.$$

If we put it in equation 2.52 we get

$$\boxed{I\delta(x) = \sigma_{c,xx}\partial_y V(x, \pm W/2) - eD_{cv,xy}\partial_x n_v(x, \pm W/2)} \tag{2.54}$$

Now let's calculate the laplacian for the valley current equation 2.51

$$\nabla \cdot \mathbf{J}_v = \nabla \times (\sigma_{c,xy}\mathbf{E}) + e\nabla \cdot (D_{v,xx}\nabla n_v)\,. \tag{2.55}$$

Now, lets analyze all the terms one by one

- For the continuity equation we have that $\nabla\cdot\mathbf{J}_v = \frac{\partial}{\partial t}n_v$, since intervalley scattering is zero, this should be zero, however we can reintroduce it by adding a exponential decay for the valley imbalance of charges $\frac{\partial}{\partial t}n_v = -\frac{1}{\tau_v}n_v$
- $e\nabla \cdot (D_{v,xx}\nabla n_v)$ is really nothing special, inside the material $D_{v,xx}$ is constsant so in the end it is equal to $eD_{v,xx}\nabla^2 n_v$
- $\nabla \times (\sigma_{c,xy}\mathbf{E})$ is equal to zero inside the material, but on the edge can be non-zero because $\sigma_{c,xy}$ changes form inside to the outside

In the end we get that

$$eD_{v,xx}\nabla^2 n_v = -\frac{1}{\tau_v}n_v - \nabla \times (\sigma_{c,xy}\mathbf{E})\,. \tag{2.56}$$

This means that at the equilibrium $n_v \neq 0$ only if you are were $\nabla\times(\sigma_{c,xy}\mathbf{E}) \neq 0$, and this is only true along the edge, so we we'll have to worry about this term only in the boundary conditions, So

$$\boxed{\left[\nabla^2 - \frac{1}{\tau_v D_{v,xx}}\right] n_v(\boldsymbol{r}) = 0} \tag{2.57}$$

The boundary condition is simply that the valley current doesn't exit the material, so

$$J_{v,y}(x, \pm W/2) = 0\,. \tag{2.58}$$

Putting it into the differential equation for J_v (eq 2.51) we get

$$\boxed{\sigma_{v,xy}\partial_x V(x, \pm W/2) + eD_{v,xx}\partial_y n_v(x, \pm W/2) = 0} \tag{2.59}$$

All the boxed equations we wrote in the in this section enable us to completely solve the system. For convenience let's write the m in a single system of equations

$$\begin{cases} \nabla^2 V(x,y) = 0 \\ \left[\nabla^2 - \frac{1}{\tau_v D_{v,xx}}\right] n_v(\boldsymbol{r}) = 0 \\ I\delta(x) = \sigma_{c,xx}\partial_y V(x, \pm W/2) - eD_{cv,xy}\partial_x n_v(x, \pm W/2) \\ \sigma_{v,xy}\partial_x V(x, \pm W/2) + eD_{v,xx}\partial_y n_v(x, \pm W/2) = 0 \end{cases}. \tag{2.60}$$

From the third equation in the system above we can see that $V(x,y)$ is even along the $\hat{\boldsymbol{x}}$ axis and odd along the $\hat{\boldsymbol{y}}$ axis.
From the fourth equation we can see that n_v has the opposite parity to V, so it's odd along the $\hat{\boldsymbol{x}}$ axis and even along the $\hat{\boldsymbol{y}}$ axis.

To be able to solve it we first have to do a Fourier transform over the $\hat{\boldsymbol{x}}$ direction. The first two equations of eq 2.60 becomes

$$\begin{cases} (\partial_y^2 - k^2)V(k,y) = 0 \\ \left[\partial_y^2 - \omega^2(k)\right] n_v(k,y) = 0 \end{cases} . \tag{2.61}$$

The solutions that respect the symmetries we talked about earlier are

$$V(k,y) = V(k)\sinh(ky)\,; \qquad n_v(k,y) = n_v(k)\cosh[\omega(k)y]\,. \tag{2.62}$$

However we still do not know what are $V(k)$ and $n_v(k)$, to obtain them we have to plug the equations above in the last two equations of 2.60

$$\begin{cases} \sigma_{c,xx} k \cosh(kw/2)V(k) - eD_{cv,xy} ik \cosh(\omega W/2) n_v(k) = I \\ -\sigma_{v,xy} ik \sinh(kw/2)V(k) - eD_{v,xx}\omega(k)\sinh(\omega W/2) n_v(k) = 0 \end{cases} . \tag{2.63}$$

This system of equation is linear in $V(k)$ and $n_v(k)$, so it can be written in this form

$$\begin{bmatrix} A & B \\ C & D \end{bmatrix} \begin{bmatrix} V \\ n_v \end{bmatrix} = \begin{bmatrix} I \\ 0 \end{bmatrix} . \tag{2.64}$$

And the inverse is simply

$$\begin{bmatrix} V \\ n_v \end{bmatrix} = \frac{I}{AD - BC} \begin{bmatrix} D \\ -C \end{bmatrix} . \tag{2.65}$$

Since we want only care to calculate the voltage we only need to evaluate

$$V = \frac{I}{A - \frac{BC}{D}} ,$$

wich turns out to be equal to

$$V(k) = \frac{I}{\sigma_c} \frac{\omega(k)/k}{\sinh(kW/2)} \left\{ \frac{\omega(k)}{\tanh(kW/2)} + \frac{k\tan^2(\theta_{VH})}{\tanh[\omega(k)W/2]} \right\}^{-1} . \tag{2.66}$$

We can plug it into equation 2.62 and evaluate it at $y = \pm W/2$

$$V(k, \pm W/2) = V(k)\sinh(\pm kW/2) = \frac{I\omega}{\sigma_c k} \left\{ \dots \right\}^{-1} , \tag{2.67}$$

where the terms inside the curly brakets are the same from the previous equation (2.66).
Finally we can calculate the non-local resistance

$$R_{\mathrm{NL}}(k) = \frac{V(k, W/2) - V(k, -W/2)}{I}\,, \tag{2.68}$$

which is equal to

$$R_{\mathrm{NL}}(k) = \frac{2\omega(k)}{k\sigma_c}\left\{\frac{\omega(k)}{\tanh(kW/2)} + \frac{k\tan^2(\theta_{VH})}{\tanh[\omega(k)W/2]}\right\}^{-1}. \tag{2.69}$$

Understanding this formula will enable us to fully model how electrons behave in Hall bars, and the study of this formula will be the main focus of the last chapter.

Chapter 3

Theory of the non-local resistance

In section 2.6 we obtained the frequency response of the non-local resistance (equation 2.69)

$$R_{\mathrm{NL}}(k) = \frac{2\omega(k)}{k\sigma_c}\left\{\frac{\omega(k)}{\tanh(kW/2)} + \frac{k\tan^2(\theta_{\mathrm{VH}})}{\tanh[\omega(k)W/2]}\right\}^{-1}. \tag{3.1}$$

Its anti-fourier transform tells us everything we would want to know about the system. Unfortunately 3.1 doesn't have an analytic Fourier transform. If there are no topological effect $\theta_{\mathrm{VH}} = 0$ and it can be solved analytically.

$$R_{\mathrm{NL}}(k)|_{\theta_{\mathrm{VH}}=0} \equiv R^{(0)}_{\mathrm{NL}}(k) = \frac{2\rho}{k}\tanh\left(\frac{kW}{2}\right), \tag{3.2}$$

$$R^{(0)}_{\mathrm{NL}}(x) = \mathcal{F}^{-1}\left[R^{(0)}_{\mathrm{NL}}(k)\right] = -\frac{2\rho}{\pi}\ln\left|\tanh\left(\frac{\pi x}{2W}\right)\right|. \tag{3.3}$$

This is the purely ohmic nonlocal signal that we have talked about in 2.36. However, if we are going to explore topological materials we cannot set $\tan(\theta_{\mathrm{VH}}) = 0$, this means that we'll have to do some approximations. Previously there had been some attempt of applying this function to understand, however only the limit $l_{\mathrm{v}} << W$ was explored [59].
In this chapter we provide a complete and accurate description on the Nonlocal resistance arising from valley-Hall. The results present in this thesis can also be applied to the spin-Hall case, this is because the frequency response function of the Nonlocal resistance in the spin-Hall case has a mathematical formulation equivalent to 3.1.

3.1 Study of the Nonlocal resistance as a function of x

Let's look at the graph of the $R_{\mathrm{NL}}(k)$ before doing any approximations: As

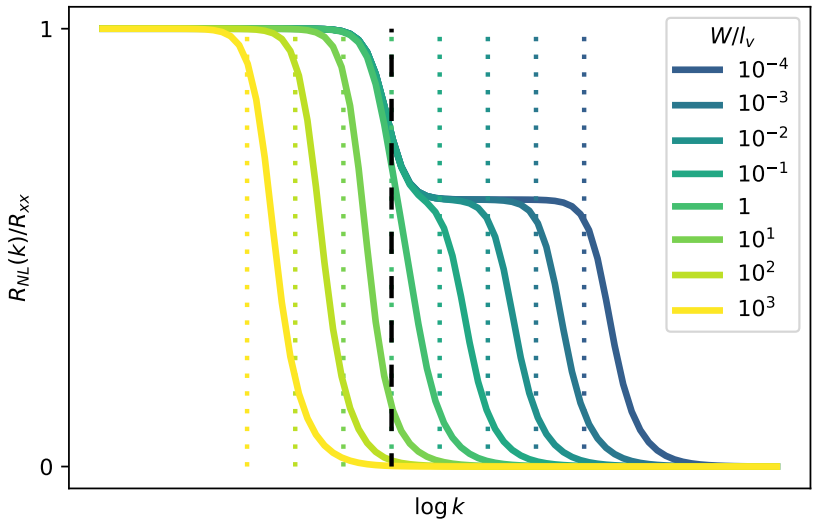

Figure 3.1: Frequency response of the non local resistance for several values of W/l_{v}. The dashed black line represents where $k = 1/l_{\mathrm{v}}$, the colored dashed line represents where $k = 1/W$

you can see from the figure 3.1

- If $W \gg l_{\mathrm{v}}$ we have a single bell like function with the width of the bell being $\approx 1/W$ and the height being R_{xx}
- If $W \ll l_{\mathrm{v}}$ we have a double-bell function, where the first bell has a height of R_{xx} and a width of $\approx 1/l_{\mathrm{v}}$, and the second one has a shorter height.

To evaluate the precise height of the secondary bell we just need to set $l_{\mathrm{v}}^{-1} \ll k \ll W^{-1}$ in equation 3.1, this gives us

$$R_{\mathrm{NL}}(l_{\mathrm{v}}^{-1} \ll k \ll W^{-1}) \approx R_{xx} \cos^2(\theta_{\mathrm{VH}})\,, \tag{3.4}$$

where $R_{xx} = \frac{W}{\sigma_{xx}}$ and $\cos^2(\theta_{\mathrm{VH}}) = \frac{1}{1+\tan^2(\theta_{\mathrm{VH}})}$

So, if we have $l_{\mathrm{v}} \ll W$ or $\theta_{\mathrm{VH}} \ll 1$ (or both) we have a single bell structure. Incidentally these are the conditions to NOT have topological effects, so the less visible the double bell is, the less visible the topological effects are. We'll also see later how one of the bell represents the ohmic nonlocal signal, while the other represents the topological nonlocal signal.

3.1.1 Small k limit

Let's start by exploring $k \ll l_{\rm v}^{-1}, W^{-1}$. This will tell us how the function behaves at long ranges $x \gg l_{\rm v}, W$. In this regime

$$\omega(k) = \sqrt{k^2 + l_{\rm v}^{-2}} \approx \frac{1}{l_{\rm v}} \left[1 + \frac{(k l_{\rm v})^2}{2}\right], \tag{3.5}$$

$$\coth(kW/2) \approx \frac{2}{kW} + \frac{kW}{6}. \tag{3.6}$$

Plugging the last two equations into equation 3.1 we have that $R_{\rm NL}(k) \approx$

$$\frac{2}{\sigma_c} \frac{1}{l_{\rm v} k} \left[\frac{1}{l_{\rm v}} \left(1 + \frac{k^2 l_{\rm v}^2}{2}\right) \left(\frac{2}{kW} + \frac{kW}{6}\right) + \frac{k \tan^2(\theta_{\rm VH})}{\tanh(W/2l_{\rm v})} + o(k^2)\right]^{-1}, \tag{3.7}$$

and after some steps we get that

$$R_{\rm NL}(k \ll l_{\rm v}^{-1}, W^{-1}) = \frac{R_{xx}}{1 + L_{\rm v}^2 k^2 + o(k^4)}, \tag{3.8}$$

where the *renormalized valley diffusion length* $L_{\rm v}^2$ is defined as

$$L_{\rm v}^2 \equiv l_{\rm v}^2 + \frac{W^2}{12} + \frac{l_{\rm v} W}{2} \frac{\tan^2(\theta_{\rm VH})}{\tanh(W/2l_{\rm v})}. \tag{3.9}$$

Now we are going to define the topological nonlocal resistance $R_{\rm NL}^T$ by taking the equation 3.8, and ignoring the $o(k^4)$ term

$$R_{\rm NL}^T(k) \equiv \frac{R_{xx}}{1 + L_{\rm v}^2 k^2}. \tag{3.10}$$

We are now ready to do the Fourier transform of equation 3.10 to get the behavior for $x \gg l_{\rm v}, W$

$$R_{\rm NL}(x \gg l_{\rm v}, W) \approx \mathcal{F}^{-1}\left[R_{\rm NL}^T(k)\right] \equiv R_{\rm NL}^T(x), \tag{3.11}$$

that is equal to

$$R_{\rm NL}^T(x) = R_{xx} \int_{-\infty}^{+\infty} \frac{e^{-ikx}}{1 + L_{\rm v}^2 k^2} \frac{dk}{2\pi} = \frac{R_{xx}}{2L_{\rm v}} e^{-\frac{|x|}{L_{\rm v}}}, \tag{3.12}$$

so,

$$R_{\rm NL}(x \gg l_{\rm v}, W) \approx R_{\rm NL}^T(x). \tag{3.13}$$

3.1.2 Large k limit

Fortunately the case for which $k \gg l_{\mathrm{v}}^{-1}$ is much simpler: in this case $\omega(k) \approx k$, so

$$R_{\mathrm{NL}}(k \gg l_{\mathrm{v}}^{-1}) = \cos^2(\theta_{\mathrm{VH}}) \frac{2\rho}{k} \tanh\left(\frac{kW}{2}\right) . \tag{3.14}$$

Using equation 3.2 we get that this last equation is $\cos^2(\theta_{\mathrm{VH}})$ times the one for the purely ohmic nonlocal signal

$$R_{\mathrm{NL}}(k \gg l_{\mathrm{v}}^{-1}) \approx \cos^2(\theta_{\mathrm{VH}}) R_{\mathrm{NL}}^{(0)}(k) . \tag{3.15}$$

This means that the Fourier transform is

$$R_{\mathrm{NL}}(x \ll l_{\mathrm{v}}) \approx \cos^2(\theta_{\mathrm{VH}}) R_{\mathrm{NL}}^{(0)}(x) . \tag{3.16}$$

3.1.3 Testing the approximations

But how do these equations fear in practice? As you can see from figure 3.2

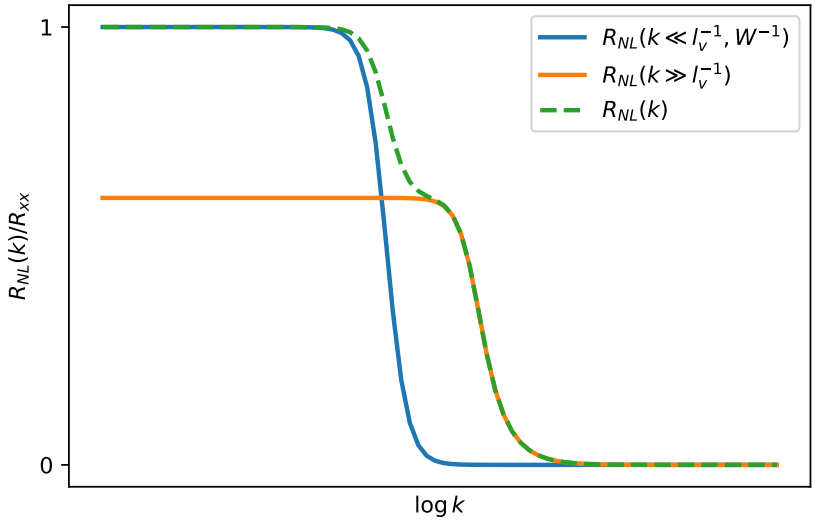

Figure 3.2: For this example $l_{\mathrm{v}} = 20W$

the two approximations work pretty well, except in the neighborhood where $k \approx l_{\mathrm{v}}^{-1}$. But what we really care about is $R_{\mathrm{NL}}(x)$.
If we plot the approximations for $x \gg l_{\mathrm{v}}, W$ (eq. 3.13) and $x \ll l_{\mathrm{v}}$ (eq. 3.16) alongside the numerical Fourier transform of $R_{\mathrm{NL}}(k)$ 3.1 we get figure 3.3

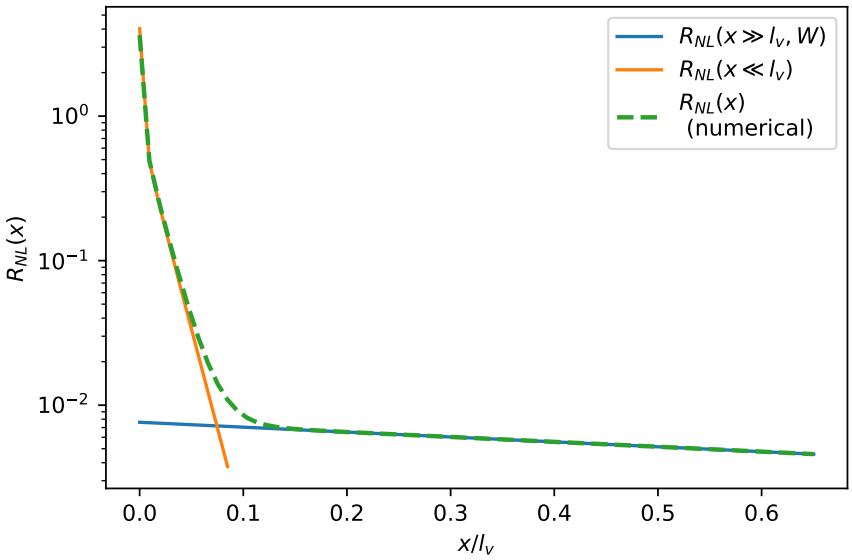

Figure 3.3: The parameters for this graph are exactly the same for the previous graph (figure 3.2)

3.1.4 Improving the approximation

We can do better than this! By combining the two approximations it's possible to have a single equation that is very accurate for both $x \gg l_\mathrm{v}, W$ and $x \ll l_\mathrm{v}$, however, in the end we'll end up with an approximation that is surprisingly good even for $x \approx l_\mathrm{v}$.

Since the Fourier transform is a linear operator, the idea is to find the linear combination of the two approximation that best approximates the $R_\mathrm{NL}(k)$ for both $k \ll l_\mathrm{v}^{-1}, W^{-1}$ and $k \gg l_\mathrm{v}^{-1}$ and then anti-transform the result.

$$R_\mathrm{NL}(k) \approx \alpha R_\mathrm{NL}(k \ll l_\mathrm{v}^{-1}, W^{-1}) + \beta R_\mathrm{NL}(k \gg l_\mathrm{v}^{-1}) =$$

$$= R_\mathrm{NL}(k) \approx \alpha R^T_\mathrm{NL}(k) + \beta \cos^2(\theta_\mathrm{VH}) R^{(0)}_\mathrm{NL}(k)\,,$$

Where α and β are the coefficient to be determined.
Since we only need to evaluate two variables, we only need to evaluate the expression above in two different points. The most reasonable points to choose are $k = 0$ and $k = +\infty$, since they are the points where the approximations work better. For doing the calculations it's best to write out the two approximations

$$R_\mathrm{NL}(k) \approx \alpha \frac{R_{xx}}{1 + L_\mathrm{v}^2 k^2} + \beta \frac{2\rho}{k} \tanh\left(\frac{kW}{2}\right) \cos^2(\theta_\mathrm{VH})\,.$$

- For $k \to +\infty$ the term that is multiplied by β is an increasingly precise estimate of $R_{\mathrm{NL}}(k)$, and it dominates over the term that is multiplied by alpha, so $\beta = 1$.
- For $k = 0$ we have that

$$R_{xx} = \alpha R_{xx} + R_{xx}\cos^2(\theta_{\mathrm{VH}})\,,$$

So, $\alpha = \sin^2(\theta_{\mathrm{VH}})$.

Putting it all together we define the resulting approximation

$$\boxed{\tilde{R}_{\mathrm{NL}}(k) \equiv \sin^2(\theta_{\mathrm{VH}})R^T_{\mathrm{NL}}(k) + \cos^2(\theta_{\mathrm{VH}})R^{(0)}_{\mathrm{NL}}(k)} \tag{3.17}$$

The thing that I personally like about this approximation is its geometrical elegance. If we write all the terms of the equation above we get

$$\tilde{R}_{\mathrm{NL}}(k) \equiv \sin^2(\theta_{\mathrm{VH}})\frac{R_{xx}}{1 + L_{\mathrm{v}}^2 k^2} + \cos^2(\theta_{\mathrm{VH}})\frac{2\rho}{k}\tanh\left(\frac{kW}{2}\right)\,. \tag{3.18}$$

And if we plot the approximation $\tilde{R}_{\mathrm{NL}}(k)$ alongside the actual values of $R_{\mathrm{NL}}(k)$ we can see that they are remarkably similar (figure 3.4)

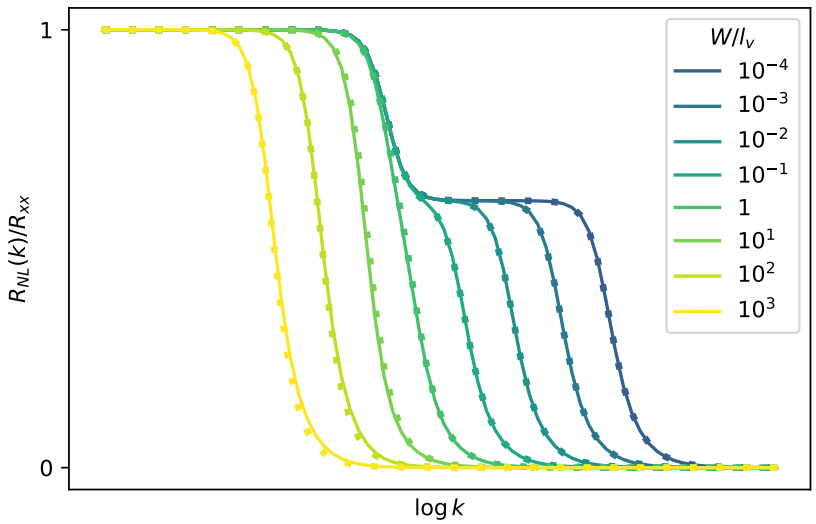

Figure 3.4: Comparison between $R_{\mathrm{NL}}(k)$ and $\tilde{R}_{\mathrm{NL}}(k)$. The continuous line represents $R_{\mathrm{NL}}(k)$, while the dashed line represents $\tilde{R}_{\mathrm{NL}}(k)$. It's unreasonably accurate!

The nice thing about this is that if two equations are similar, then their

Fourier transform will be too. This means that $\tilde{R}_{\mathrm{NL}}(x)$ will be a good approximation of $R_{\mathrm{NL}}(x)$, where

$$\boxed{\tilde{R}_{\mathrm{NL}}(x) = \sin^2(\theta_{\mathrm{VH}}) R^{T}_{\mathrm{NL}}(x) + \cos^2(\theta_{\mathrm{VH}}) R^{(0)}_{\mathrm{NL}}(x)} \tag{3.19}$$

We can write out the full formula using equations 3.13 and 3.16

$$\tilde{R}_{\mathrm{NL}}(x) = \frac{R_{xx}}{2L_{\mathrm{v}}} e^{-|x|/L_{\mathrm{v}}} \sin^2(\theta_{\mathrm{VH}}) - \frac{2R_{xx}}{\pi W} \ln \left| \tanh\left(\frac{\pi x}{2W}\right) \right| \cos^2(\theta_{\mathrm{VH}}) \,. \tag{3.20}$$

Infact if we re-create figure 3.3 with the equation above we get figure 3.5

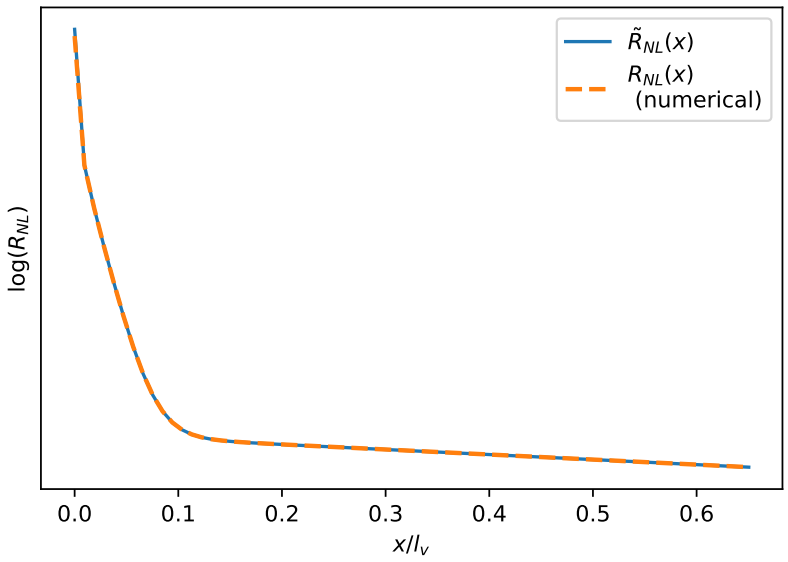

Figure 3.5: As you can see it's impossible to distinguish the difference between the two functions to the naked eye. The parameters are the same as figure 3.5

3.2 Behavior of the nonlocal resistance as function of the longitudinal resistivity

Hall effect experiments are generally done in Hall-bars. These are samples of material with a shape like the one in figure 3.6, it also means that more often than not in experimental setups we cannot change x without changing the geometry of the sample.
In the previous section we studied how R_{NL} depended on x, but since Hall-bars can only measure a single x one of the ways to have multiple measurements with the same Hall-bar is to change the resistivity of the material by changing the temperature of the setup, and study R_{NL} as we change ρ_{xx}.

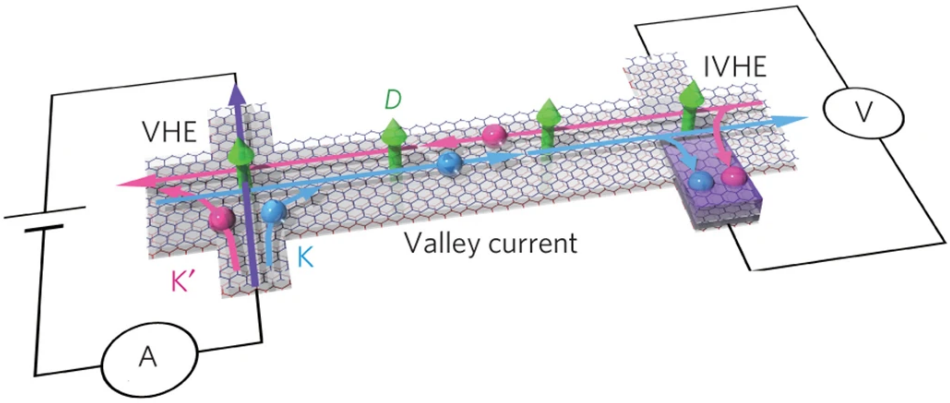

Figure 3.6: Example of Hall bar the currents are injected and measured in the rectangular contacts that come out from the main strip. Image taken from [62].

If you were to conduct an experiment where you measure R_{NL} as you change the resistivity of the material ρ you would have in general something that looks like figure 3.7.

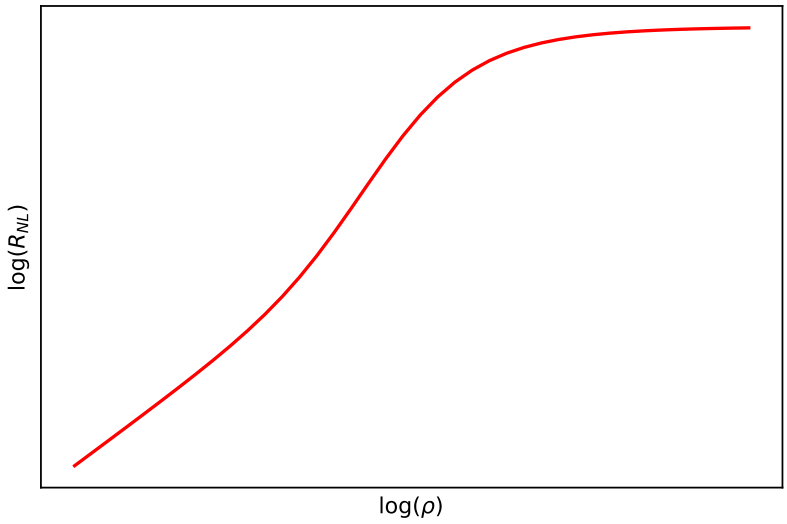

Figure 3.7: Looking at the image you can see that at the start it increases linearly, then it starts to increase even faster just before reaching a plateau.

The objective of this section is effectively to be able to understand this graph.

Just like before to understand the general behavior of $R_{\mathrm{NL}}(\rho)$ we'll ex-

amine $\rho \to 0$ and $\rho \to \infty$. For convenience let's re-write equation 3.1

$$R_{\mathrm{NL}}(k) = \frac{2\omega(k)}{k\sigma_c}\left\{\frac{\omega(k)}{\tanh(kW/2)} + \frac{k\tan^2(\theta_{\mathrm{VH}})}{\tanh[\omega(k)W/2]}\right\}^{-1}.$$

3.2.1 Low resistivity limit ($\rho \to 0$)

Sending $\rho \to 0$ is effectively equal to sending $\tan(\theta_{\mathrm{VH}}) = \sigma_{\mathrm{v}}\rho \to 0$. To be more precise we are going to assume that

$$\frac{k\tan^2(\theta_{\mathrm{VH}})}{\tanh[\omega(k)W/2]} \ll \frac{\omega(k)}{\tanh(kW/2)} \qquad \forall k\,.$$

Which means that $\tan^2(\theta_{\mathrm{VH}}) \ll 1$. So now we do a Taylor series expansion of the above equation around $\tan^2(\theta_{\mathrm{VH}}) = 0$.

$$R_{\mathrm{NL}}(k) \approx R_{\mathrm{NL}}(k)|_{\tan^2(\theta_{\mathrm{VH}})=0} + \frac{\partial}{\partial\tan^2(\theta_{\mathrm{VH}})}R_{\mathrm{NL}}(k)|_{\tan^2(\theta_{\mathrm{VH}})=0}\,,$$

that we are going to re-define as

$$R_{\mathrm{NL}}(k) \approx R^{(0)}_{\mathrm{NL}}(k) + R^{(1)}_{\mathrm{NL}}(k)\tan^2(\theta_{\mathrm{VH}})\,.$$

The zeroth order term gives us our good old ohmic response in the frequency domain (eq. 3.2)

$$R^{(0)}_{\mathrm{NL}}(k) = \frac{2\rho}{k}\tanh\left(\frac{kW}{2}\right).$$

This makes sense because as we lower ρ/ρ_{v} the hall current will be increasingly smaller and so the ohmic response will dominate.
And if we do the Fourier transform to get the x dependent form we get the ohmic nonlocal resistivity 2.36

$$R^{(0)}_{\mathrm{NL}}(x) = \frac{2\rho}{\pi}\ln\left|\coth\left(\frac{\pi x}{2W}\right)\right|. \tag{3.21}$$

Now let's calculate the first order term

$$R^{(1)}_{\mathrm{NL}}(k)\tan^2(\theta_{\mathrm{VH}}) = -2\rho\frac{\omega(k)}{k}\left[\frac{\omega(k)}{\tanh(Wk/2)}\right]^{-2}k\frac{\tan^2(\theta_{\mathrm{VH}})}{\tanh(\omega(k)W/2)} =$$

$$= -2\rho^3\sigma_{\mathrm{v}}^2\tanh^2\left(\frac{kW}{2}\right)\left\{\omega(k)\tanh\left[\frac{\omega(k)W}{2}\right]\right\}^{-1} \equiv \rho^3 F(k)\,,$$

where $F(k)$ is defined as follows

$$F(k) \equiv -2\sigma_{\mathrm{v}}^2\tanh^2\left(\frac{kW}{2}\right)\left\{\omega(k)\tanh\left[\frac{\omega(k)W}{2}\right]\right\}^{-1}. \tag{3.22}$$

And it doesn't depend on ρ. Its Fourier transform is

$$F(x) = -2\sigma_v^2 \int_{-\infty}^{+\infty} \tanh^2\left(\frac{kW}{2}\right)\left\{\tanh\left[\frac{\omega(k)W}{2}\right]\right\}^{-1} \frac{e^{-ikx}}{\omega(k)}\frac{dk}{2\pi}\,. \quad (3.23)$$

Putting it all together we get that

$$\lim_{\rho\to 0} R_{\mathrm{NL}}(x) = \frac{2\rho}{\pi}\ln\left|\coth\left(\frac{\pi x}{2W}\right)\right| + \rho^3 F(x) + o(\rho^5)\,. \quad (3.24)$$

3.2.2 Large resistivity limit ($\rho \to \infty$)

Now let's study what happens when $\rho, \tan(\theta_{\mathrm{VH}}) \to \infty$. First off let's rewrite equation 3.1 and bring the $\omega(k)$ and k inside the curly braces.

$$R_{\mathrm{NL}}(k) = 2\rho\Bigg\{\underbrace{\frac{k}{\tanh(kW/2)}}_{\substack{\text{cannot be}\\ \text{ignored for } k=0}} + \frac{k^2}{\omega(k)}\frac{\tan^2(\theta_{\mathrm{VH}})}{\tanh[\omega(k)W/2]}\Bigg\}^{-1}. \quad (3.25)$$

This limit is a bit tricky to evaluate. First off even thought the right-most term inside the curly braces dominates everywhere except for $k = 0$ this "*small detail*" is crucial. From image 3.8 we can see that the larger ρ gets, the smaller the area around $k = 0$ where the first term dominates.
For high values of $\rho, \tan(\theta_{\mathrm{VH}})$ the parabola becomes really narrow, and it overtakes the first term. This means that for the values of $\tan(\theta_{\mathrm{VH}})$ such that the parabola manages to overtake the $k\tanh^2(kW/2)$ term before $k = 2/W$ we can approximate the first term as being always equal to $2/W$. To be more precise

$$\left(\frac{2}{W}\right)^2 \frac{1}{\omega(2/W)}\frac{\tan^2(\theta_{\mathrm{VH}})}{\tanh[\omega(2/W)W/2]} \gg \frac{2}{W}\,,$$

so,

$$\tan^2(\theta_{\mathrm{VH}}) \gg \sqrt{1+\frac{W^2}{4l_{\mathrm{v}}^2}}\tanh\left(\sqrt{1+\frac{W^2}{4l_{\mathrm{v}}^2}}\right). \quad (3.26)$$

This means that in that case

$$R_{\mathrm{NL}}(k) \approx 2\rho\Bigg\{\frac{2}{W} + \frac{k^2}{\omega(k)}\frac{\tan^2(\theta_{\mathrm{VH}})}{\tanh[\omega(k)W/2]}\Bigg\}^{-1}. \quad (3.27)$$

Ok, low let's take a look at this function as we make ρ bigger and bigger.
As you can see from figure 3.9 are three regimes here. The first one in for $k < l_{\mathrm{v}}^{-1}$, the second one is for $l_{\mathrm{v}}^{-1} < k < W^{-1}$ and the third one is for $W^{-1} < k$

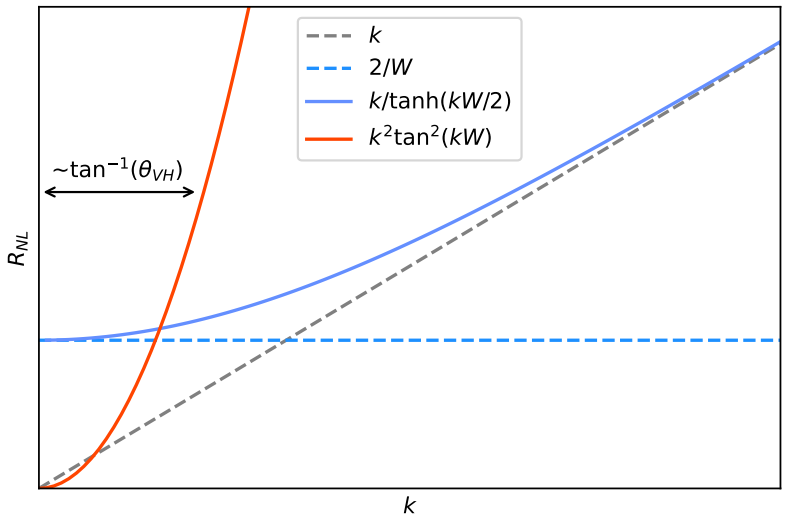

Figure 3.8: This graph shows the elements inside the curly brakets in equation 3.25. The continuous blue line represents the first term, the blue dashed line represents its approximation around $k = 0$ and the gray dashed lines represent its approximation for $k \to \infty$.
The orange parabola represents the right-hand side term $\frac{k^2}{\omega(k)} \frac{\tan^2(\theta_{\mathrm{VH}})}{\tanh[\omega(k)W/2]}$

First regime

In the first regime ($k < l_{\mathrm{v}}^{-1}$) $R_{\mathrm{NL}}(k)$ is similar to a Lorentzian function.

$$\lim_{\rho\to\infty} R_{\mathrm{NL}}(k) = 2\rho\left\{\frac{2}{W} + l_{\mathrm{v}}k^2\frac{\tan^2(\theta_{\mathrm{VH}})}{\tanh[W/2l_{\mathrm{v}}]}\right\}^{-1}. \tag{3.28}$$

We can re-parametrize it As

$$\lim_{\rho\to\infty} R_{\mathrm{NL}}(k) = \frac{R_{xx}}{1+(k/\Gamma)^2}, \tag{3.29}$$

Where

$$\Gamma = \frac{1}{\tan(\theta_{\mathrm{VH}})}\sqrt{\frac{2}{l_{\mathrm{v}}W}\tanh\left(\frac{W}{2l_{\mathrm{v}}}\right)}.$$

Therefore ρ and the standard deviation of the Lorentzian Γ are inversely proportional.
If we do the anti-Fourier transform of this equation to get the position dependent Non-local resistivity we get

$$\mathcal{F}^{-1}\left[\frac{R_{xx}}{1+(k/\Gamma)^2}\right] = \frac{1}{2}\rho W\Gamma e^{-|x|\Gamma} =$$

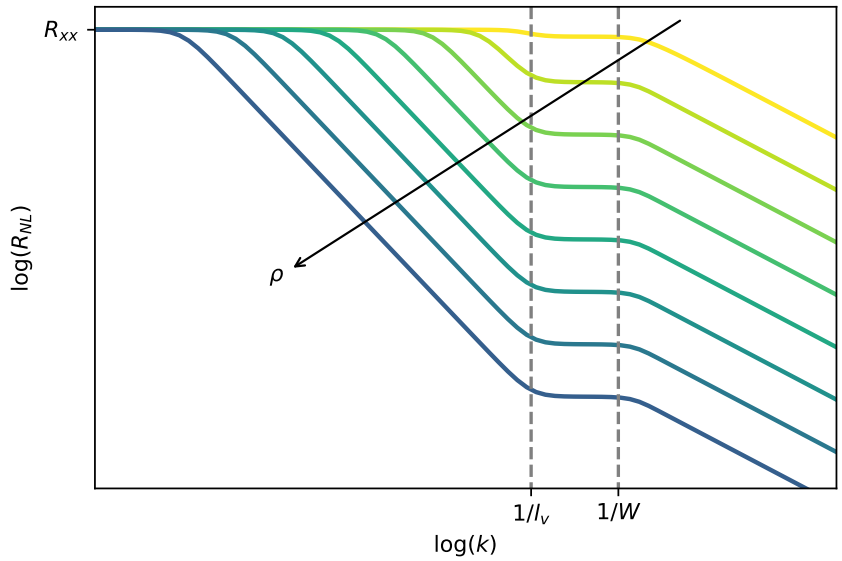

Figure 3.9: In this graph we show several graphs of the nonlocal resistance as a function of k. The darker the line color is, the bigger is the value of ρ. Notice how, as we increase ρ the first regime becomes more dominant

$$= \frac{\rho W}{\tan(\theta_{\mathrm{VH}})}\sqrt{\frac{2}{l_{\mathrm{v}}W}\tanh\left(\frac{W}{2l_{\mathrm{v}}}\right)}\exp\left[\frac{-|x|}{\tan(\theta_{\mathrm{VH}})}\sqrt{\frac{2}{l_{\mathrm{v}}W}\tanh\left(\frac{W}{2l_{\mathrm{v}}}\right)}\right]. \tag{3.30}$$

Since $\tan(\theta_{\mathrm{VH}}) = \rho\sigma_{\mathrm{v}}$, for $\rho \to +\infty$ the equation above converges pointwise to the following saturation constant S

$$\lim_{\rho\to\infty}\mathcal{F}^{-1}\left[\frac{R_{xx}}{1+(k/\Gamma)^2}\right] = \frac{1}{\sigma_{\mathrm{v}}}\sqrt{\frac{2W}{l_{\mathrm{v}}}\tanh\left(\frac{W}{2l_{\mathrm{v}}}\right)} \equiv S\,. \tag{3.31}$$

Second regime and third regime

Now that we have calculated how it behaves in the regime where is similar to a Lorenztian, let's calculate the second regime. We have already calculated the value the plateau assumes in equation 3.4

$$R_{\mathrm{NL}}(k) \approx \rho W\cos^2(\theta_{\mathrm{VH}})\,, \tag{3.32}$$

While in the third and last regime

$$R_{\mathrm{NL}}(k) \approx \frac{2\rho}{k}\cos^2(\theta_{\mathrm{VH}})\,. \tag{3.33}$$

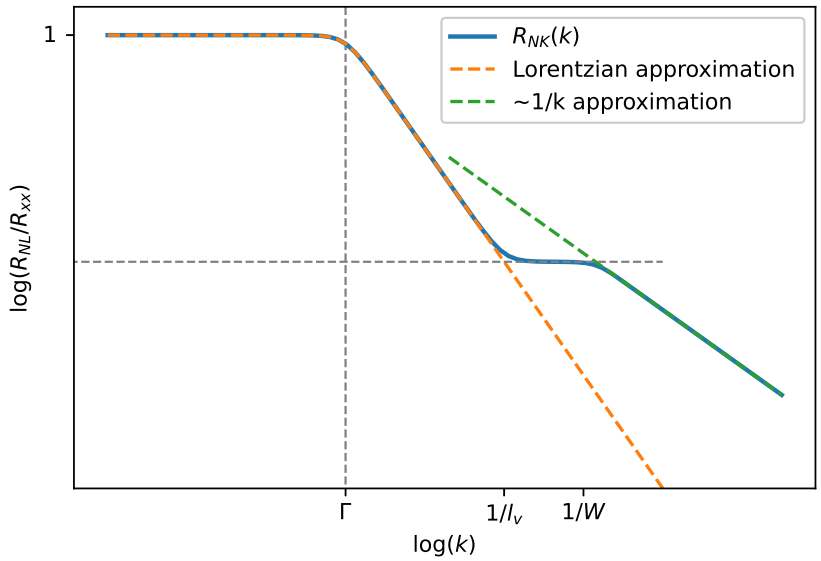

Figure 3.10: The main regimes of the nonlocal resistance as a function of k

Notice how the equations for the second and third regime are both proportional to $\rho\cos^2(\theta_{\mathrm{VH}})$. This means we can write equation 3.27 as approximately

$$\lim_{\rho\to\infty} R_{\mathrm{NL}}(k) = \frac{R_{xx}}{1+(k/\Gamma)^2} + \rho\cos^2(\theta_{\mathrm{VH}})C(k)\,, \tag{3.34}$$

Where $C(k)$ is a function that doesn't depend on ρ or $\tan(\theta_{\mathrm{VH}})$ and it comprehends the second, third regime and eventual corrections in between the approximations[1].
Now let $G(x)$ be it's Fourier anti-transform, then we have that

$$\lim_{\rho\to\infty} R_{\mathrm{NL}}(x) = S + \frac{1}{\rho}G(x)\,, \tag{3.35}$$

Where here we have used that $\lim_{\rho\to\infty}\rho\cos^2(\theta_{\mathrm{VH}}) = 1/\rho$. This means that for $\rho\to+\infty$ the right hand side term vanishes, unless it diverges. And indeed $G(x)$ diverges for $x=0$. Therefore, the limit above has pointwise convergence in $\{x\in\mathbb{R}\,|\,x\neq 0\}$

$$\lim_{\rho\to\infty} R_{\mathrm{NL}}(x) = \frac{1}{\sigma_{\mathrm{v}}}\sqrt{\frac{2W}{l_{\mathrm{v}}}\tanh\left(\frac{W}{2l_{\mathrm{v}}}\right)} \qquad \text{for } x\neq 0\,. \tag{3.36}$$

[1]The corrections also are proportional to $\rho\cos^2(\theta_{\mathrm{VH}})$

3.2.3 Putting it all together

The main result from subsection 3.2.1 we showed that for $\tan^2(\theta_{\mathrm{VH}}) \ll 1$ we had equation 3.24

$$R_{\mathrm{NL}}(x) = \frac{2\rho}{\pi} \ln \left| \coth\left(\frac{\pi x}{2W}\right) \right| + \rho^3 F(x) + o(\rho^5)\,,$$

While, in subsection 3.2.2 we had that for

$$\tan^2(\theta_{\mathrm{VH}}) \gg \sqrt{1 + W^2/(4l_{\mathrm{v}}^2)} \tanh\left(\sqrt{1 + W^2/(4l_{\mathrm{v}}^2)}\right)$$

(eq. 3.26) we had equation 3.36.

$$R_{\mathrm{NL}}(x) = \frac{1}{\sigma_{\mathrm{v}}} \sqrt{\frac{2W}{l_{\mathrm{v}}} \tanh\left(\frac{W}{2l_{\mathrm{v}}}\right)}\,.$$

If we plot the approximations on top of the actual function we get something that looks like figure 3.11. This behavior has been observed when in atomically thin MoS_2 [72].

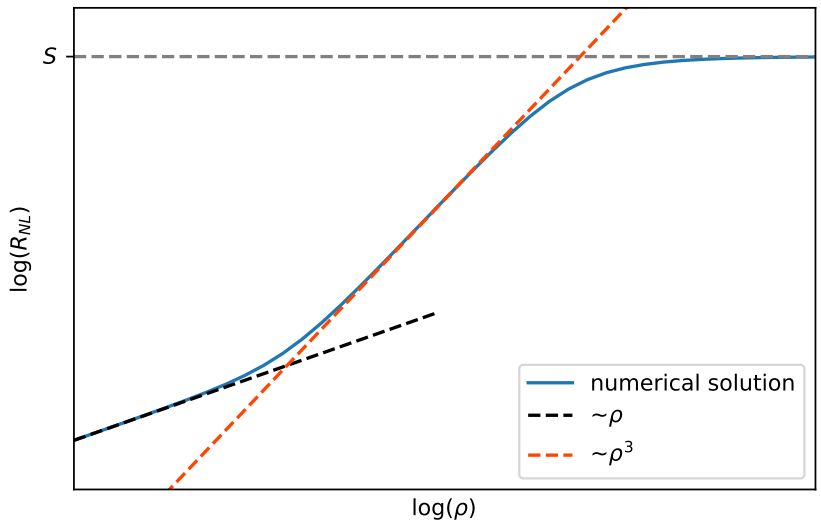

Figure 3.11: The main regimes of the nonlocal resistance as a function of the resistivity

3.2.4 Altertative way of studying the non local resistance as we change the resistivity

Up until now we have studied $R_{\mathrm{NL}}(x)$ as we change ρ starting directly from the frequency response function (eq. 3.1). This is the most rigorous way for doing this analysis, but it can be cumbersome to work with and doesn't really offer much insight in the topology behind.

A much simpler, but less rigorous way of approaching the problem would be to start from the approximate form of $R_{\mathrm{NL}}(x)$ (eq. 3.19). As you might remeber, this equation had the advantage of being able to distinguish the ohmic effect from the topological ones giving us a strong tool to be able to analyze the graphs.

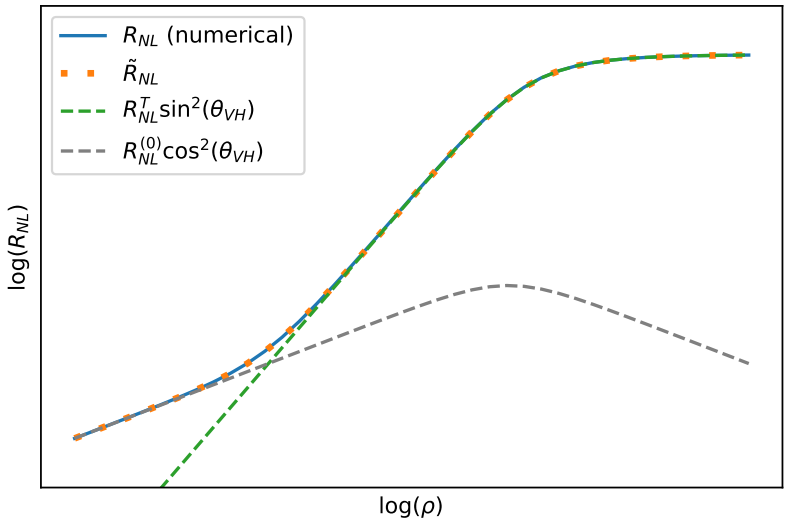

Figure 3.12: R_{NL} (continuous blue line, calculated numerically) and its approximation $\tilde{R}_{\mathrm{NL}}$ (dotted orange line) are virtually indistinguishable. The topological component of $\tilde{R}_{\mathrm{NL}}$ is the green dashed line and the ohmic is the grey dashed line.

From image 3.12 it is clear that the linear part at low $\tan(\theta_{\mathrm{VH}})$ is due to the ohmic effect. This makes sense even intuitively, infact the current will prefer choosing the path of least resistance, and since at low $\tan(\theta_{\mathrm{VH}})$ the ohmic resistivity is much less than the hall resistivity, we have a mostly ohmic behavior.

This image also shows that the topological component is the one responsible for the ρ^3 behavior, and then the saturation value.

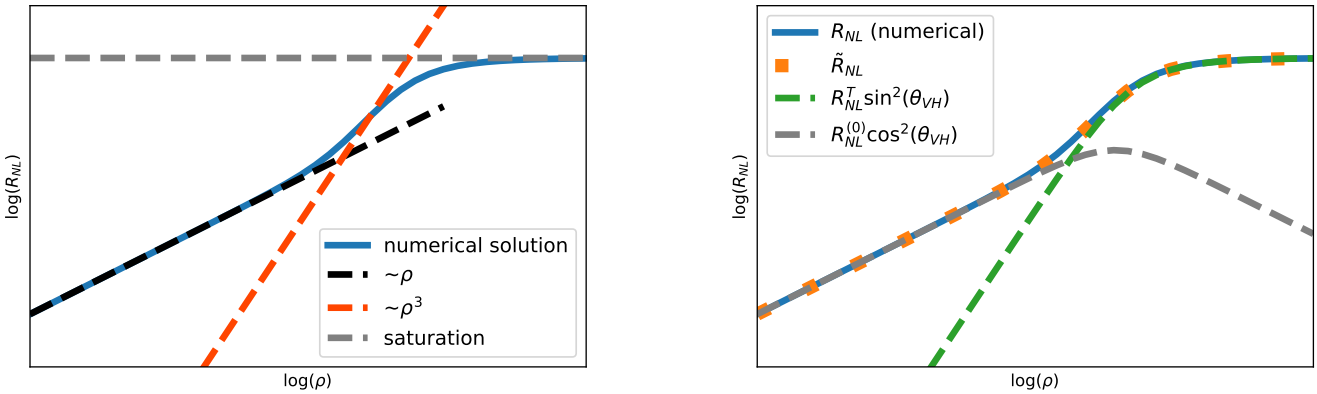

Figure 3.13: This is an example where the valley diffusion length l_v and the width of the sample W are comparable, as you can see the ρ^3 behavior disappears

A few small details

In the discussion about R_{NL} as we change ρ we choose parameters to highlight the behaviors we talked about. However sometimes certain behaviors disappear, for example if we increase the ohmic contributions by decreasing the width of the bar, figures 3.11 and 3.12 become like in figure 3.13

In the following section we'll see how this applies to lab measurements

Does this generalize?

Up until now we talked about valley currents, however this also applies to spin-hall effect and spin-orbit effect since the differential equations that govern the system are equivalent

3.3 Comparison with experimental data

Experimental setups have a few limitations compared to the theoretical treatment, for example you do not have complete freedom of changing the resistance, rather the resistance is changed by changing the temperature of the sample. This has a few consequences:

- Since out sample is a semiconductor, the lower the temperature, the higher the resistance, but if the temperature gets too low we enter the ballistic regime, and our treatment is no longer valid.
- If the temperature gets too high, the quantization of the hall effect disappears

This restricts us to a couple order of magnitude of the resistivity.

Now we compare the results with the experimental data. Let's start from analyzing the data from [73].
In this paper the authors measured the valley hall effect of a heterostructure made of bilayer-graphene on top of boron nitride at different angles ϕ between the graphene and the boron nitride. The sample has a width $W = 1.7\mu$m, and inter-valley scattering length $l_{\mathrm{v}} = 1.6\mu$m and the distance of the contact from the injection point is $x = 2.3\mu$m

The angles ϕ that were explored are $0, \pi/6$ and $\pi/3$. If you plot the measurements you get figure 3.14.

We then analyze the data by comparing the output of the model thus far

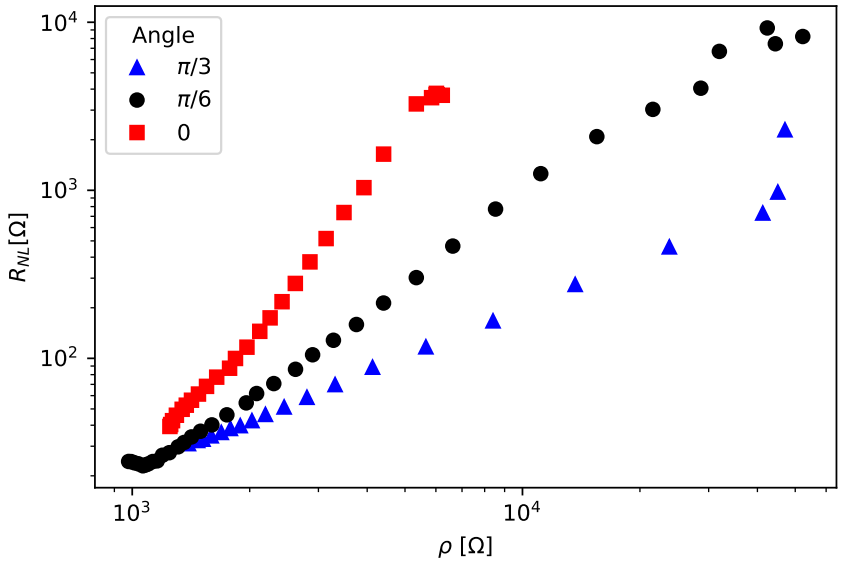

Figure 3.14: Datapoints from [73]

developed to the data, we did not fit the data, rather we used the knowledge we already have about the parameters W, l_{v}, x and plot the result on top of the datapoints.

- For $\phi = \pi/3$ we have that the response is fully ohmic, and so we get a completely linear response (figure 3.15)
- For $\phi = \pi/6$ we have a hall effect, however, since $W \approx l_{\mathrm{v}}$ the ohmic and the topological response mix together, so we never see the full-fledged ρ^3 behavior.[2]

[2] A more detailed explanation was given in the details of subsection 3.2.4

- For $\phi = 0$ the response does not match the model we developed, further investigations should be done to address the discrepancy

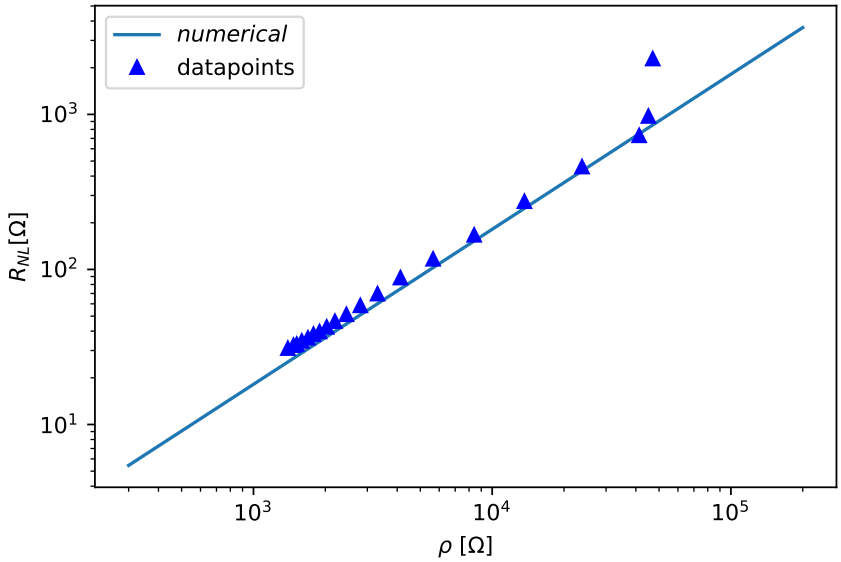

Figure 3.15: Comparison between the data points and the theoretical expectation for $\phi = \pi/3$. With the exception of the last experimental point, the data follows the theoretical prediction

3.4 Conclusions

In this thesis we provided a complete and accurate description on the Nonlocal resistance arising from valley-Hall. It expands on top of the work done by Beconcini et al. [59] where they manage to explain the results Shimazaki et al. obtained [62] where they found a that the non-linear resistance on bilayer graphene depended on the cube of the longitudinal resistivity ($R_{\mathrm{NL}} \propto \rho^3$) for low resistivities and then it saturates.
The work done by Beconcini et al. was only able to explain the behavior of the nonlocal resistance if the width of the material is much smaller than the valley diffusion length ($l_v \ll W$). In this thesis we found an accurate description for any valley diffusion length and width and we compared the results with the work done by Arrighi et al. [73]. The results we obtained can also be used to study the non-local resistance of other anomalous Hall effect such as spin-Hall effect.

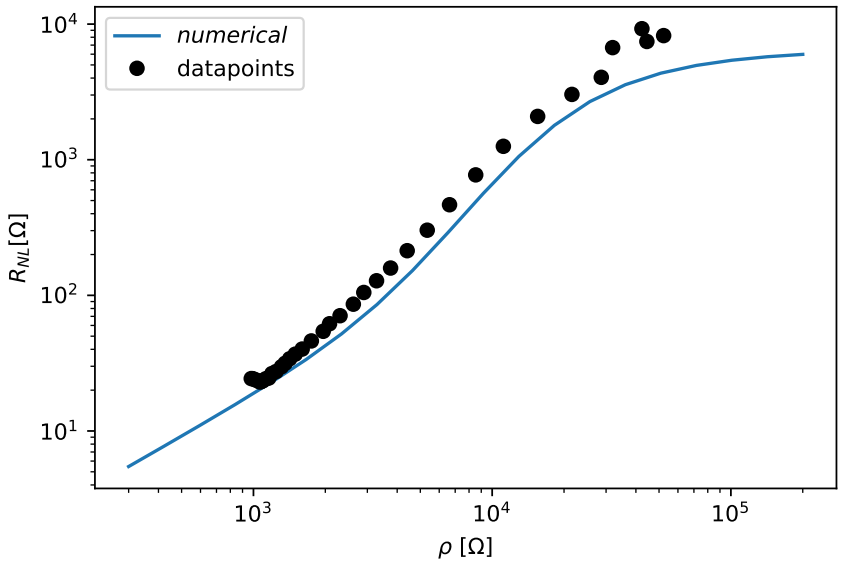

Figure 3.16: Comparison between the data points and the theoretical expectation for $\phi = \pi/6$. The model has a lower precision for higher values of ρ, R_{NL}, however we can say that the data follow the theoretical prediction

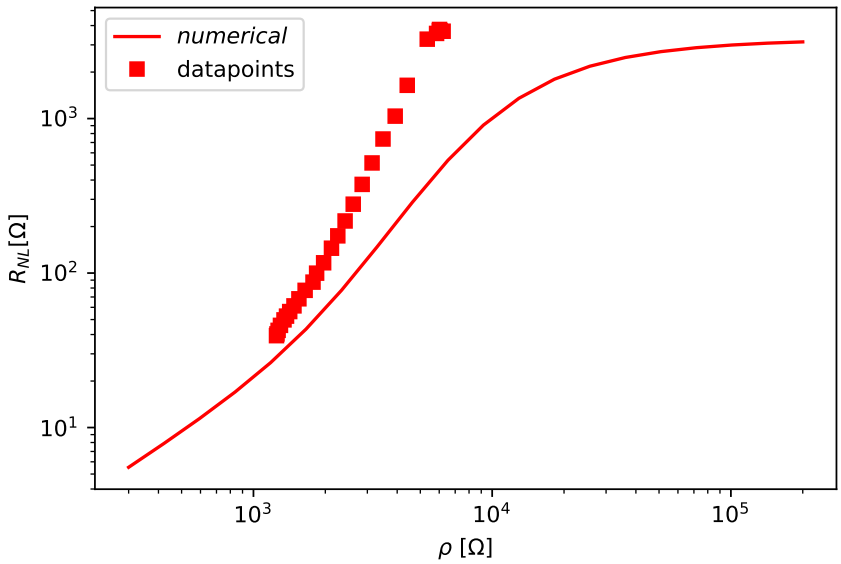

Figure 3.17: Comparison between the data points and the theoretical expectation for $\phi = 0$. The model does not satisfactorily reflect the data.

Bibliography

[1] T. course team, *Online course on topology in condensed matter*. 2021.

[2] D. Tong, *Topics in Quantum Mechanics*. 2017.

[3] B. I. Halperin, "Quantized hall conductance, current-carrying edge states, and the existence of extended states in a two-dimensional disordered potential," *Physical Review B*, vol. 25, no. 4, p. 2185, 1982.

[4] M. Z. Hasan and C. L. Kane, "Colloquium: Topological insulators," *Reviews of modern physics*, vol. 82, no. 4, p. 3045, 2010.

[5] R Jackiw and C. Rebbi, "Vacuum periodicity in a yang-mills quantum theory," *Physical Review Letters*, vol. 37, no. 3, p. 172, 1976.

[6] D. Tong, "Lectures on the quantum hall effect," *arXiv:1606.06687*, 2016.

[7] S. Weinberg, *Lectures on Quantum Mechanics*. Hyperion New York, 2013.

[8] G. Grosso and G. P. Parravicini, *Solid state physics*. Academic press, 2013.

[9] D. J. Thouless, M. Kohmoto, M. P. Nightingale, and M. den Nijs, "Quantized hall conductance in a two-dimensional periodic potential," *Physical review letters*, vol. **49**, no. 6, p. 405, 1982.

[10] D. Thouless, "Quantization of particle transport," *Physical Review B*, vol. **27**, no. 10, p. 6083, 1983.

[11] M.-C. Chang and Q. Niu, "Berry phase, hyperorbits, and the hofstadter spectrum," *Physical review letters*, vol. **75**, no. 7, p. 1348, 1995.

[12] Y. Yao *et al.*, "First principles calculation of anomalous hall conductivity in ferromagnetic bcc fe," *Physical review letters*, vol. **92**, no. 3, p. 037 204, 2004.

[13] K. S. Novoselov *et al.*, "Electric field effect in atomically thin carbon films," *science*, vol. **306**, no. 5696, pp. 666–669, 2004.

[14] A. C. Neto, F. Guinea, N. M. Peres, K. S. Novoselov, and A. K. Geim, "The electronic properties of graphene," *Reviews of modern physics*, vol. **81**, no. 1, p. 109, 2009.

[15] F. Bloch, "Über die quantenmechanik der elektronen in kristallgittern," *Zeitschrift für physik*, vol. **52**, no. 7, pp. 555–600, 1929.

[16] J. C. Slater and G. F. Koster, "Simplified lcao method for the periodic potential problem," *Physical Review*, vol. **94**, no. 6, p. 1498, 1954.

[17] M. GIBERTINI and D. M. POLINI, "Ground-state properties of inhomogeneous graphene sheets,"

[18] M. Cardona and Y. Y. Peter, *Fundamentals of semiconductors*. Springer, 2005, vol. 619.

[19] D. DiVincenzo and E. Mele, "Self-consistent effective-mass theory for intralayer screening in graphite intercalation compounds," *Physical Review B*, vol. 29, no. 4, p. 1685, 1984.

[20] F. D. M. Haldane, "Model for a quantum hall effect without landau levels: Condensed-matter realization of the" parity anomaly"," *Physical review letters*, vol. 61, no. 18, p. 2015, 1988.

[21] C. L. Kane and E. J. Mele, "Quantum spin hall effect in graphene," *Physical review letters*, vol. **95**, no. 22, p. 226 801, 2005.

[22] E. McCann and M. Koshino, "The electronic properties of bilayer graphene," *Reports on Progress in physics*, vol. **76**, no. 5, p. 056 503, 2013.

[23] A. Kuzmenko, I. Crassee, D. Van Der Marel, P Blake, and K. Novoselov, "Determination of the gate-tunable band gap and tight-binding parameters in bilayer graphene using infrared spectroscopy," *Physical Review B*, vol. **80**, no. 16, p. 165 406, 2009.

[24] E. McCann and V. I. Fal'ko, "Landau-level degeneracy and quantum hall effect in a graphite bilayer," *Physical review letters*, vol. 96, no. 8, p. 086 805, 2006.

[25] M Mucha-Kruczyński, E McCann, and V. I. Fal'Ko, "Electron–hole asymmetry and energy gaps in bilayer graphene," *Semiconductor Science and Technology*, vol. 25, no. 3, p. 033 001, 2010.

[26] V. B. Mbayachi, E. Ndayiragije, T. Sammani, S. Taj, E. R. Mbuta, *et al.*, "Graphene synthesis, characterization and its applications: A review," *Results in Chemistry*, vol. 3, p. 100 163, 2021.

[27] R. S. Edwards and K. S. Coleman, "Graphene synthesis: Relationship to applications," *Nanoscale*, vol. 5, no. 1, pp. 38–51, 2013.

[28] R. Van Noorden, "Production: Beyond sticky tape," *Nature*, vol. 483, no. 7389, S32–S33, 2012.

[29] F. Liu *et al.*, "Synthesis of graphene materials by electrochemical exfoliation: Recent progress and future potential," *Carbon Energy*, vol. 1, no. 2, pp. 173–199, 2019.

[30] S. Yang, M. R. Lohe, K. Müllen, and X. Feng, "New-generation graphene from electrochemical approaches: Production and applications," *Advanced Materials*, vol. 28, no. 29, pp. 6213–6221, 2016.

[31] W. Luheng, D. Tianhuai, and W. Peng, "Influence of carbon black concentration on piezoresistivity for carbon-black-filled silicone rubber composite," *Carbon*, vol. 47, no. 14, pp. 3151–3157, 2009.

[32] S. S. Shams, L. S. Zhang, R. Hu, R. Zhang, and J. Zhu, "Synthesis of graphene from biomass: A green chemistry approach," *Materials Letters*, vol. 161, pp. 476–479, 2015.

[33] H. HIBINO, H. KAGESHIMA, and M. NAGASE, "Graphene growth on silicon carbide," *NTT Technical Review (Web)*, vol. 8, no. 8, 2010.

[34] Z.-Y. Juang *et al.*, "Synthesis of graphene on silicon carbide substrates at low temperature," *Carbon*, vol. 47, no. 8, pp. 2026–2031, 2009.

[35] Y. Pan *et al.*, "Highly ordered, millimeter-scale, continuous, single-crystalline graphene monolayer formed on ru (0001)," *Advanced Materials*, vol. 21, no. 27, pp. 2777–2780, 2009.

[36] D. A. Brownson and C. E. Banks, "The electrochemistry of cvd graphene: Progress and prospects," *Physical Chemistry Chemical Physics*, vol. 14, no. 23, pp. 8264–8281, 2012.

[37] F. Yavari, Z. Chen, A. V. Thomas, W. Ren, H.-M. Cheng, and N. Koratkar, "High sensitivity gas detection using a macroscopic three-dimensional graphene foam network," *Scientific reports*, vol. 1, no. 1, pp. 1–5, 2011.

[38] Y. Seekaew, D. Phokharatkul, A. Wisitsoraat, and C. Wongchoosuk, "Highly sensitive and selective room-temperature no2 gas sensor based on bilayer transferred chemical vapor deposited graphene," *Applied Surface Science*, vol. 404, pp. 357–363, 2017.

[39] H. An, W.-J. Lee, and J. Jung, "Graphene synthesis on fe foil using thermal cvd," *Current Applied Physics*, vol. 11, no. 4, S81–S85, 2011.

[40] F. Ghaemi, L. C. Abdullah, P. M. Tahir, and R. Yunus, "Synthesis of different layers of graphene on stainless steel using the cvd method," *Nanoscale research letters*, vol. 11, no. 1, pp. 1–6, 2016.

[41] D. Vanderbilt, *Berry phases in electronic structure theory: electric polarization, orbital magnetization and topological insulators*. Cambridge University Press, 2018.

[42] E. H. Hall, "Xviii. on the "rotational coefficient" in nickel and cobalt," *The London, Edinburgh, and Dublin Philosophical Magazine and Journal of Science*, vol. **12**, no. 74, pp. 157–172, 1881.

[43] R. Karplus and J. Luttinger, "Hall effect in ferromagnetics," *Physical Review*, vol. **95**, no. 5, p. 1154, 1954.

[44] P. B. Smith, "The resonant scattering integral; application to the analysis of elastic proton scattering," *Physica*, vol. **24**, no. 6-10, pp. 1085–1091, 1958.

[45] L. Berger, "Side-jump mechanism for the hall effect of ferromagnets," *Physical Review B*, vol. **2**, no. 11, p. 4559, 1970.

[46] N. Nagaosa, J. Sinova, S. Onoda, A. H. MacDonald, and N. P. Ong, "Anomalous hall effect," *Reviews of modern physics*, vol. **82**, no. 2, p. 1539, 2010.

[47] V. Dugaev, P Bruno, M Taillefumier, B Canals, and C Lacroix, "Anomalous hall effect in a two-dimensional electron gas with spin-orbit interaction," *Physical Review B*, vol. **71**, no. 22, p. 224 423, 2005.

[48] Y. Tian, L. Ye, and X. Jin, "Proper scaling of the anomalous hall effect," *Physical review letters*, vol. **103**, no. 8, p. 087 206, 2009.

[49] D. Xiao, W. Yao, and Q. Niu, "Valley-contrasting physics in graphene: Magnetic moment and topological transport," *Physical review letters*, vol. **99**, no. 23, p. 236 809, 2007.

[50] M. D'yakonov and V. Perel, "Spin orientation of electrons associated with the interband absorption of light in semiconductors," *Soviet Journal of Experimental and Theoretical Physics*, vol. **33**, p. 1053, 1971.

[51] S. Wolf *et al.*, "Spintronics: A spin-based electronics vision for the future," *science*, vol. **294**, no. 5546, pp. 1488–1495, 2001.

[52] J. D. Jackson, *Classical electrodynamics*, 1999.

[53] Y. A. Bychkov and É. I. Rashba, "Properties of a 2d electron gas with lifted spectral degeneracy," *JETP lett*, vol. **39**, no. 2, p. 78, 1984.

[54] Y. K. Kato, R. C. Myers, A. C. Gossard, and D. D. Awschalom, "Observation of the spin hall effect in semiconductors," *science*, vol. 306, no. 5703, pp. 1910–1913, 2004.

[55] J. Wunderlich, B. Kaestner, J. Sinova, and T. Jungwirth, "Experimental observation of the spin-hall effect in a two-dimensional spin-orbit coupled semiconductor system," *Physical review letters*, vol. 94, no. 4, p. 047 204, 2005.

[56] V Sih, W. Lau, R. Myers, V. R. Horowitz, A. Gossard, and D. Awschalom, "Generating spin currents in semiconductors with the spin hall effect," *Physical review letters*, vol. 97, no. 9, p. 096 605, 2006.

[57] N. Stern, S Ghosh, G Xiang, M Zhu, N Samarth, and D. Awschalom, "Current-induced polarization and the spin hall effect at room temperature," *Physical review letters*, vol. 97, no. 12, p. 126 603, 2006.

[58] H. Weng, X. Dai, and Z. Fang, "From anomalous hall effect to the quantum anomalous hall effect," *arXiv preprint arXiv:1509.05507*, 2015.

[59] M. Beconcini, F. Taddei, and M. Polini, "Nonlocal topological valley transport at large valley hall angles," *Physical Review B*, vol. **94**, no. 12, p. 121 408, 2016.

[60] R. Gorbachev *et al.*, "Detecting topological currents in graphene superlattices," *Science*, vol. **346**, no. 6208, pp. 448–451, 2014.

[61] M. Sui *et al.*, "Gate-tunable topological valley transport in bilayer graphene," *Nature Physics*, vol. **11**, no. 12, pp. 1027–1031, 2015.

[62] Y. Shimazaki, M. Yamamoto, I. V. Borzenets, K. Watanabe, T. Taniguchi, and S. Tarucha, "Generation and detection of pure valley current by electrically induced berry curvature in bilayer graphene," *Nature Physics*, vol. **11**, no. 12, pp. 1032–1036, 2015.

[63] D. Xiao, G.-B. Liu, W. Feng, X. Xu, and W. Yao, "Coupled spin and valley physics in monolayers of mos 2 and other group-vi dichalcogenides," *Physical review letters*, vol. **108**, no. 19, p. 196 802, 2012.

[64] K. F. Mak, K. L. McGill, J. Park, and P. L. McEuen, "The valley hall effect in mos2 transistors," *Science*, vol. **344**, no. 6191, pp. 1489–1492, 2014.

[65] J. Lee, Z. Wang, H. Xie, K. F. Mak, and J. Shan, "Valley magnetoelectricity in single-layer mos2," *Nature materials*, vol. **16**, no. 9, pp. 887–891, 2017.

[66] S. O. Valenzuela and M Tinkham, "Direct electronic measurement of the spin hall effect," *Nature*, vol. **442**, no. 7099, pp. 176–179, 2006.

[67] D. Abanin, A. Shytov, L. Levitov, and B. Halperin, "Nonlocal charge transport mediated by spin diffusion in the spin hall effect regime," *Physical review B*, vol. **79**, no. 3, p. 035 304, 2009.

[68] C Brüne *et al.*, "Evidence for the ballistic intrinsic spin hall effect in hgte nanostructures," *Nature Physics*, vol. **6**, no. 6, pp. 448–454, 2010.

[69] D. Abanin *et al.*, "Giant nonlocality near the dirac point in graphene," *Science*, vol. **332**, no. 6027, pp. 328–330, 2011.

[70] J. Balakrishnan and K. W. Koon, "G., jaiswal, m., castro neto, ah & özyilmaz, b. colossal enhancement of spin–orbit coupling in weakly hydrogenated graphene," *Nat. Phys*, vol. **9**, pp. 284–287, 2013.

[71] Z. Wang, C. Tang, R. Sachs, Y. Barlas, and J. Shi, "Proximity-induced ferromagnetism in graphene revealed by the anomalous hall effect," *Physical review letters*, vol. **114**, no. 1, p. 016 603, 2015.

[72] Z. Wu *et al.*, "Intrinsic valley hall transport in atomically thin mos2," *Nature communications*, vol. 10, no. 1, pp. 1–8, 2019.

[73] E Arrighi *et al.*, "Non-identical moiré twins in bilayer graphene," *arXiv: 2205.01760*, 2022.